1-1-1986

Novel application of light scattering in condensed matter physics/

Scott A. Kuehl
University of Massachusetts Amherst

NOVEL APPLICATION OF LIGHT SCATTERING IN CONDENSED MATTER PHYSICS

A Dissertation Presented

By

Scott A. Kuehl

Submitted to the Graduate School of the

University of Massachusetts

in partial fulfillment of the requirements for

the degree of

DOCTOR OF PHILOSOPHY

September 1986

Polymer Science and Engineering

NOVEL APPLICATIONS OF LIGHT SCATTERING

IN CONDENSED MATTER PHYSICS

A Dissertation Presented

By

Scott A. Kuehl

Approved as to style and content by:

Prof. James C. W. Chien
Co-chairperson of Committee

Prof. Frank E. Karasz
Co-chairperson of Committee

Prof. Kenneth H. Langley
Co-chairperson of Committee
and outside member

Prof. Edwin L. Thomas, Head
Department of Polymer Science
and Engineering

ACKNOWLEDGEMENT

This work is dedicated in part to those individuals, especially teachers, authors of text and reference books and those contributing to published literature used so often as basic reference material who contributed silently to my education. Without their groundwork any contributions I have made would surely have been impossible. More specifically, I'd like to recognize the seemingly Herculean effort expended by the members of my committee and the Polymer Science department in general in the acquisition of the financial and material sustenance making my graduate work both pleasant and expedient. Special thanks to Dr. Chien and Dr. Charles Dickinson who provided moral and financial support during my association with Dr. Chiens research group. Special thanks to Professors Karasz and Langley for providing financial and material support during my association with them while I carried out Part II of this dissertation. It was Dr. Karasz who most graciously invited me into his research group in midstream and provided the funding for the publication costs of my first paper. He also unselfishly provided badly needed funds even after my statute of limitations had ended and absorbed some hefty telephone bills. Finally, I'd like to thank my parents (especially them) and the mentors Dr. Bruce Cleare and Dr. Mandelkern for support before and during my stay and experiences at the University of Massachusetts. Thanks to the members of 608 over the years for their hospitality and advisement. All of the above surely proved to me that patience is a virtue.

PREFACE

A doctoral dissertation meeting the requirements of the department of Polymer Science and Engineering, the graduate school at the University of Massachusetts and my thesis committee has been completed and its content presented in a split two topic thesis format. The circumstances that both inspired and directed the course of the scientific expositions contained in this thesis are wide and complex as they usually are in any research project. Through hindsight the process can be best related as a chronological history. As a split thesis, this dissertation is not a discourse singular in theme, however, the subject matter can be summed up under the general title of "Novel Applications of Light Scattering in Condensed Matter Physics." The two separate and independent scientific inquiries which will be described have nothing to do specifically with polymeric or macromolecular systems but both topics do address certain problems of the structure and behavior of condensed material phases analyzed by the techniques of elastic and inelastic light scattering.

Part I entitled "Raman Scattering Topology in an Anisotropic conjugated Molecule: A Novel Approach Through Single Crystal Raman" was the first project which I brought to a decisive conclusion while in the Polymer Science Department. It was performed while working with Dr. Chien, as a member of his group attempting to characterize

the conducting polymer polyacetylene. The project at the time it was conceived (1980) was designed to be a broad assault into revealing the macromolecular nature and electronic properties of polyacetylene as reflected in its electronic and vibrational spectroscopy. What was known about the polymer in this regard and at that time was new and controversial and needless to say, many fine academic and industrial concerns had for years made advances and accomplishments with a speed and detail never to be matched by workers such as myself naive in the field of solid state physics or trained in its experimental methods. Even with such competition, it was felt that significant contributions could be made, a virtual certainty under the directorship of Dr. Chien, making a significant contribution being the basic requirement for achieving Ph.D. status.

Of primary interest in polymer physics is the characterization of one or more material properties of a macromolecule or polymeric system as a function of the molecular weight or chain length. Coincident and sometimes precedential to this strategy is the characterization of the chain conformation/configuration of the macromolecular species contributing to the properties of the bulk state as well as determining the morphology of the bulk state itself. Over the years, many characterization techniques have been invented or adopted from other areas of science and applied to the inherently more complex polymeric systems. Sometimes one is confronted with a polymer which exhibits properties which do not lend themselves to characterization

by these conventional techniques. One such polymer was polyacetylene, an air sensitive, insoluble, opaque and polycrystalline polymer lacking mechanical resilience. Its novel property is that its electrical conductivity increases by 18 orders of magnitude, from that of a pure insulator to the semimetallic regime when it is introduced to chemicals causing charge transfer reactions. In some circles, the electronic conductivity was thought to be a result of the extended π electron conjugation simulating an effective one dimensional semiconductor. The electronic properties would then be closely related to chain architecture, bulk morphology, molecular weight and the chemistry of the doped and undoped states. The presence of a mobile soliton structure was proposed as the mechanism for electronic conduction (Chien, Heeger). A group with an alternative explanation lead by C. B. Duke, proposed a percolation model for conduction where the claim was made that polyacetylene is not an organic semiconductor and only appears to be semiconducting as a result of the polymer stabilizing conducting domains of inhomogeneously distributed dopant species. A conduction mechanism based on this scenerio would downplay the structure and chemistry of the polymer treating it as an inert matrix except to the extent that it provides a suitable charge-transfer chemical environment for the dopant species. In an attempt to deduce the electronic conduction mechanism, one is tempted to adopt procedures used in the field of crystalline metallic conductors and semiconductors. Conductivity measurements applied to a polycrystalline chemically complex material yields average and bulk

properties which can cloud a clear interpretation and perpetuate controversy. Decoupling the complex interplay of interactions and structural features which govern the behavior of the material would be required to fully understand the conduction mechanism and ideally one would like to study the properties of an individual chain specifically. Like the polymer oriented electronic conduction mechanism, the extended conjugation or sharing of π electrons along the chain in its Peierls distortion configuration governs the vibrational and electronic spectroscopy of the material. Moreover, it can provide single chain information. At the time this study was conceived, the Raman Spectra of polyacetylene was under close scrutiny, the hot topics being the force-resonance problem and the hot luminescence/cis-trans sequence distribution controversy. As spectoscopists sometimes do, a clever device was employed which is common in the field of polymer science, a textbook example being its application to intractable polyacetylene. A material parameter or property characteristic of the size of a single molecule is followed in a series of low molecular weight analouges where these properties are more easily identified and interpreted and then this information is extrapolated to the higher molecular weights indicative of the polymer, effects of morphology excluded. This procedure had been done to predict the crystal structure of polyacetylene using the members of the diphenylpolyene series. This study had four objectives based on this approach using the diphenylpolyene series. These are the model compounds of choice due to their air stability and high melting

point.

1) Solution and solid state spectra (IR and Raman) were to be recorded for diphenylpolyenes of different conjugation lengths in an effort to tabulate their vibrational mode frequencies and band intensities. A normal coordinate analysis supplemented with a Huckel level SCF-MO approach to the π bond force field was to be carried out on this series as a theoretical modelling effort to characterize the potential energy distribution of those modes involved in the force resonance effect and to determine the symmetry of those modes.

2) An understanding of the molecular packing and a determination of the crystalline field interactions if any through their effect on their Raman spectra where desired.

3) An investigation of the resonance Raman effect involved in the Raman scattering of these molecules and the polymer itself was to be carried out to determine the role of the π manifold on the polarization of the scattered light.

4) Characterization of the polymer in its doped and undoped states using the information accumulated from the model compound study.

This grand design or blueprint although noble in its intentions did suffer from flaws. After much work had been performed on the four objectives, it became obvious that further attention would be futile

when one compared the information that was desired with what could be found in the volumes of new material rapidly appearing in the literature or addressed there indirectly previously. Coupled with a lack of enthusiasm on behalf of my committee, I decided to place all emphasis on an interesting offshoot related to objective three which revealed itself only after I had developed a good historical foundation in the field of spectroscopy.

The distilled essence of this work is Part I of this dissertation and was published in 1984 (J.C.P., 81, 607 (1984)). The study was a discourse in molecular spectroscopy, having nothing to do with polymer science and shedding little light on the polyacetylene problem. It is a paper which has condensed and focused in on a number of spectroscopic fundamentals such as the resonance-Raman selection rules and the consequences of scattering from the crystalline state in a most vivid example of classical Raman scattering.

Due to a diminished interest in the area on behalf of my committee and myself, the completion of Part I signaled the termination of my association with the polyacetylene project and with molecular spectroscopy. A brighter future with a new committee and project was sought, one which would facilitate the completion of my Ph.D. work. At this time I was reacquainted with Dr. Frank Karasz whom I'd had some contact with during the polyacetylene project and was introduced to his collaborator in the physics department Dr. Ken Langley. In discussions, a research project was proposed which would

hopefully produce a piece of work supplementing Part I yielding a split but complete thesis. The research area concerned the solution properties of rigid rod polymers as reflected by their Brownian dynamics, the experimental technique would be static and quasielastic light scattering. In general, this area is and has been very popular, workers quickly exhausting the supply of interesting polymers to be characterized. New projects could only be initiated only after synthesis of sufficiently interesting new polymers. Amongst all possible methods of characterization for the Brownian dynamics of polymers in general and rod like polymers in particular, the dynamic light scattering technique has dintinguished itself in the easy measurement of the translational and rotational diffusion constants. In particular, the rotational diffusion constant is a quantity hard to access and can provide a wealth of supplemental and complementary information to the translational diffusion constant. It, however, can only be measured by this technique when the polymer exhibits optical anisotropy. Frustration grew in searching for a polymer exhibiting the necessary properties and one which would generate sufficient interest warranting the investment of time and energy. At this time, one Dr. Kevin Kidnie (now at 3M) mentioned that he had encountered an optically anisotropic colloid particle in his thesis work in the Chemistry department at UMASS. After some acquaintance and feasibility studies were made on this Teflon (Fluon, ICI) colloid and once the literature had been examined in this area, it became apparent that a valuable discovery had been made. The field of Brownian dynamics of

particles which interact with each other in solution, like the Coulombically interacting polystyrene latex spheres, is and has been very active but by no means have definitive conclusions been drawn. Lagging behind the experimental work were a few untested theoretical treatises on this subject of Coulombic interactions between colloid particles, specifically as they are reflected in the concentration dependence of the translational diffusion constant. Moreover, the rare find of an optically anisotropic colloid particle allows for the first time the study of rotational Brownian dynamics in a large Coulombically interacting system. This information would be a valuable supplement to the simultaneous measurement of the translational diffusive behavior. This wide and complex subject characterizes and concludes Part II of this dissertation.

ABSTRACT

NOVEL APPLICATIONS OF LIGHT SCATTERING

IN CONDENSED MATTER PHYSICS

(September 1986)

Scott A. Kuehl, B.S. Florida State University, Tallahassee, FLA 1979

Ph.D. University of Massachusetts, Amherst 1986

Part I Directed by James C. W. Chien
Part II Directed by Frank E. Karasz and Kenneth H. Langley

Part I of this two part split thesis is a comprehensive investigation into the Raman scattering topology of a polyene chain carried out through polarized Raman spectroscopy on a single crystal of diphenyloctatetraene. By using the crystallographic data of the monoclinic modification of diphenyloctatetraene, the relative magnitudes of the components of the Raman scattering tensor for those normal modes subject to resonance enhancement have been obtained. These vibrations correspond to the double bond and some single bond stretch modes and two phenyl ring modes, these being the most intense bands observed in the Raman spectrum enhanced by lasing in the preresonance region. Intensity measurements were carried out in the principal coordinate system of the electrical susceptibility tensor. The intensity data obtained are appropriately interpreted with an oriented gas model. Furthermore, recognizing the high anisotropy of the scattering topography, a novel simplification is used enabling a transformation which results in the relative magnitudes and signs of

the complete molecular Raman scattering tensor in molecular fixed coordinates.

Part II of this thesis describes the measurement of the concentration dependence of the translational and rotational diffusion constants for a colloidal suspension of Coulombically interacting optically anisotropic Teflon (ICI) particles by Quasielastic Light Scattering. The particles exhibit a small degree of size and shape dispersity. The dilute suspensions were stable, dispersed with the aid of a surface active agent, it being responsible for weak interparticle Coulomb forces. A retardation of free diffusion with concentration is observed for both relaxation modes indicating that the interparticle potential has both radial and anisotropic components. The effect of these interactions is also evidenced by the form of some absolute static structure factors measured through the wavevector dependence of the depolarized scattered light. These structure factors indicate positional and positional-orientational correlations amongst the particles. The experimental results for translational self-diffusion have been interpreted successfully through a theoretical calculation by Hess and Klein and the main features of this approach is evaluated. No precedent for the behavior observed in rotational diffusion can be found, however, a feasible mechanism consistant with that governing translational diffusion can be proposed.

TABLE OF CONTENTS

PART II

STATIC AND QUASIELASTIC LIGHT SCATTERING OF TRANSLATIONAL AND ROTATIONAL BROWNIAN DYNAMICS IN A COULOMBICALLY INTERACTING MACROFLUID

LIST OF TABLES

PART I

PART II

LIST OF FIGURES

PART I

PART II

P A R T I

RAMAN SCATTERING TOPOLOGY IN AN ANISOTROPIC CONJUGATED MOLECULE: A NOVEL APPROACH THROUGH SINGLE CRYSTAL RAMAN

C H A P T E R I

A. Abstract

A comprehensive investigation into the Raman scattering topology of a polyene chain is carried out through polarized Raman spectroscopy on a single crystal of diphenyloctatetraene. By using the crystallographic data of the monoclinic modification of diphenyloctatetraene, the relative magnitudes of the components of the Raman scattering tensor for those normal modes subject to resonance enhancement have been obtained. These vibrations correspond to the double bond and some single bond stretch modes and two phenyl ring modes, these being the most intense bands observed in the Raman spectrum enhanced by lasing in the preresonance region.

Intensity measurements were carried out in the principal coordinate system of the electrical susceptibility tensor. The intensity data obtained are appropriately interpreted with an oriented gas model. Furthermore, recognizing the high anisotropy of the scattering topography, a novel simplification is used enabling a transformation which results in the relative magnitudes and signs of the complete molecular Raman scattering tensor in molecular fixed coordinates.

B. Introduction

Analysis of the optical properties of molecules in both condensed and gas phases has been of great theoretical and experimental interest. The study of Rayleigh and Raman scattering as well as the bulk optical properties of a material all reduce to a discussion of the molecular polarizability tensor. In this regard, most of the experimental attention has been given to Rayleigh scattering of small gas phase molecules where tabulation of bond and molecular polarizabilities and anisotopies leads to easy comparison and to a better understanding of molecular shape and electronic structure.[1] Here, the polarized and depolarized Rayleigh intensities provide information on the tensor invariants and in some cases leads to extraction of the absolute values of the mean polarizability and anisotropy.[2] Bond polarizability data acquired on model systems can then be used to construct molecular polarizability tensors for more complex molecules through bond-atom polarizability models. This, and attempts to determine the shape of larger molecules with conformational degrees of freedom through bond-atom polarizability models,[3] suffer from the apparently large intramolecular dipole-induced dipole interaction. The failure of the bond-atom tensor addition model without incorporating internal field affects is evidence for the strong and long range nature of dipole correlation in even a simple σ bond network.[4] In a π bond system, delocalization causes extensive electron correlation, and modeling of molecular

polarizability through isolated atomic properties is even less feasible. The interpretation of Raman intensity profiles suffers from the same difficulties while additionally being dependent on knowledge of the normal coordinates of the vibration.[5] The use of normal coordinate analysis supplemented with extended quantum mechanical calculations[6] has been a very powerful method in elucidating the role the electronic manifold plays in the preresonance or resonance Raman enhancement; and the role played by those same enhanced modes on the vibrational progressions observed in the fluorescence and excitation spectrums of conjugated molecules. This treatment of the polarizability using a quantum mechanical approach does a very good job in reproducing observed trends in conjugated systems,[7] however it is much more complicated than the bond-atom tensor addition approach applied to the σ bond systems.

Often, it is desirable to determine the symmetry of a Raman vibration. To distinguish a non-totally symmetric band from a totally symmetric one, it is sufficient to determine its depolarization ratio in solution or gas phase. This information will not differentiate between those possibly allowed non-totally symmetric vibrations nor provide knowledge of the relative magnitudes of the tensor elements themselves. The single crystal Raman technique has emerged in recent times[8] as a very powerful method leading to unambiguous assignments of the symmetry character of a Raman band. This has been most successful[9] for molecules of particular symmetry where the non-totally

symmetric modes of the molecule are easily identified by observation of its relative intensity along different crystal axes. In this case, only one molecular tensor element is active and the relative intensity between each orientation is proportional to the molecular direction cosines only. For the totally symmetric modes, the relative intensities depend in a more complicated way on all three diagonal tensor elements as well as the orientation direction cosines. This was overcome, however, in a study of single crystal napthalene by Hanson and Gee.[10]

As a result of the new approach developed here, actual measurement of the relative values of the complete derived polarizability tensors for the totally symmetric modes becomes possible in the special case of high anisotropy within the preresonance regime. With the wide variety of information on the vibronic and electronic structure of diphenyloctatetraene that this quantity brings forth, a brief review of the classical polarizability theory of Raman scattering, the selection rules governing resonance enhancement, and the spectroscopic consequences of scattering in the crystalline phase is undertaken.

relative intensity along different crystal axes. In this case, only one molecular tensor element is active and the relative intensity between each orientation is proportional to the molecular direction cosines only. For the totally symmetric modes, the relative intensities depend in a more complicated way on all three diagonal tensor elements as well as the orientation direction cosines. This was overcome, however, in a study of single crystal napthalene by Hanson and Gee.[10]

As a result of the new approach developed here, actual measurement of the relative values of the complete derived polarizability tensors for the totally symmetric modes becomes possible in the special case of high anisotropy within the preresonance regime. With the wide variety of information on the vibronic and electronic structure of diphenyloctatetraene that this quantity brings forth, a brief review of the classical polarizability theory of Raman scattering, the selection rules governing resonance enhancement, and the spectroscopic consequences of scattering in the crystalline phase is undertaken.

C H A P T E R II

EXPERIMENTAL: THE SINGLE CRYSTAL RAMAN TECHNIQUE

A. Preparation

Single crystals of prepurified t-diphenyloctatetraene (DPO, ALDRICH) were grown via slow solvent evaporation from a supersaturated solution of ethyl acetate. The crystals precipitated as large flat platelets were of excellent quality, free of cracks or twinning, and having well-formed faces making them suitable for use in the Raman experiment as well as the x-ray crystallographic study.[11] The monoclinic modification of t-DPO was found to have a C^5_{2h}-P^2_1/c space group with two molecules per unit cell (fig. 2.1a). Examination of the crystals' macroscopic morphology indicated the large flat face to be (001) and the major cleavage plane to be (010). These planes and the location of the optical indicatrix were determined through polarized light microscopy. Following crystallographic convention,[12] the obtuse bisectrix is coincident with the unique axis [010] and is labeled Y. The plane of the optic axes is perpendicular to (010) and lies such that the acute bisectrix, X, approximately bisects the monoclinic angle ($\beta = 90.76^\circ$, $X\Lambda a = 45.76^\circ$). The optic normal, Z, lies perpendicular to both (fig. 2.1b). The choice of a molecular coordinate system is made to conform with the requirements of the absolute molecular symmetry. For molecules of high enough symmetry, three mutually perpendicular

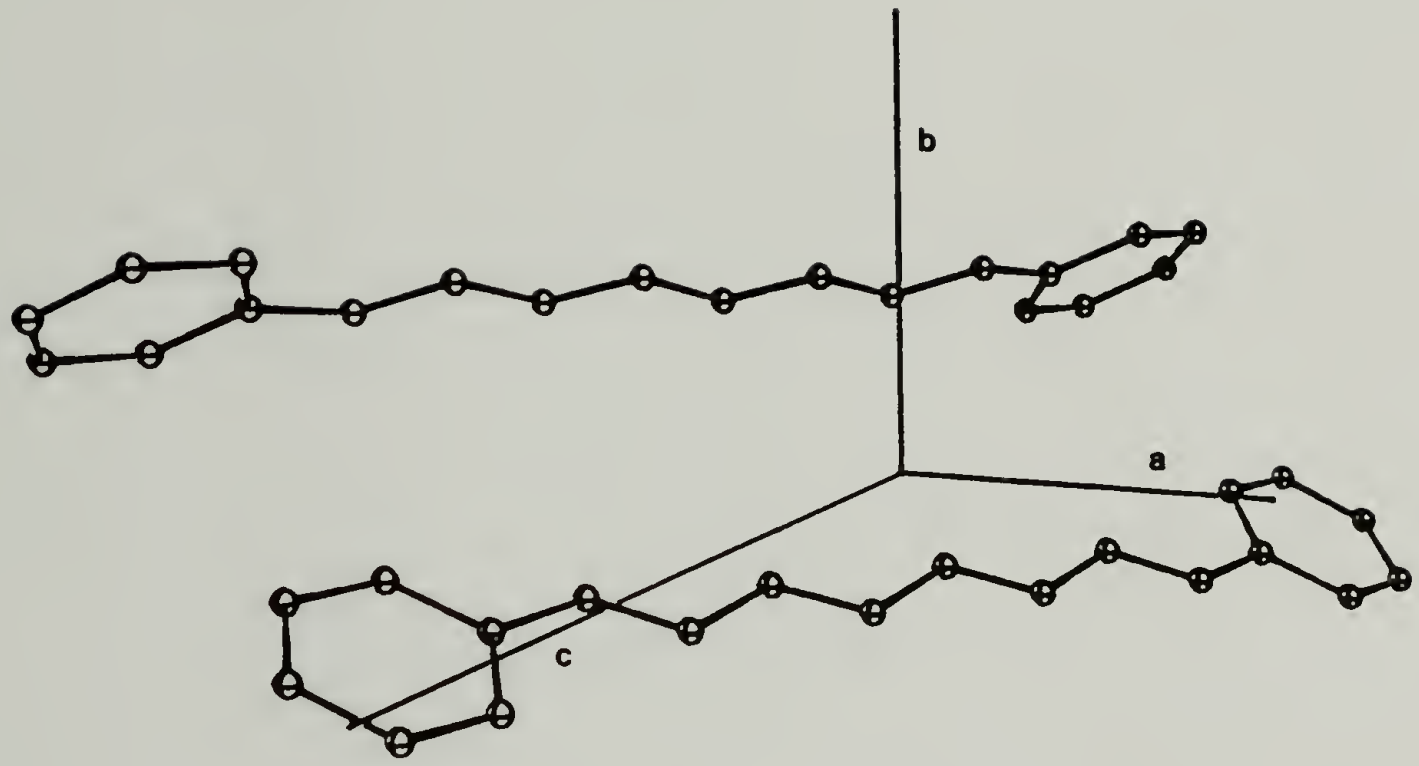

Figure 2.1 (a) Contents of a unit cell.

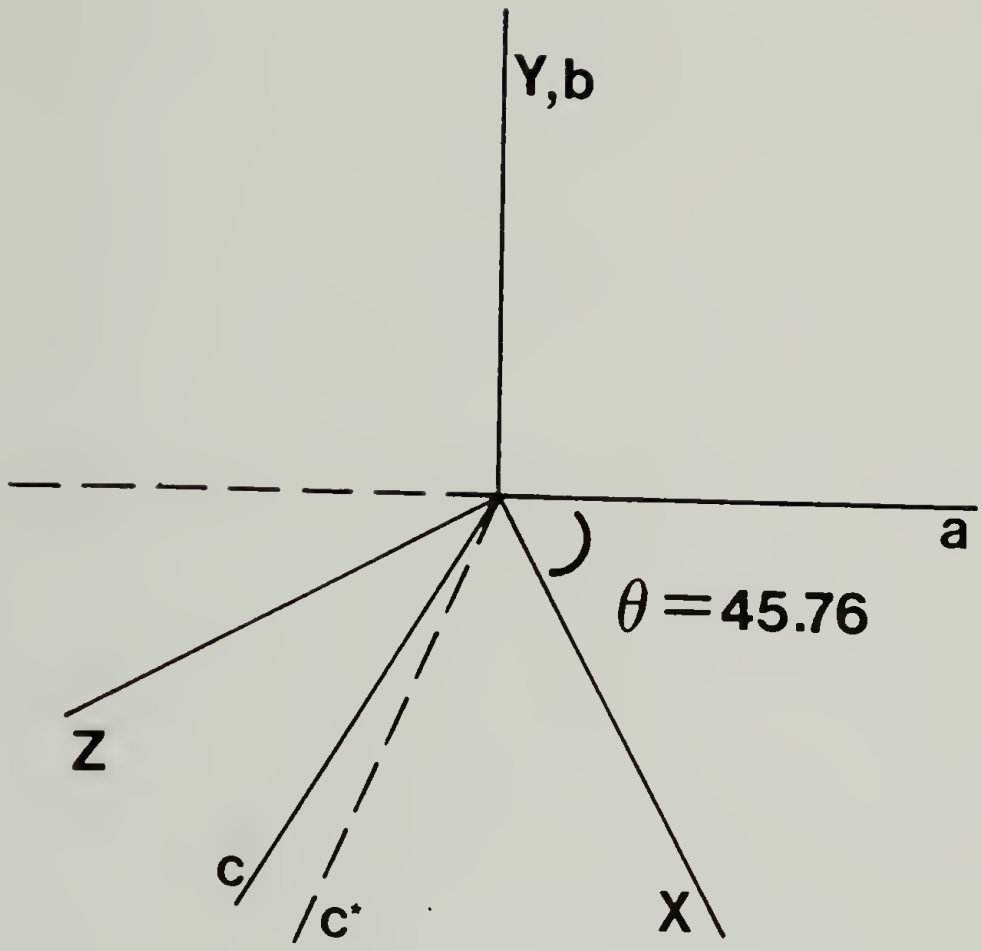

Figure 2.1 (b) Orientation of the indicatrix with respect to the unit cell coordinate axes.

reflection planes, and the symmetry axes perpendicular to them, can serve as a principal coordinate system from which polarizability parameters can be interpreted. For molecules of low symmetry the choice is arbitrary, but a coordinate system can usually be defined to coincide with important molecular directions or upon the local symmetries of fragments. In the monoclinic modification of DPO, the phenyl groups are bent and twisted out of the plane defined by the polyene chain by about 11.3 degrees so that molecules lie on sites of C_i symmetry. In having only an inversion center and no symmetry axes, the assignment of molecular coordinate axes becomes one of convenience. The local symmetry of the polyene chain segment is C_{2h} and its C_2 axis provides one locally unique axis in the direction of the π orbitals along the chain. This y axis was determined from the least squares mean plane calculated from the atomic coordinates of the polyene chain. The long axis of the polyene chain, labeled z, is defined as the intersection of this mean plane with the (010) crystal plane. It lies in the plane of the chain and through the centers of the middle five bonds along the backbone. The x axis becomes the cross product of y and z and lies approximately along the direction of the hydrogens (fig. 2.1c and 2.1d). As symmetry dictates, this is not a principal coordinate system for either the Rayleigh or Raman tensors of DPO. Tensor elements, especially off diagonal elements, must be regarded as a consequence of the particular geometrical perspective as well as the nature of the excitation topology.

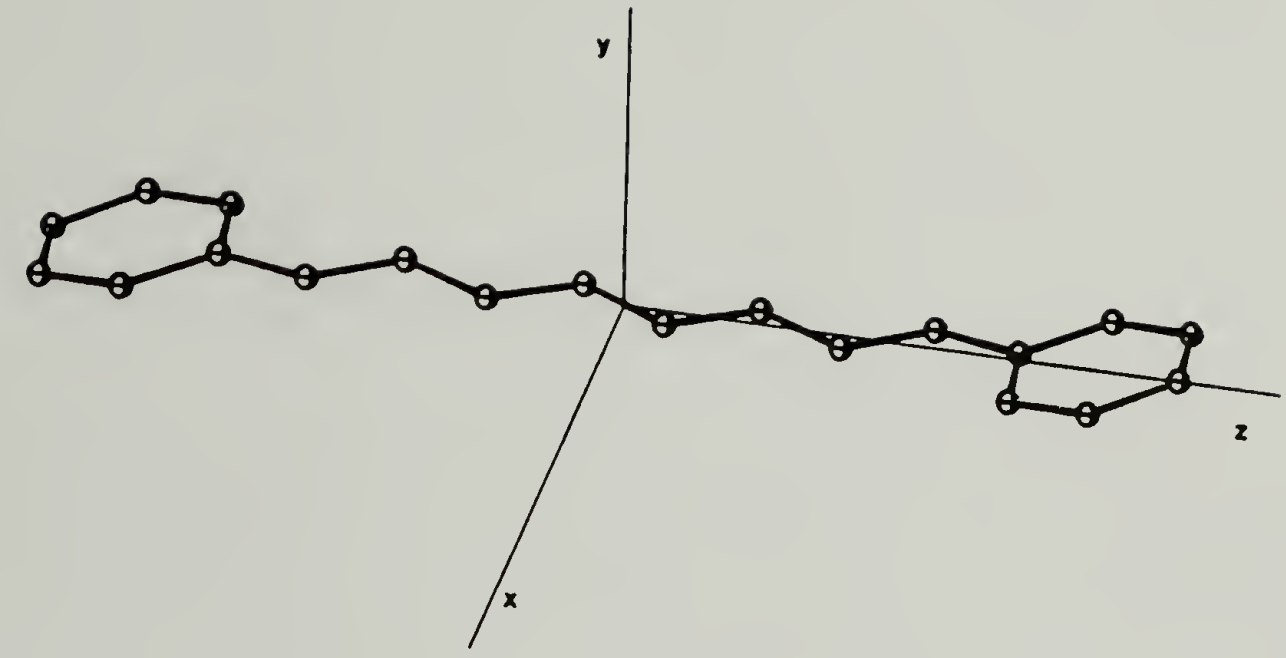

Figure 2.1 (c) Molecular coordinate axes.

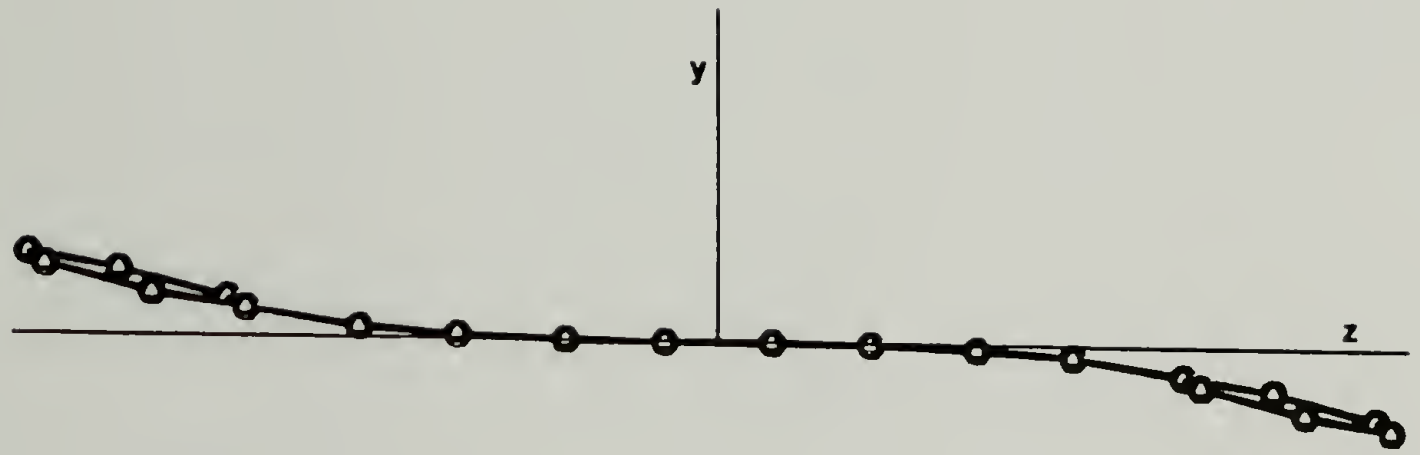

Figure 2.1 (d) Molecular coordinate axes. View in the yz plane.

The 514.5 nm line of a Spectra Physics Argon ion laser operating at constant light was used as the excitation source. The optical arrangement is shown in figure 2.2 in which geometry 1 of Table 2.1 is used as an example. The completely vertically polarized beam of 120 mW was passed through a 90% and a 70% neutral density filter to reduce the power down to about 75mW. This power was well below the threshold required to vaporize and degrade the crystal through absorption processes. Spectra were recorded with a Jobin-Yvon HG.2S Raman spectrometer. All spectra were recorded at a spectral slit width of .8 cm^{-1}. An f/17 aperture was employed to reduce the contribution of light with off axis polarization being collected. Extreme care was taken in the positioning of the crystal such that indicatrix axes and lab axes were coincident. This was possible within the accuracy of a three circle goniometer, in which angles were measured with respect to the well-defined crystal planes. The focus of the incident beam, with a diameter of 50 μm was placed just inside the boundary of the crystal's body so that edge effects were reduced and to reduce the incident and scattered light path lengths. The image was maximized in each geometry to insure proper optical and spectrometric efficiency. The spectra were recorded using computerized photon counting techniques and stored on floppy disk. Peak heights were used as the measure of relative intensity and were found to be consistent with measurements of peak area as is the case when dealing in very high intensities, high signal to noise ratio, and when band shape is conserved within

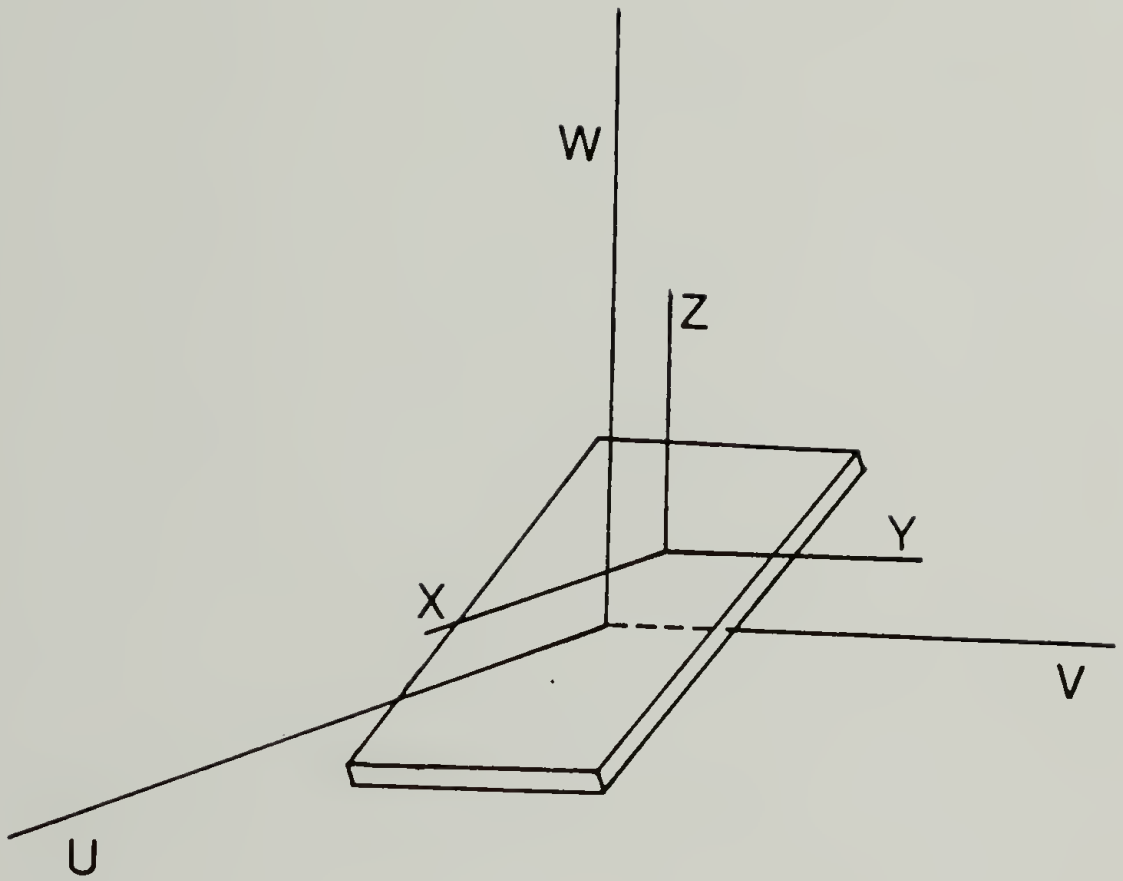

Figure 2.2 The optical arrangement of the indicatrix(where geometry 1 is used as an example) and lab coordinate systems.

Table 2.1. The possible configurations of the crystal fixed indicatrix axes X, Y, and Z, coincident with the lab axes U, V, and W; and the intensity tensor element involved in each polarization.

Geometries	Lab Axes U	V	W	Polarization	Elements VV	HV
1	X	Y	Z		I_{ZZ}	I_{XZ}
2	Y	X	Z		I_{ZZ}	I_{YZ}
3	Z	X	Y		I_{YY}	I_{ZY}
4	Z	Y	X		I_{XX}	I_{ZX}
5	Y	Z	X		I_{XX}	I_{YX}
6	X	Z	Y		I_{YY}	I_{XY}

different configurations.

B. Procedure

Classically, in the dipolar approximation to the scattering field, the intensity and polarization of a Raman band is related to the square of the induced dipole moment. In a molecule of low symmetry, this moment will be related in a complicated way to the derived polarizability tensor, α'. In scattering from an isotropic array of molecules, the tensor property must be space averaged and can be expressed as the dyadic product, $\langle\alpha':\alpha'\rangle$ or in terms of tensor invariants. For a molecule or crystal oriented identically in space, the associated tensor becomes space fixed as well. Tensor elements, be they from the molecule or unit cell, become associated with a particular coordinate axis, incident, and exit polarizations. The intensity, I_{ij}, observed by irradiating a space fixed coordinate system with light polarized in the i direction and analyzing at 90° the j polarized component of the scattered light can be related to the space fixed derived polarizability tensor α' through a tensor A_{ij} where $A_{ij} = \alpha'^{2}\delta_i\delta_j$, such that $I_{ij} = I_o A_{ij}$. The constant I_o is related to the square of the incident electric field, a quantity which in an anisotropic, transparent condensed phase is modified by the electrical susceptibility tensor. The principal coordinate system of the susceptibility tensor is called the optical indicatrix and three principal values are required to describe this biaxial crystal system.

Intensity measurements were carried out in the geometry of the optical indicatrix in order to eliminate the possibility of introducing birefringence phenomenon.[8] This coordinate system also allows for internal standardization of the electric displacement suffered by the incident electric field while in the body of the crystal, a quantity different for light polarized along its three unique directions. This is achieved by mounting a crystal, cut to a dimension of 3x1.5x1/4 mm, on the three circle goniometer. Vertically polarized incident laser light was used in the excitation of the Raman spectrum. The crystal, attached to the goniometer, was positioned in a series of geometries so as to probe all six possible orientations of the indicatrix in the lab coordinate system. These configurations and the intensity tensor elements involved with them are listed in Table 2.1. Analyzing the scattered light vertically and horizontally in each geometry provides the two unique intensity profiles arising from the two different unit cell tensor components involved.

The direction of the z molecular axis of both molecules in the unit cell are parallel as dictated by the unit cell symmetry. As shown in figure 2.1a, the Z indicatrix axis lies along this unique crystallographic direction. The location of this unique direction as distinguished from X was determined by doing VV scattering in geometries 1 and 4 where I_{XX} and I_{ZZ} are observed respectively. When polarized light is incident and scattered parallel to z and therefore to Z, very high intensities are observed. A vector mark in the

direction of Z was then placed on the goniometer insuring the correct geometrical convention throughout the experiment.

Intensity data was taken for the three frequency regions in the first five geometries. Employing the redundancies of the elements of I which occur in different geometries (see Table 2.1), and assuming the tensor is symmetric, a normalization is carried out reducing the data to tensor form such that the magnitude of all six elements are normalized with respect to the largest, that being I_{ZZ}. This procedure insures that the intensity values are normalized with respect to the different macroscopic scattering volumes encountered in each geometry, and insures simultaneous correction for the differences in electric displacement or local field occurring along each indicatrix axis. This normalization scheme permits the construction of an intensity tensor as a quantity rendered independent of the exact shape or form of the hypothetical Lorentz cavity used to model the internal field around any lattice site. The internal field correction to the absolute scattering intensity has been successfully applied to both Rayleigh[13] and Raman[14] scattering of isotropic solutions. The assumed symmetry of the unit cell tensor A_{ij} follows from the assumed symmetry of the molecular scattering tensor α', a point to be discussed in detail and justified in a later section.

C H A P T E R III

SPECTRA ANALYSIS

A. Excited state topology

The nature of polyene excitation has been studied in depth and the considerable amount of experimental and theoretical[15] work have established a clear picture of the phenomenon. An exhaustive analysis of the absorption and emission spectra of DPO has been carried out by Hudson and Kohler.[16] In this and in more recent studies,[17] the existence of a dipole forbidden excited state has been proven, it being lower in energy than the classical strongly allowed excited state characterized by the HOMO-LUMO transition in polyenes. This lower excited state, S_1, is believed to involve doubly excited configurations and borrow intensity from the strongly allowed excited state S_2 by a vibronic coupling mechanism or through a symmetry breaking molecular distortion. Its low oscillator strength, however, would imply a negligible contribution to the Raman scattering. The excited state which will characterize the intermediate state acting in the preresonance Raman enhancement is the strongly dipole allowed $\pi \rightarrow \pi^*$ (λ_{max}=400nm) non-degenerate singlet excited state (S_2) of symmetry $^{o}Ag \rightarrow {}^{1}Au$ in the C_i point group. The transition is polarized[18] predominately along the long axis (z) of the molecule and because it includes the phenyl groups, it is not entirely in the plane of the

polyene chain. In frozen solution and especially the crystalline state, the radiative relaxation has been shown to occur from a Franck-Condon state.[19] Here, the scattering event occurs much more quickly than the molecular relaxation to the newly created S_2 potential surface minima, and faster than the time involved for intermolecular relaxation through exciton mechanisms. Radiative relaxation with production of the Raman effect occurs through this singlet manifold while secondary states, multiply excited states, Rydberg states, or intramolecular exciton states do not contribute.

For this molecule and other related polyene systems, the symmetry of the ground state is retained in the excited state while the structure itself deviates only by a totally symmetric distortion. Thus only totally symmetric normal modes are active in the vibrational progressions of the emission and absorption spectra. The vibrational progressions observed in the spectra by Kohler arise from the totally symmetric double and single bond stretch modes centered around 1600 and 1200 cm^{-1}. The other totally symmetric modes which are observed in the Raman spectrum are obscured within the linewidths of their experiment. Interpretation of polarizability parameters on the basis of the ground state electronic and geometrical structure is appropriate when those factors which can mix in excited state properties, i.e., Dushinski effect,[20] molecular distortions with a possible change in symmetry, and contribution by the excited state polarizability are negligible.

B. Raman spectra

A typical unpolarized Raman spectrum of powdered crystalline DPO is shown in figure 3.1. All bands in the Raman spectrum taken in any geometry or polarization have identical frequencies. In the low frequency region the lattice modes are shown. The band at $46cm^{-1}$ is the z axis libration. The moments of inertia about the x and y axes are nearly the same in magnitude and their librational frequencies are redundant and occur at $21cm^{-1}$. The relative intensity of these two bands display strong polarization behavior and pronounced temperature dependence.

A formal normal coordinate analysis treatment of DPO has not been carried out, however unambiguous assignments of the Raman bands of DPO are available. The assignments of Raman bands arising from the crystalline phase of DPO presents no difficulties as properties governing the Raman scattering for the internal modes, in the zeroth approximation, are identical to those in the liquid or gas phase. This, the oriented gas approximation, is applicable to DPO and will be described in a later section. The assignment of the Raman bands of DPO are available in previous studies done on this and similar compounds. The spectrum is characterized by three major regions on which intensity measurements were made. All bands within each region displayed the same relative intensity in each geometry and polarization.

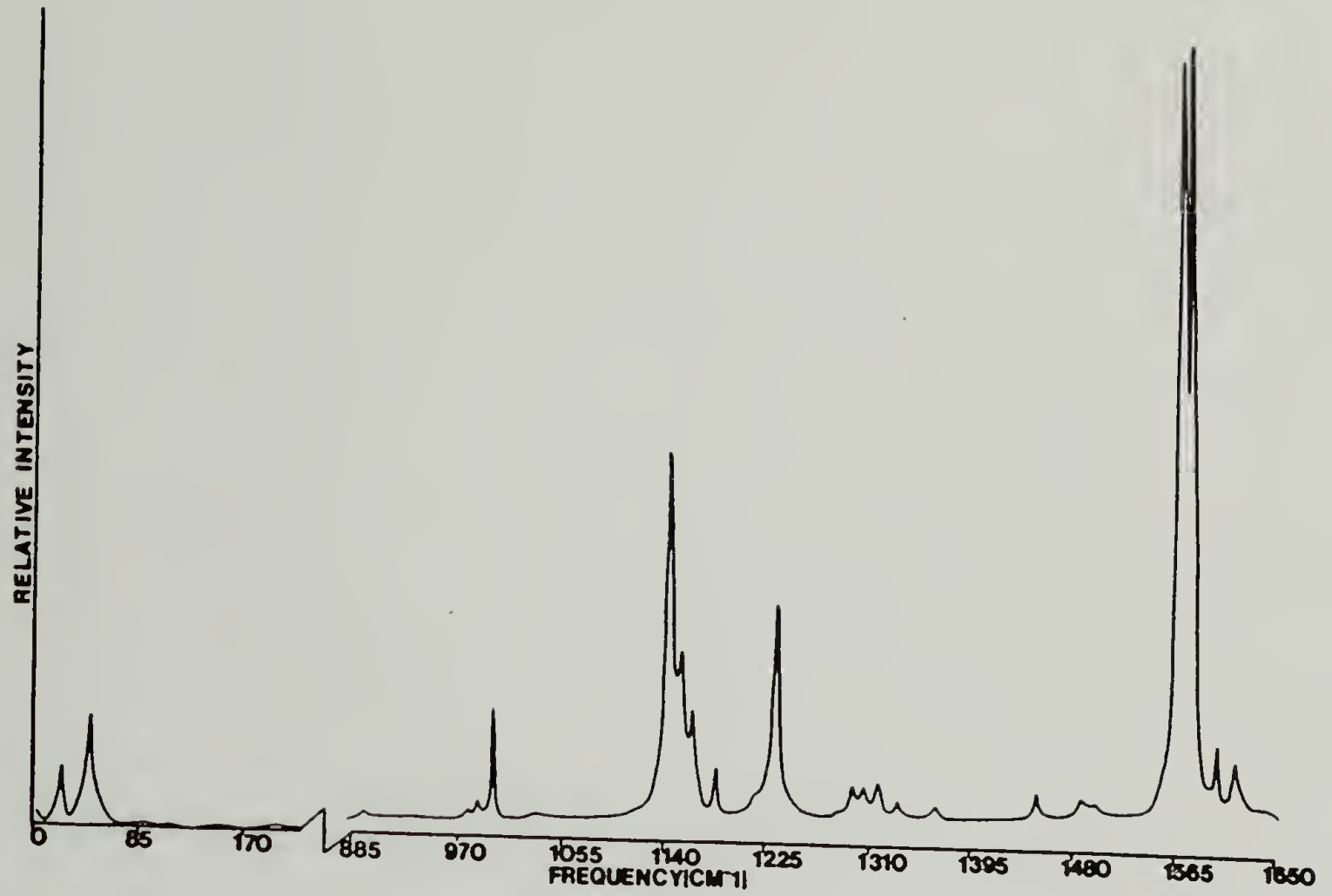

Figure 3.1 An unpolarized Raman spectrum of powdered crystalline diphenyloctatetraene.

1. 996.8cm-1 Band

This band has been identified as the totally symmetric breathing vibration[16, 21] associated with the terminal phenyl groups. The normal coordinates are assumed to have the same character as the ν_1(Ag) mode[22] in benzene. The normal coordinate vectors for this vibration are shown in figure 3.2a.

2. 1100-1250cm-1 Region

The single bond stretch region has five major bands. The band at 1142.5 is known to be the totally symmetric single bond stretch vibration[16, 17] of the polyene chain. The bands at 1151, 1160, and 1180 are believed to be associated with the chain but of mixed character incorporating single bond stretch, c-c-c angle bending, and H-c-c angle bending contributions.[23] The 1230cm^{-1} band is the totally symmetric chain-phenyl stretch.[21] Its intensity decreases relative to the single bond stretch band in the longer members of the diphenylpolyene series. These two vibrations are shown in Figures 3.2b and c.

3. 1550-1630cm^{-1} Region

The double bond stretch region shows two bands. The band at 1567.6cm^{-1} is the totally symmetric double bond stretch vibration.[16, 17] The normal coordinates for this and the totally symmetric single bond stretch are believed to be similar to the normal coordinates of

	BAND (cm^{-1})
a	998
b	1143
c	1250
d	1567
e	1574

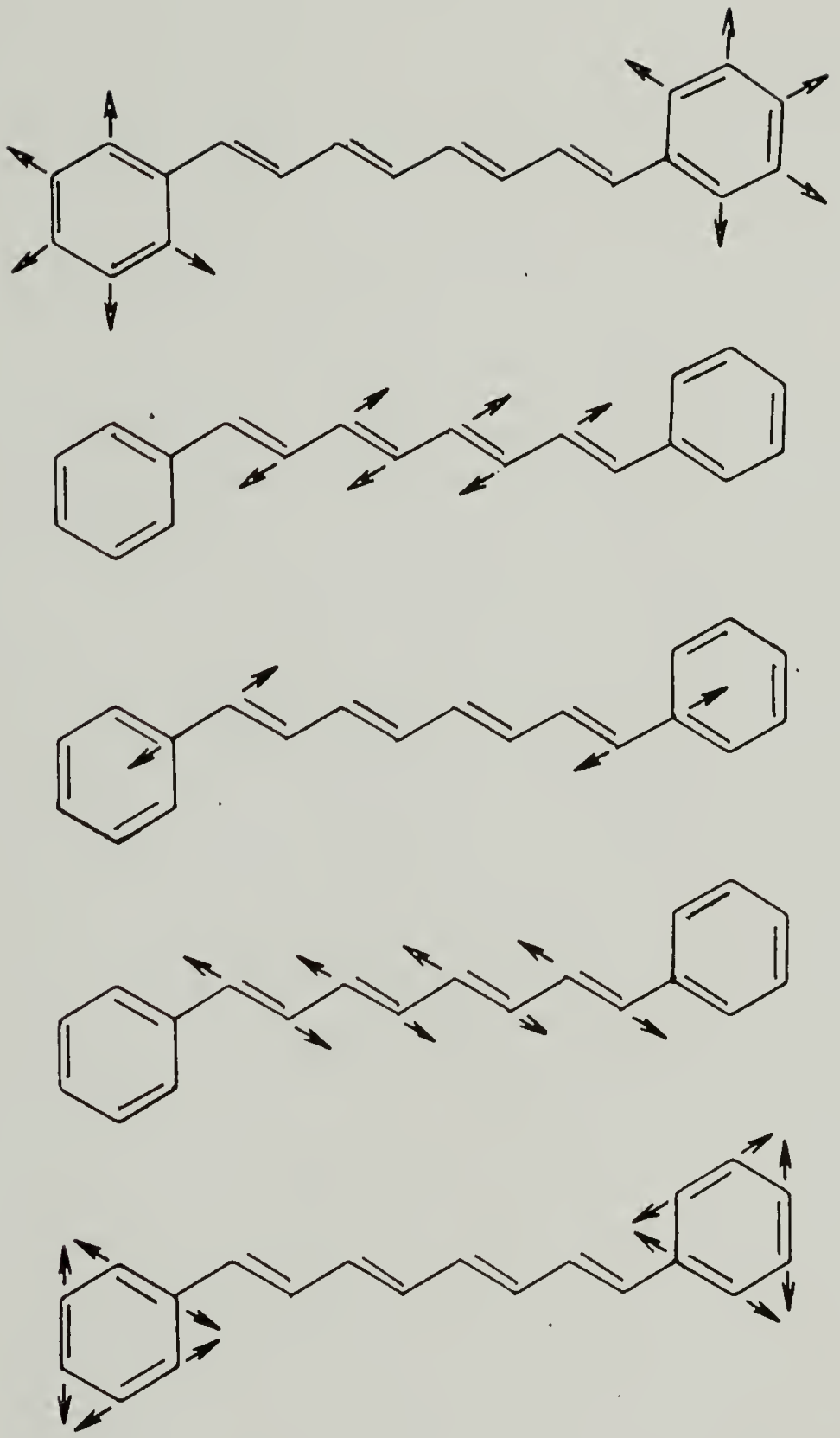

Figure 3.2 Normal coordinates of the resonance enhanced vibrations observed in the Raman spectrum of DPO.

β-carotene and other linear polyene systems.[24] The band at 1574.5cm^{-1} is like the degenerate $\nu_8(e_{2g})$ (benzene) carbon stretching mode[22] of the terminal phenyl groups. These two vibrations are shown in Figures 3.2d and e.

CHAPTER IV

RAMAN SCATTERING IN A CONDENSED PHASE

A. The oriented gas approach

A discussion of the hierarchy of effects at work in the condensed phase which might tend to influence the polarizability is in order if a complete description of the differential polarizability is desired. In the gas phase, a molecule's electrons reside in a square well potential defined by its nuclear framework. In the crystalline phase this potential is expected to become more rounded in shape allowing the electron cloud to become more expansive resulting in an increase of the absolute values of the principal polarizabilities. This event is not isotropic as the anisotropic crystal field of this biaxial crystal system would dictate resulting in an observed increase in polarizability anisotropies. Dunmur et al.[25] found a rotation of the principal axes of polarizability away from the molecular symmetry axes by a small amount in some aromatic polyene systems of high symmetry. The polarizability in aromatic systems, however, is dominated by two low-lying nearly degenerate electronic transitions of orthogonal polarization, both of which are skewed in direction with respect to each nearest neighbor in the crystalline state. In crystalline DPO, all the z axes and therefore the z polarized transition moments are parallel, thus cancelling out any angularly dependent dipole-dipole

interactions. This in turn would decrease the amount of distortion below that observed in the aromatic systems. A measure of intermolecular forces large enough to alter the strong valence bond forces is observation of a solution to crystal frequency shift in a Raman band. Frequency shifts in flexible polyenes usually are derived from small structural changes involving torsions about weaker bonds which tends to weaken the molecular potential field. The exact character of a vibrational mode can be a factor in the extent to which it could be perturbed by the crystal field. Vibrations most susceptible would be those including the hydrogens whose intermolecular repulsive interactions are mostly responsible for the crystal packing[26] although these vibrations may not be Raman active. Vibrations least susceptible are vibrational motions localized within the primary or skeletal structure of the molecule. In DPO these are the Raman active and resonance enhanced carbon-carbon motions of interest in this study. These modes show a frequency shift of about 1% and display an even smaller low temperature dependence. Thus these resonance enhanced modes ideally meet the criterion of what is referred to as the "oriented gas model." This model has been used previously with success in the determination of vibrational assignments of other non-polar molecular crystals such as napthalene and anthracene.[9]

In a conjugated molecule like DPO, an induced dipole and therefore the polarizability is not localized. The structure of DPO

consists of a σ and π bond network where the polarizability will be a composite of both systems.[6] In a conjugated system where valence bond electrons, especially π electrons are highly delocalized, excitation involves correlation of all electrons in the creation of the induced dipole. In such a system, a localized bond-atom polarizability model is extremely inappropriate in the description of molecular polarizability. In the dipole approximation, it is appropriate to assign a polarizability ellipsoid encompassing the entire electron cloud which will act as the optical and geometrical surface used to describe the electrical response. In Rayleigh scattering, one measures optical size and shape with tensor elements defining the polarizability. In Raman scattering, one measures the polarizability gradients. The transition amplitudes defining the polarizability do not have regional character as the ellipsoid itself encloses the entire molecule. A vibration occurring within this envelope would not be expected to display the character of the local bond-atom polarizability environment where the vibration occurs. Vibrational modes of similar character would then display similar polarizability derivative behavior. This interpretation will be expounded upon the following sections.

B. Selection rules

The prescription in the treatment of Raman scattering from a crystalline substance begins with the construction of the unit cell transition amplitudes out of a linear combination of molecular

transition amplitudes. This is equivalent to approaching the event as a pairwise interaction which can be described from the standpoint of a symmetry coordinate. For a molecule belonging to the C_i symmetry group, all elements of α' are allowed and only totally symmetric vibrations are Raman active. In the unit cell of group C_{2h}, normal modes from each molecule pair up to be either symmetric or asymmetric with respect to the mirror plane (010). This relationship can be visualized using the correlation diagram in Table 4.1 where the number of modes expected in each irreducible representation is also shown. As predicted from the oriented gas model and documented by experiment, the A_g and B_g crystal modes occur at degenerate frequencies. What is observed in any orientation is always a superposition of these two symmetry species. This superposition description is a consequence of the oriented gas approach to single crystal Raman.

Relating the derived polarizability tensor of the free molecule α', to the a b c* crystal axes proceeds through direct tensor transformation. The orientation matrix relating the molecular fixed (x, y, z) coordinate system of molecule 1 to the crystal fixed (a, b, c*) system given by[27]:

$$\phi_1 = \begin{bmatrix} 0.58438 & 0.55063 & 0.59605 \\ -0.38549 & 0.83474 & -0.39319 \\ -0.71406 & 0.0 & 0.70008 \end{bmatrix}$$

The orientation matrix of molecule 2 is related to the first by the (010) reflection operation or $\phi_2 = \sigma_b \phi_1$. In transforming both

Table 4.1. The correlation diagram between the molecular point group and the factor group of the unit cell.

Correlation Diagram			
Molecule C_i		Site C_i	Factor (uc) C_{2h}
Raman	54 Ag	54 Ag	Raman: 54 + 3r Ag; 54 + 3r Bg
IR	54 Au	54 Au	IR: 54 + 2t Au; 54 + t Bu

molecule 1 and 2 into the working a, b, c* system we have:

$$\alpha'_{1(uc)} = \phi_1 \alpha' \phi_1^t$$

$$\alpha'_{2(uc)} = \phi_2 \alpha' \phi_2^t \qquad 1)$$

Construction of the total differential increment of the unit cell polarizability gives:

$$\alpha_{(uc)} = \alpha'_{1(uc)} Q_1 + \alpha'_{2(uc)} Q_2 \qquad 2)$$

Decomposition of this equation is achieved by reverting to the two orthogonal symmetry coordinate transformations appropriate for the C_{2h} unit cell:

$$Q_1 = (S_{Ag} + S_{Bg})/2^{1/2}$$

$$Q_2 = (S_{Ag} - S_{Bg})/2^{1/2} \qquad 3)$$

Where S_{Ag} and S_{Bg} are the symmetry coordinates of the molecular pair. Replacing equations 1 and 3 into 2 and taking the derivative with respect to these symmeterized unit cell coordinates:

$$\alpha'_{Ag} = \left[\frac{\partial \alpha_{(uc)}}{\partial S_{Ag}}\right] = (\phi_1 \alpha' \phi_1^t + \phi_2 \alpha' \phi_2^t)/2^{1/2}$$

$$\alpha'_{Bg} = \left[\frac{\partial \alpha_{(uc)}}{\partial S_{Bg}}\right] = (\phi_1 \alpha' \phi_1^t - \phi_2 \alpha' \phi_2^t)/2^{1/2} \qquad 4)$$

Mathematically, the superposition of these symmetry species represents simple addition of these two orthogonal tensor equations to give:

$$\alpha'_{ij(uc)} = \alpha'_{Ag(uc)} + \alpha'_{Bg(uc)} = 2^{1/2} (\phi_1 \alpha' \phi_1^t)_{ij} \qquad 5)$$

The intensity observed in any of the particular unit cell orientations

is proportional to the square of an element of $\alpha'_{ij(uc)}$, i.e.,

$$A_{ij} = \alpha'_{ij(uc)}. \qquad 6)$$

As described earlier, a direct relationship between the measured intensity tensor I_{ij} and the molecular tensor α' can be defined:

$$I_{ij} = I_o A_{ij} = I_o(\phi_1 \alpha' \phi_1^t)^2_{ij} \qquad 7)$$

where I_o becomes a constant after proper normalization.

This equation is intractable in any procedure involving an inverse transformation. Each element of $(\phi_1 \alpha' \phi_1^t)_{ij}$ is a function of all six unique components of α' each combined with a pair of elements belonging to ϕ. An intensity is proportional to the square of an ij th element which would have thirty-six different combinations of these six unknowns. A set of six equations and thirty-six unknowns is an intractable system. The square root of each element in I_{ij} could be taken and the transformation preformed, however, the sign ambiguity requires resolution. The signs, of course, are determined by knowledge of the elements of ϕ as well as the signs and magnitudes of elements of α' which are not known in general except in some very special cases.

Elements of both the Rayleigh and Raman tensors having the same polarization as the transition dipoles of the contributing excited states become exaggerated in magnitude under conditions approaching resonance. In DPO, the presence of one strong low lying, non-degenerate and z polarized excited state leads to the dispersion

of only the α'_{zz} element so that the values of the elements of $(\phi_1 \alpha' \phi_1^t)_{ij}$ are dominated by the α'_{zz} element and those direction cosines involved with it. The prescription used in the exact solution of this equation involves the assignment of the correct sign to each square-rooted element of I_{ij}. This assignment is simply based on the sign of α'_{zz} and the signs of the direction of the cosines involved with it. The sign of α'_{zz} is positive as determined by previous studies where the absolute magnitude and signs of the totally symmetric carbon-carbon bond stretch modes were determined for benzene, ethane, ethylene and acetylene.[5] To transfer this information to the totally symmetric carbon-carbon stretch modes of DPO seems reasonable. Empirically, in a diatomic or linear molecule, the polarizability of the molecule should be greater in the extended state and smaller in the contracted state thus giving a positive value for the axial tensor element. In DPO, all the enhanced modes are characteristic of a molecular extension and contraction along the z axis. Thus for the normal modes investigated here in this polyatomic system, the sign of α'_{zz} is expected to be positive and as resonance is approached, large. The inverse transformation can be preformed in this special case of high optical anisotropy.

C H A P T E R V

RESULTS

The polarized spectra of crystalline DPO was taken in each of the first five geometries listed in Table 2.1. This data, expressed as the ratio of the HV and VV polarized intensity components observed in each geometry, is displayed in Table 5.1. Setting the value of I_{ZZ} for each frequency region equal to 1., the values of the other elements relative to I_{ZZ} are constructed by employing the redundancies of elements belonging to I_{ij} occurring in different geometries. These normalized unit cell tensors are listed in Table 5.2.

The unitary transformation taking $I_{ij}(XYZ)$ into $I_{ij}(abc^*)$ is given by:

$$\begin{bmatrix} \cos\theta & 0.0 & \sin\theta \\ 0.0 & 1.0 & 0.0 \\ -\sin\theta & 0.0 & \cos\theta \end{bmatrix} \qquad \theta = X\Lambda a = 45.76^{\circ}$$

After applying the coordinate transformation, the inverse transformation can be preformed:

$$(\phi_1^{-1})(\pm I^{1/2})(\phi_1^{-1})^t = \alpha' \qquad 8)$$

In this geometry, the sign of the product of α'_{zz} with the direction cosines makes $I^{1/2}_{ab}$, $I^{1/2}_{ba}$, $I^{1/2}_{c^*b}$, and $I^{1/2}_{bc^*}$ have negative signs

Table 5.1. Intensity data taken on the three frequency regions measured in the first five geometries of Table 2.1 and reduced to ratio form.

Geometry	Elements	Bands (cm^{-1})		
		998	1100/1250	1574/1567
1	I_{XZ}/I_{ZZ}	0.058	0.046	0.048
2	I_{YZ}/I_{ZZ}	0.138	0.147	0.157
3	I_{YY}/I_{ZY}	0.297	0.244	0.254
4	I_{XX}/I_{ZX}	0.171	0.156	0.151
5	I_{YX}/I_{XX}	0.361	0.467	0.458

Table 5.2. Normalized unit cell tensors constructed from the intensity ratios listed in Table 5.1. $I_{ij}=I_{ji}$*

Band (cm^{-1})	I_{XX}	I_{XY}	I_{XZ}	I_{YY}	I_{YZ}	I_{ZZ}
998	0.0	0.0	0.058	0.041	0.138	1.0
1100/1250	0.0	0.0	0.046	0.035	0.147	1.0
1574/1567	0.0	0.0	0.048	0.040	0.157	1.0

*Tensor elements less than 1% of I_{ZZ} in Table 5.2 and α'_{zz} in Table 5.3 were set equal to 0.0.

while the others have a positive sign. Preforming this calculation and normalizing gives the derived polarizability tensors for these normal modes. These are listed in Table 5.3.

Table 5.3. Normalized derived molecular polarizability tensors for the normal modes in the three frequency regions. $\alpha'_{ij} = \alpha'_{ji}$

Band (cm^{-1})	α'_{xx}	α'_{xy}	α'_{xz}	α'_{yy}	α'_{yz}	α'_{zz}
998	0.0	0.0	0.063	0.053	0.120	1.0
1100/1250	0.0	0.0	0.059	0.038	0.115	1.0
1574/1567	0.0	0.0	0.063	0.037	0.110	1.0

CHAPTER VI

DATA ANALYSIS AND CONCLUSION

A variety of information is contained in the derived polarizability tensors for these normal modes. The observations which must be addressed for a complete interpretation are: 1) why are these modes enhanced out of the fifty-four total Raman active modes; 2) the largest tensor element is indeed α'_{zz}; 3) the forms these tensors take for normal modes of different mechanical location are very similar; 4) the presence of off diagonal elements; 5) all the tensor elements are positive. The interpretation of these facts starts through a brief and simple phenomenological understanding of the dispersion equation and the relationships among the quantities therein.

The scattering tensor, as derived by Kramers and Heisenberg[28] and later by Dirac[29] using perturbation theory is given by the dispersion relation:

$$\alpha_{ij})_{mn} = 1/h \sum_{r} \left[\frac{(M_i)_{rn}(M_j)_{mr}}{\nu_{rm} - \nu_o} + \frac{(M_i)_{mr}(M_j)_{rn}}{\nu_{rn} + \nu_o} \right] \qquad 9)$$

This equation, originally derived for atomic light scattering is equally applicable to molecular light scattering. The terminology is given a different basis such that α_{ij} is an element of the polarizability tensor along the i and j th molecular coordinate axes;

m and n are the initial and final vibronic states both of which lie in the ground state; ν_0 is the frequency of the incident light; represents the possible intermediate states involved while M_i and M_j are the molecular transition moment amplitudes along the i and j th directions. The molecular transition moment always occurs as a product of two directionally dependent transition amplitudes arising as a consequence of modeling the scattering process as a double event in the perturbation treatment. Scattering becomes a concerted process, first of absorption of a quanta of radiation raising the state from m to r, where r can be a real or virtual state, then a spontaneous emission process where the atom or molecule radiatively decays from r to n. These two events are not necessarily uncoupled depending on the absolute molecular symmetry.[30] Due to the low symmetry and the absence of principal symmetry axes in DPO, both i and j (belonging to x, y and z) belong separately to the same totally symmetric representation. The product of the transition moment amplitudes in this case is not expected to vanish identically, so that off diagonal elements are allowed and may be important depending upon the size of the electronic coupling along any pair of directions.

In the preresonance region, some very meaningful simplifications can be made as was first pointed out by Shorygin.[31] In the preresonance region of DPO the one low lying dipole allowed transition is the only effective excited state contributing to the polarizability, therefore the sum over r may be dropped and replaced

by this one effective state labeled e. The frequency of this transition from the ground state vibrational level m to this state e, ν_{me}, and from e back to n, ν_{en}, is very large compared to the frequency of the normal mode ν_{nm}. The transition moment amplitudes M_{me} and M_{en} can also be assumed approximately equal for any ij pair. The indices m and n can then be replaced by an effective ground vibrational state k where k can be defined as the average of n and m. Both of these approximations act such that the same polarizability ellipsoid becomes the parent body governing the Rayleigh scattering of the molecule, as well as scattering of all resonance enhanced Raman active modes occurring within it. Therefore normal modes of similar character, such as these resonance enhanced modes with normal coordinates acting as to deform the length of the z axis, would be expected to display very similar polarizability gradients. The polarizability ellipsoid essentially "breathes" at the frequency of the normal vibration[22] by an oscillating distortion of the z axis length while preserving the orientation of the coordinate axes.

Applying these simplifications gives:

$$\alpha_{ij})_k = 2/h \left[\frac{(M_i)(M_j)_{ek}\nu_{ek}}{\nu_{ek}^2 - \nu_o^2} \right] \qquad 10)$$

The tensor remains symmetric upon exchange of the i and j components. In the preresonance region, tensor symmetry is expected and the original assumption of tensor symmetry is justified. This is

in contradiction to the findings of Margulies.[32] Taking the derivative of $\alpha_{ij})_k$ with respect to a normal mode q gives the strain dependence of the polarizability. This procedure gives a result which means essentially the same thing as the second term in the Taylor expansion of the ground state polarizability introduced by Placzek.[33] Thus, the ground state approach, which neglects the possible intermediate states can be related to them through differentiation of the dispersion equation.

$$\frac{\partial \alpha_{ij})_k}{\partial q} = 2/h \left[\frac{\nu_{ek}}{(\nu_{ek}^2 - \nu_o^2)} \cdot \frac{\partial (M_i)(M_j)_{ek}}{\partial q} + (M_i)(M_j)_{ek} \frac{(\nu_{ek}^2 + \nu_o^2)}{(\nu_{ek}^2 - \nu_o^2)} \cdot \frac{\partial \nu_{ek}}{\partial q} \right] \quad (11)$$

It has been shown theoretically by Shorygin[31] and experimentally[34] for a series of diphenylpolyenes including DPO that the preresonance Raman intensities are derived from the first term in this expression. In this product, the frequency factor is mainly responsible for the enhancement of the Raman intensity over the usual non-resonance ν^4 dependence. The $\partial(M_i M_j)/\partial q$ term contains the electronic transition moments which govern the polarization of the radiation and also the Franck-Condon integrals which are responsible for the selection of a Raman active vibration as one capable of resonance enhancement.

In compliance with selection rules based on the C_i point group, only totally symmetric modes are allowed in the Raman spectrum. Of

these, only those totally symmetric modes with normal coordinates having a large projection along the multi-centered Franck-Condon vectors will have exaggerated Franck-Condon integrals and significant preresonance Raman intensity. These particular normal modes studied here meet this criterion because all couple with the system and are the only significant bands observed in the Raman spectrum. Aside from the frequency factor, assumed to be approximately the same for all these vibrations, the relative intensity between these modes is a function of the square of the Franck-Condon integrals contained in the $\partial(M_i M_j)/\partial q$ term. The magnitude of these integrals are different for different modes taking part to a greater or lesser degree in the excitation. The relative intensity between the α'_{zz} elements of the 996., 1142., and the 1567./1574.cm^{-1} modes are in the ratio of 1:3:5.5, indicating the relative contributions of the Franck-Condon integrals. The intensity of the single and double bond modes eventually become equal in the case of the infinite polyene, polyacetylene.[35]

The transition moments and their derivatives govern the magnitude of the scattering tensors for both the Rayleigh and Raman radiation respectively. The selection rules state that these particular normal modes are capable of resonance enhancement, the predominant z polarization of the electronic transition moment dictates that they all will have exaggerated α'_{zz} tensor elements.

On the basis of a pseudo C_{2h} point group for DPO, thirty-seven

totally symmetric and seventeen non-totally symmetric modes would be allowed in the Raman spectrum. As indicated, no non-totally symmetric modes are observed in the Raman or absorption/emission spectra. The tensors for a totally symmetric mode in the C_{2h} group would have identically vanishing α'_{xy}, α'_{yz} tensor elements while the non-totally symmetric modes would have all elements vanish except α'_{yx}, and α'_{yz}. Clearly this is not the case here. As a result of the low symmetry in DPO and the absence of principal axes, the off diagonal elements observed are a result of the geometrical perspective in which the Raman scattering tensor is measured. Interpretation of a diagonallized α'_{ij} tensor would clearly be inconsistent because the principal directions of α_{ij} and α'_{ij} would no longer be coincident nor would this optical measurement coincide with the molecular coordinate axes assigned to the geometrical structure. In this coordinate system, existence of other elements besides α'_{zz} indicate the presence and strength of the electronic coupling between the z polarized transition and the x and y directions. The similar tensor form that these normal modes share arise from the fact that even though these modes have different normal coordinates and mechanical location, they all are subject to the same global excitation topology.

During these totally symmetric vibrations, all polarizability gradients are positive indicating that the polarizability in the extended state is larger than in the contracted phase of the vibrations. Dispersion of the α'_{zz} element in relation to other

possibly allowed elements is expected to occur as the approaches resonance. Dispersion of the zz element as the chain becomes infinitely long is expected as the symmetry approaches pure C_{2h}. The depolarization ratios calculated from the data in Table 5.2 are all nearly 1/3. The depolarization ratios measured in isotropic solution are also nearly 1/3 within experimental error. This ratio is at the limit for the value of a completely anisotropic rod. Intermolecular effects of emission from a non-Franck-Condon state would have little effect on this high anisotropy and thus a negligible effect on the depolarization ratio.

In conclusion, it would be interesting to attempt to make such measurements on crystalline compounds of higher symmetry where a violation of the selection rules might take place in the solid state due to the deviations that the principal coordinate system of the optical-electronic structure might experience in relation to the geometrical one.

Acknowledgements:

Thanks are due to Professor J. C. W. Chien for valuable suggestions at various stages of this work and for financial support. I also acknowledge Professor S. L. Hsu for kindly providing his Raman Spectroscopy Laboratory. Assistance from the Materials Research Laboratories and AFOSR are gratefully acknowledged.

REFERENCES

1. K. G. Denbigh, Trans. Faraday Soc. 36, 936 (1940).

2. (a) R. L. Rowell and R. S. Stein, J. Chem. Phys. 47, 2985 (1967). (b) H. A. Szymanski, Raman Spectroscopy, vol. 1 (Plenum Press, 1967).

3. R. L. Jernigan and P. J. Flory, J. Chem. Phys. 47, 3104 (1967).

4. B. M. Ladanyi and T. Keyes, Mol. Phys. 37, 1809 (1979).

5. (a) R. G. Snyder, J. Mol. Spec. 36, 204-221, 222-231, (1970). (b) H. Schrotter and H. Bernstein, J. Mol. Spec. 12, 1-17 1964). (c) W. F. Murphy and S. Montero, Mol. Phys. 11, 1-11 (1981).

6. A. C. Albrecht, J. Chem. Phys. 34, 1476 (1961).

7. (a) A. Warschel and P. Dauber, J. Chem. Phys. 66, 5477 (1977). (b) F. Inagaki, M. Tasumi, and T. Miyazawa, J. Mol. Spec. 50, 286-303 (1974). (c) H. A. Szymanski, Raman Spectroscopy, vol. 2 (Plenum Press, 1967).

8. I. Beattie and T. Gilson, Proc. Roy. Soc. A307, 407-429 (1968).

9. M. Suzuki, T. Yokoyama, M., and M. Ito, Spectrochim Acta 24, 1091 (1967).

10. D. Hanson and A. R. Gee, J. Chem. Phys. 51, 5052 (1969).

11. Unpublished work, crystallographic data for the monoclinic modifications of diphenyl-hexatriene and octatetraene. R. O. Day: Dept. of Chemistry, University of Massachusetts, Amherst, Massachusetts 01003; S. A. Kuehl, J. C. W. Chien: Dept. of Polymer Sci. & Eng., University of Massachusetts, Amherst, Massachusetts 01003.

12. E. E. Wahlstrom, Optical Crystallography (John Wiley & Sons, Inc., 1969).

13. A. Burnham, G. Alms, and W. Flygare, J. Chem. Phys. 62, 3289 (1975).

14. (a) J. R. Nester and E. R. Lippincott, J. Ram. Spec. 1, 305 (1973). (b) G. Fini, P. Mirone, and P. Patella, J. Mol. Spec. 28, 144-160 (1968).

15. (a) A. Warschel and M. Karplus, J. Amer. Chem. Soc. 94, 5612 (1972). 2). (b) A. Warschel, J. Chem. Phys. 62, 214 (1975). (c) K. L. Kip, N. O. Lipari, C. B. Duke, B. S. Hudson, and J. Diamond, J. Chem. Phys. 64, 4020 (1976).

16. B. S. Hudson and B. E. Kohler, J. Chem. Phys. 59, 4984 (1973).

17. (a) B. S. Hudson and B. E. Kohler, Chem. Phys. Letters 14, 299 (1972). (b) K. Schulten and M. Karplus, Chem. Phys. Letters 14, 305 (1972). (c) J. B. Birks, G. N. R. Tripathi, and M. D. Lumd, Chem. Phys. 33, 185 (1978).

18. (a) R. S. Mulliken, J. Chem. Phys. 7, 364 (1939). (b) L. J. Parkhurst and B. G. Anex, J. Chem. Phys. 45, 862 (1966).

19. M. Ashraf El-Bayoumi and F. M. Abdel Halim, J. Chem. Phys. 48, 2536 (1968).

20. B. E. Kohler, T. A. Spiglanin, R. J. Hemley, and M. Karplus, J. Chem. Phys. 80, 23 (1984).

21. R. H. Dyck and D. S. McClure, J. Chem. Phys. 36, 2326 (1962).

22. G. Hertzberg, Infrared and Raman Spectroscopy, (D. Van Nostrand Co., Inc., 1950).

23. (a) R. Gavin and S. Rice, J. Chem. Phys. 55, 2675 (1971). (b) R. Gavin, S. Saloman, and S. Rice, J. Chem. Phys. 58, 3160 (1973).

24. F. Inagaki, M. Tasumi, and T. Miyazawa, J. Ram. Spec. 3, 335 (1975).

25. (a) P. Cummins and D. Dunmur, Chem. Phys. Letters 22, 519 (1973). (b) D. Dunmur, Mol. Phys. 23, 109 (1972).

26. D. P. Craig, R. Mason, P. Pauling, and D. P. Santry, Proc. Roy. Soc. A286, 98 (1965).

27. Direction cosines constructed from the calculated mean plane and its intersection with the (010) crystal plane.

28. H. A. Kramers and W. Heisenberg, Z. Physik 31, 681 (1925).

29. P. A. M. Dirac, Proc. Roy. Soc. (London) 114, 710 (1927).

30. C. H. Ting, Spectrochim Acta 24A, 1177 (1968).

31. (a) P. P. Shorygin. Zh. Fiz. Khim. 21, 1125 (1947). (b) P. P. Shorygin, Izv. Akad. Nauk SSSR Fiz. Zemli 12, 576 (1948). (c) P. P. Shorygin, Pure Appl. Chem. 4, 87 (1967). (d) See also J. Berhinger and J. Brandmuller, Z. Elektrochem. 60, 643, (1956).

32. L. Margulies and M. Stockburger, J. Ram. Spec. 8, 26 (1979).

33. G. Placzek, Handbuch der Radiologie, edited by E. Marx, (Akademische Verlagsgellschaft, Leipzig, 1934), Vol. VI, part 2, p. 205.

34. E. Schmidt and B. Brosa, J. Chem. Phys. 58, 3871 (1973).

35. H. Shirakawa, T. Ito, and S. Ikeda, Polymer J. 4, 460 (1973).

P A R T II

STATIC AND QUASIELASTIC LIGHT SCATTERING STUDIES OF TRANSLATIONAL AND ROTATIONAL BROWNIAN DYNAMICS IN A COULOMBICALLY INTERACTING MACROFLUID

C H A P T E R I

A. Abstract

Measurements of the concentration dependence of the translational and rotational self-diffusion constants have been made on a colloidal suspension of Coulombically interacting optically anisotropic Teflon (ICI) particles by Quasielastic Light Scattering. The particles exhibit a small degree of size and shape dispersity. The dilute suspensions were stable, dispersed with the aid of a surface active agent. Both the translational and rotational self-diffusion constants display a retardation of free diffusion with concentration indicating the presence of both radial and anisotropic interparticle interactions respectively. The particulate system acts as a liquidlike macrofluid, the pairwise interparticle interactions adequately represented by a screened Coulomb potential with renormalized surface potential and screening length resulting from the strong deviations from ideal behavior ususally treated with the simple Debye-Huckel theory. The effect of these interactions is also embodied in the static structure of the solutions. Short range order at a volume fraction as low as $\phi = 1.6 \times 10^{-5}$ is indicated by the presence of weak maximums in the absolute static structure factor measured from the wavevector dependence of the depolarized scattered light. Unlike structure factors presented by other authors for isotropic systems, the structure factors obtained from the depolarized scattering of anisotropic systems contain information on orientational correlations

between particles as well as particle center correlations. The affect of this complication is discussed. The novel anisotropic optical properties exhibited by these semicrystalline particles in colloidal suspension has allowed for the first time the observation of hindered rotational self-diffusion in a Coulombically interacting macrofluid.

The experimental results for translational self-diffusion have been successfully interpreted through the theoretical calculations of Hess and Klein for macroions interacting through a radially symmetric screened Coulomb potential. In choosing the basic transport equation of Fokker-Planck and solving the N-particle dynamical system for self-diffusion within the projection operator formalism, they derive a simple relation between self-diffusion and concentration for the interacting macroions using a mode-mode coupling approximation. These results are consistent with previous measurements made on interacting macrofluids. A brief discussion of other theoretical results for translational self-diffusion is undertaken as the differences are related to the physics of the models applied and will therefore illuminate the nature of the system studied here. At this time, no theoretical explanation exists for the description of the concentration dependence of the rotational self-diffusion results, although results from studies into dielectric and orientational relaxation of molecular liquids have been adopted. A plausible explanation as to the mechanism of the observed concentration dependence is related to an interparticle torque exerted through an effective

monopole-dipole interaction arising from the large static electric polarizability of the counterion atmosphere surrounding each particle. The postulated mechanism is selfconsistent with the trends observed simultaneously in translational and rotational self-diffusion.

B. Introduction

Transport processes have been studied in great detail since the time of Einstein when particular emphasis was given to Brownian dynamics and diffusion. Brownian motion, the most common example of a stochastic process, has been the centerpiece around which the development of statistical mechanical methods have evolved. Recently, much attention has been focused on the theoretical treatment of the concentration, frequency, and wavevector dependence of various Brownian variables such as the friction factor and the self or mutual diffusion constants in interacting and non-interacting systems. In the area of interacting colloidal macrofluids, most of this attention has dealt with translational diffusion, rotational diffusion being a topic of less interest. This is due in part to the absence of a body of experimental data which can be drawn upon as data can only be obtained in some special circumstances. Also, rotational diffusion is conceptually and mathematically more difficult to treat while it is also considered to be a local effect having little influence on the macroscopic and collective properties of a particulate system. A

considerable amount of experimental and theoretical work has been put forth, however, concerning the rotational motion of interacting non-Brownian diffusers such as molecular liquids. With the extraordinary and sophisticated advances made in mathematical physics, namely statistical and quantum mechanics, a variety of approaches in the solution of these complicated N-body problems have appeared. As such, the literature contains many theoretical treatises all based on either Smoluchowski or Fokker-Planck dynamics solved by different techniques to various levels of approximation in the direct and/or indirect interparticle interaction, addressing different density regimes and different aspects of Brownian motion. These results, some of which are conflicting, are deemed to be valid to the degree of approximation and level of rigor in the solution scheme. Experimental endeavors have not in general supplied a body of clear cut evidence by which the success of these various foundations and approaches can be judged. Computer simulations of both the structure and dynamics of interacting macrofluids have been a good beginning. Alternatively, the static structure, the time average of the dynamic properties, has been studied in greater detail in an effort to characterize solutions, most of these in the area of molecular liquids. In strongly interacting Brownian systems, this static structure is reflected in the dynamic behavior. A solution of infinitely dilute non-interacting particles will, for instance, be completely disordered in space and will move about unhindered with purely Gaussian statistics. In a solution of interacting particles, with for example a radially symmetric pairwise

repulsive interaction, the particles will be statistically coupled and will tend to localize themselves in space at maximum distances from each other. Depending on the form of possible anisotropic interparticle forces which could be present, a correlation could exist between the orientation of a pair of particles and/or possibly affect a hindrance of free rotational diffusion without orientation correlations. This correlation in position and possibly orientation with respect to nearest neighbors will be reflected in their dynamics as well. Movement about these virtual lattice sites with respect to the spacial or angular variable component will be slow in comparison to a free particle, as a slowly varying configurationally dependent and long-lived restoring force is always superimposed upon the rapidly varying randomly directed Brownian force. Although a number of excellent experimental investigations have been done into the statics and dynamics of strongly interacting Brownian systems, none have addressed in particular the concentration dependence of translational or rotational diffusion directly. Moreover, none of the theoretical results on concentration dependence which do exist have risen to distinction because of the lack of a direct study of this kind. This work has as its aim the presentation of experimental results on the concentration dependence of translational and rotational self-diffusion in a strongly interacting system of macroions. The frequency dependence of these parameters has also been investigated briefly. A review of the enormous and complex quantity of theoretical work is not the intention of this work. Excellent reviews have been

compiled by the best experts in the field[1,2] and much of the basic discussion presented here has been summarized from their work. What will be attempted is a comparison and contrast between a few theoretical results specifically addressing translational self-diffusion of strongly interacting macroions without hydrodynamic interaction. Notably, the approach of Hess and Klein will be emphasized. With regards to rotational self-diffusion, the observations which will be presented here have not been seen or postulated before, no exact treatments are at hand to be used as a tool. A wealth of work, however, has been accumulated for the static and dynamic behavior of dense molecular fluids by depolarized light scattering, neutron scattering and dielectric measurement techniques. The relevant similarities between the behavior of dense fluids and the theoretical results (sometimes treating particles as non-Brownian diffusers) describing its structure, dynamics and dielectric properties which can be invoked for the interpretation of the observations seen in the Brownian macrofluid studied here will be identified when required. The presentation will be structured as follows.

In Chapter II, Brownian theory is introduced through basic Langevin dynamics. Concepts and terms are defined here for free Brownian diffusion. Next, the behavior of interacting systems is discussed. The sources of interparticle interactions is revealed in light of historical documentation. The correct form of the Coulomb potential characteristic of finite sized and highly charged macroions

is followed from the exact solution to the Poisson equation and is contrasted with the Debye-Huckel form used almost universally in this field. The spacial order characteristic of interacting macrofluids is described briefly through the structure factor function, S(q) which in this system contains information on orientational and position correlations. Next, a zeroth order approximation to the dynamics of a Coulombically interacting system of particles is presented through a harmonically bound Brownian particle model. Finally, the more advanced and complete treatments of translational diffusion as an N-body problem are discussed. The physical bases and approximations used in the successful theory by Hess and Klein are contrasted and compared with other models available in terms of reasonable physical intuition into the physics of the problem.

Chapter III will show how the techniques of laser light scattering is applied in the measurement of the static and dynamic properties of the macrofluid investigated here. The methodology and practice of static and quasielastic light scattering is highly evolved and enjoys broad application in the study of solution properties. Derivation of the static structure factor and the dynamic field time correlation function from the scattered intensity is first introduced for a simple isotropic system of small particles. Next, equations applicable for the analysis of the polarized (Vv) and depolarized (Hv) intensity scattered from a system of optically anisotropic small Brownian particles are introduced. Having sufficiently laid the basic

foundations of light scattering from optically anisotropic systems, inclusion of large size and interparticle interactions is made possible yielding forms for the absolute static structure factor, particle form factor and the polarized and depolarized time correlation functions which are valid for the systems studied here. The influence of intraparticle interference, particle anisotropy memory effects and polydispersity on the q^2 dependent decay rates are discussed. The formalism behind the accumulation and extraction of the decay rates from the measured correlation functions by the cumulant method is reviewed.

Chapter IV describes the physical characteristics of these Teflon particles in solution. The particles' unique internal organization is revealed and a particle fixed coordinate system is assigned. Important parametes characterizing the particle size and shape distribution are listed and the nature of the particles' surface charge arising from a surfactant coating is described. This is followed by sample preparation procedures and measurements of their concentrations. Finally, the validity of the Born approximation (multiple scattering) is reviewed.

Chapter V details the procedures involved in measuring the angularly dependent polarized and depolarized static light scattering intensities and dynamic time correlation functions. The important features of the absolute static structure factor and particle form factor are described. The form of the polarized and depolarized time

correlation functions are considered in both their time and concentration dependence. The decay rates extracted from them and the influence of certain "non-idealities" identified. Finally, the results of the concentration dependent translational and rotational self-diffusion constants are plotted.

Chapter VI of Part II of this dissertation concludes with a discussion of the trends observed in the concentration dependence of translational and rotational diffusion. The relationships and self-consistencies between the concentration dependence of translational and rotational self-diffusion are revealed and documented by experimental evidence while the relationship between the dynamic behavior of this interacting system as emboddied by the measured diffusion constants and the static structure factor are identified. Conclusions are drawn for translational diffusion in light of the theoretical predictions based on both weak and strong coupling theories. A plausible mechanism as to the nature of the concentration dependence of rotational diffusion is postulated and justified, the mechanism proposed being self-consistent with the known source of the Coulomb potential, historical documentation regarding the behavior of the ionic polarizability and the trends observed in translational and rotational self-diffusion simultaneously.

C H A P T E R II

DIFFUSION: THEORETICAL BACKGROUND

A. Non-interacting Particles

The simplest way of introducing the statistical mechanical foundations of Brownian motion is to consider a classical differential equation of motion derived from Newton's laws which describe the process. In this model, let a single particle be subject to a driving force F(t) and also subject to viscous damping. Our differential equation becomes:

$$m\left(\frac{dv(t)}{dt}\right) + fv(t) = F(t) \qquad (1)$$

where V (t) is the velocity at time t and f is the damping constant. This non-homogeneous differential equation is commonly called the Langevin equation. The statistical mechanics is introduced at this point by defining the properties of the driving force F(t) and the velocity v(t) with time, a requirement if an exact solution to eq.II.1 is desired. F(t) must be defined here to represent the randomly fluctuating Brownian force arising from the delta function forces from all the solvent-macroparticle bombardments, these forces having a characteristic fluctuation time τ_B. At the times on the order of $\tau_B(10^{-8}s)$, the velocity and displacement will be discontinuous in time making the particles non-Brownian and a solution to eq. II.1 most

difficult. If the long time $t >> \tau_B$ behavior is desired, the force F(t) becomes an isotropically distributed random variable and important statistical properties derived for stochastic processes may be applied. Over long times, the average force acting on a particle is zero thus $\langle F(t)\rangle = 0$. In this simple single particle example where interactions of any kind are absent, the Markovian approximation (no memory effects) is valid whereby the long time values of the force-force, force-velocity and force-position correlation functions are zero; i.e., $\langle F(t)F(t+\ )\rangle = 0.$, $\langle F(t)v(t)\rangle = 0.$, $\langle F(t)x(t)\rangle = 0.$ A formal solution to eq.II.1 in the velocity representation may be written as:

$$v(t) = v(0)\exp(-\frac{f}{m}t) + \int_o^t \exp-[\frac{f}{m}(t-\tau)]F(\tau)d\tau \qquad (2)$$

Using the relations defined above, this equation can be reduced to a convenient form written in terms of a velocity autocorrelation function:

$$\phi(t) = \langle v(t)v(0)\rangle = \langle v(0)^2\rangle \exp-(\frac{f}{m}t) \qquad (3)$$

Borrowing concepts from the kinetic gas theory, equipartition of energy yield:

$$\langle v(t)v(0)\rangle = \langle v^2\rangle$$

where $\frac{1}{2} m\langle v^2 \rangle = \frac{3}{2} kT$

so that $$\phi(t) = \frac{3kT}{2} \exp-(\frac{f}{m})t \qquad (4)$$

The translational diffusion constant is defined as the integral of the velocity autocorrelation function (Green-Kubo relation):

$$D = \frac{1}{3}\int_o^\infty \phi(t)dt \qquad (5)$$

Thus the diffusion constant is related to the average distance a particle travels over a long period of time, $t >> \tau_B$. Putting eq. II.4 in II.5 gives D = kT/f which is the Einstein relation. The friction coefficient f, is dependent upon the size and shape of the particle and upon the shear viscosity of the solvent η_o . Stokes[3], Einstein[4] and Perrin[5] have derived the translational and rotational friction factors for particles of a variety of shapes through linear hydrodynamics based on the Navier-Stokes equations for fluid flow. For translational diffusion of spheres, $f = 6\pi\eta_o a$, where a is the particle radius. Similar but more complicated arguments have been invoked with regard to rotational diffusion. The Brownian force not only affects a translation of a particle with time but also imparts microscopic torques during the solvent bombardment which do not cancel, this being the mechanism causing rotational diffusion. For spheres, the rotational diffusion coefficient is given by: $\Theta = kT/8\pi\eta_o a^3$.

An alternative method for treating diffusion is based on transport theory for a material continuum. In Brownian motion, the flux of particles in space and time must obey the equations of continuity, i.e., mass or density conservation etc. The time rate of change of a configuration of particles within some volume element is related to the spacial velocity gradients of the particles within that volume element. Creating a single particle space-time distribution function G(r,t), one can write:

$$\frac{\partial G(r,t)}{\partial t} = D\nabla^2 G(r,t) \tag{6}$$

where D is now a transport coefficient. This equation is called Ficks law[6] of diffusion and has a form reminiscent of wave equation encountered in quantum mechanics describing electron densities. This similarity of form will have an important bearing on how more advanced treatments of diffusion can be developed. Analogously, if a N-particle distribution function is defined such as the concentration C(r,t), one can write:

$$\frac{\partial C(r,t)}{\partial t} = D_m \nabla^2 C(r,t) \tag{7}$$

where the coefficient is now a mutual diffusion coefficient as it is a relation concerning the time evolution of a collective variable. Analogous treatments may be applied for rotational diffusion. These will be developed in Chapter III. In a system of non-interacting

particles, the self and mutual diffusion coefficients are equal as the N-particle distribution function can be factored into N one-particle distribution functions[7], each satisfying equation II.6. Self diffusion describes the motion of a single particle at equilibrium and in a concentration gradients in the absence of interparticle interactions. The self-diffusion constant is usually extracted from tracer experiments, forced Rayleigh scattering or dynamic light scattering at a very large value of the scattering wavevector. The mutual diffusion constant describes the transport of particles in a concentration gradient where osmotic forces drive equilibration processes through diffusion. The mutual diffusion constant can also be measured by dynamic light scattering at very low wavevectors, or it can be obtained through mixing experiments. The size of the wavevectors needed to extract the self and mutual diffusion constants through dynamic light scattering will be discussed in Chapter III. Modifications to this theory of free Brownian diffusion are required for the analysis of interacting particles.

B. Interacting Particles

1. The Sources and Form of the Interparticle Potential

In the past, diffusion or sedimentation experiments have usually centered around obtaining a value for the friction factor from which a particle dimension could be obtained using the results of hydrodynamic modelling such as the Perrin equations. An extrapolation of diffusion

data to zero concentration is required in some cases to eliminate the effect of interparticle interactions which can confuse a simple interpretation and lead to misleading conclusions. Recently, these interparticle interactions, which in the past were regarded as a nuisance, have become a subject of interest for both experimentalists and theoreticians. The development of theoretical machinery capable of accurately predicting the effect of interparticle interactions on diffusion is of interest to physicists and presents them with yet another N-body problem. Experimentalists can gather more subtile and esoteric information into the nature of solvated macroparticles by studying their Brownian motion at densities where these effects can be of influence. A range of interparticle interaction strengths can occur as mean interparticle spacings become small enough to place particles within a potential field of approximately kT or greater. Two classes of interactions have been identified which can influence free particle motion; direct interactions and indirect hydrodynamic interactions. Hydrodynamic interactions result from the propagating velocity fields set up in the solvent by the movement of all the Brownian particles. These are very weak at low densities and can be neglected. Direct interactions, found to be much more significant, are the short ranged hard sphere (excluded volume) interaction and the long ranged Coulombic interactions. Pertinent to any discussion of the static and dynamic properties of pure liquids or macrofluids is the specification of the pair potential function between particles. In systems displaying Coulombic interactions, these functions can be

written explicitly in terms of forms derived from ideal models. The validity of these expressions in general applications must be justified.

Many types of particles (biopolymers, ionomers, viruses, surfactant micelles, latexes, etc.), when dispersed in water, can carry a charge due to spontaneous ionization of surface carboxylate groups. The character of the resulting Coulomb potential is determined by the structure of the surrounding ion atmosphere. The symmetry of the particle and the instantaneous symmetry of its' counterion atmosphere will determine which terms in the multipole expansion of the charge distribution contribute to the potential field while the surface charge density, the screening effect and dielectric properties of the atmosphere determines the strength of the field at arbitrary distances from the surface. The range and strength of the Coulomb potential is in some cases great enough to affect a crystallization[8] of the colloidal particles yielding crystallites several millimeters in dimension containing many unit cells of a primitive Bravis lattice type (BCC,FCC). These systems characterize the colloidal crystal regime where interparticle potential energies are many kT while systems at reduced density below a critical volume fraction or with weaker forces will be "liquidlike," having short range order like a hard sphere dense liquid.

The mathematical form and character of the Coulomb potential present in electrolyte solutions, one of the central problems of

colloidal science, is still being addressed having been researched for years with considerable controversy, exact solutions and accurate predictions available only for special ideal cases. Unfortunately, the system under investigation here is not one of those ideal situations as it exhibits some novel peculiarities which have only been addressed in the literature quite recently. This necessitates a brief discussion of the most fundamental approach to the problem, then a discussion of the modifications and ramifications of the more complete theory which corrects for deviations from ideality.

To calculate the potential field ψ at a point in a volume element containing free charge, Poisson's equation (eq. II.8) must be solved self consistently. The distribution of excess free charge, ρ , within that volume element, determines the potential while at the same time the potential will determine the distributional charge thus setting up a criterion for self consistency.

$$\nabla^2\psi = \frac{\rho}{\varepsilon\varepsilon_o} \tag{8}$$

The approximate solution which has enjoyed broad use and universal acceptance in the field of electrolytes is that by Debye and Huckel[9] (DH). Their approximate scheme rests on a variety of assumptions. Namely, they calculate the monopole field about a finite sized central ion of charge Q, in the case where the counterion has symmetrical charge, i.e., -Q, and where the system is very dilute. To solve the

Poisson differential equation, they assumed that the counterion particles were pointlike, allowing the time averaged distribution of free charge to be written as continuous function in space and that the potential energy $|\psi Q|$, anywhere in space, including near the central ions surface is much less than the thermal energy kT. They assumed that the distribution of ions around the central ion could be given by the Boltzmann distribution[6], and where the N-body potential can be treated in a superposition approximation. It is given as:

$$\rho = -2NQ\left[\frac{Q\psi}{kT} + \frac{1}{3!}\left(\frac{Q\psi}{kT}\right)^3 + \frac{1}{5!}\left(\frac{Q\psi}{kT}\right)^5 + \ldots\ldots \right] \qquad (9)$$

Keeping only the first linear term in this expansion, Poisson's equation is linearized and may be solved explicitly to give a screened Coulomb potential given by:

$$\psi(r) = \frac{A}{r} e^{-\kappa r} \qquad (10)$$

where A is related to the surface charge density and κ is a screening parameter related to the concentration of neutralizing counterions in the vicinity of the central ion.

Similarly, all solutions to the Poisson equation for any geometry will give this exponential screening when it is assumed that the bare Coulomb field is screened linearly by the counterions. In the DH approximation, the cloud of pointlike counterions effectively screens

the bare charge of a central ion when it is viewed at distances greater than the Debye length κ^{-1}. In every study of interacting colloids in either the liquid or crystalline states, experimentalists discovered that when a DH screened Coulomb potential is applied in the modelling of the interparticle interaction as it is reflected in both static and dynamic behavior, on the basis of best fit criterion, rescaled particle valencies and screening lengths (κ^{-1}) were found to yield consistant trends, these being unexpectedly below and above respectively from those estimated empirically. These findings motivated Hastings to reconsider earlier Kirkwood predictions concerning the applicability of the original DH assumptions as applied to the newly researched systems where those assumptions are invalidated, these being systems of highly charged and large macroions surrounded by finite sized counterions and possibly added salt ions also of finite size. Hastings[10a] and Kirkwood[11] found that the solutions to Poissons's equation is not given by the simple form of eq. II.10 but is reduced to a differential-difference integral equation possessing non-linear screening in the vicinity of the central ion. In sharp contrast to the DH theory, this important modification predicts that at a critical ionic strength such that $2\kappa a=2.79$ (a=particle radius), a macroionic system will undergo crystallization, the potential being long range and oscillatory in space exhibiting a stratification with zones of excess positive and negative charge, the macroions occupying lattice sites corresponding to the potential energy minima. Contrast this with the results of the DH theory which

is only valid for $\kappa a \ll 1$, predicting no such transition and implying that any interaction gets weaker as κa gets larger. The modified theory predicts an undamped oscillatory potential for values of $2\kappa a > 2.79$, this potential being undefined as it would be unbounded while below 2.79, the potential is damped and oscillatory. Equating the critical wavelength of the oscillation with the expected lattice spacing places a constraint on the minimum valence required by the macroions for crystallization to occur, $Z_c = 2.5(2a)^{\frac{1}{2}}$. The macroionic crystallization phenomenon was found to be only weakly dependent upon the presence of added salt. This arises as the density of finite sized ions in the screening cloud cannot increase above a certain level as could be done with point ions. This suggests the possibility that particles in a sufficiently dilute suspension for which $2\kappa a > 2.79$ might yet exhibit a liquidlike spacial arrangement while from a Brownian dynamics standpoint, particles might interact weakly as well, visa vi a κa which might appear to be smaller than estimated empirically. Solidlike behavior observed[12] in dilute solutions of turnip yellow mosaic virus by critical shear stress measurements also suggest the presence of long range Coulomb forces at higher ionic strengths. The calculated value of κa for these solutions is much greater than 1 (about 50). The effective value of κa found by Hastings[10b] in a theoretical modelling study which appears to govern the behavior of this solution is about 1. A raising and subsequent lowering of shear moduli with increasing ionic strength has been observed previously in concentrated suspensions of polystyrene latex spheres. It has been

speculated that some mechanism might be responsible for the suppression of the apparent ionic strength of a suspending medium thus increasing the magnitude of the effective inverse screening length. Alexander,[13] et. al. addressed this problem in some respects by solving the exact Poisson equation numerically for macroions at high potentials in a spherical Wigner-Seitz cell geometry. He showed that in the vicinity of a macroion with real charge Ze^-, the counterions a strongly accumulated at the expense of numbers in the bulk between the macroions. At the regions close to the cell boundry corresponding to L/2(L= interparticle spacing) the actual potential simulates the screened Columb form but with a particle valence and screening length corresponding to a renormalized valence Z*, Z* being smaller than Z. Z* was found to saturate at a value such that the maximum surface potential energy of a counterion (ψe^-) on a sphere of any size is about 10kT due to electrostatic chemical potential considerations at the highly charged surface. This was found even though the inter-macroion potential energies of the colloidal crystals in which they refer can be many kT. The increase in charge Q and drastic increase in the distance between the charged particles (L) as compared to e^- and the small macroion-counterion distance does not seem to be proportional indicating a discrepancy. All workers have found that as long as particles are observed while interacting over large distances L such that $\kappa L<1$, the renormalized screened Coulomb form will accurately represent the actual potential and thus suffice in the modelling of any static or dynamic property. This interpretation has also been

reiterated by Shih, et. al.[14]

Also typically present in colloidal solutions is a weakly attractive short range van der Waals dispersion force which can be responsible for coagulation in dispersions which are not prevented from reaching close interparticle separations by a sufficiently large and longer range monopole field. In the presence of dominant repulsive interactions, configurations of particles which probe this short range attractive part or the hard sphere repulsive part are rarely sampled so that the structure and dynamics of macroionic solutions is determined entirely by the Coulomb potential. A schematic of this composite potential is shown in figure 2.1. The colloidal chemistry of such systems has been reviewed in depth by Verwey and Overbeek.[15] The potential used universally to model Coulombically interacting colloidal systems is that incorporating the hard sphere repulsion and the screened Coulomb DH result. The hard sphere part acting as a reference system upon which the Coulomb repulsion is treated as a perturbation. this potential, proposed by Derjagium and Landau[16] and by Verwey and Overbeek[15] has been given the name the DLVO potential and can be written for two macroions of radius R as:

$$U(r) = \begin{cases} \infty \\ 4\pi\varepsilon\varepsilon_o R^2 \psi_o^{*2} \frac{1}{r} e^{-\kappa^* r} \end{cases} \qquad (11)$$

where ε_o is the dielectric constant of the solvent, κ^* is the

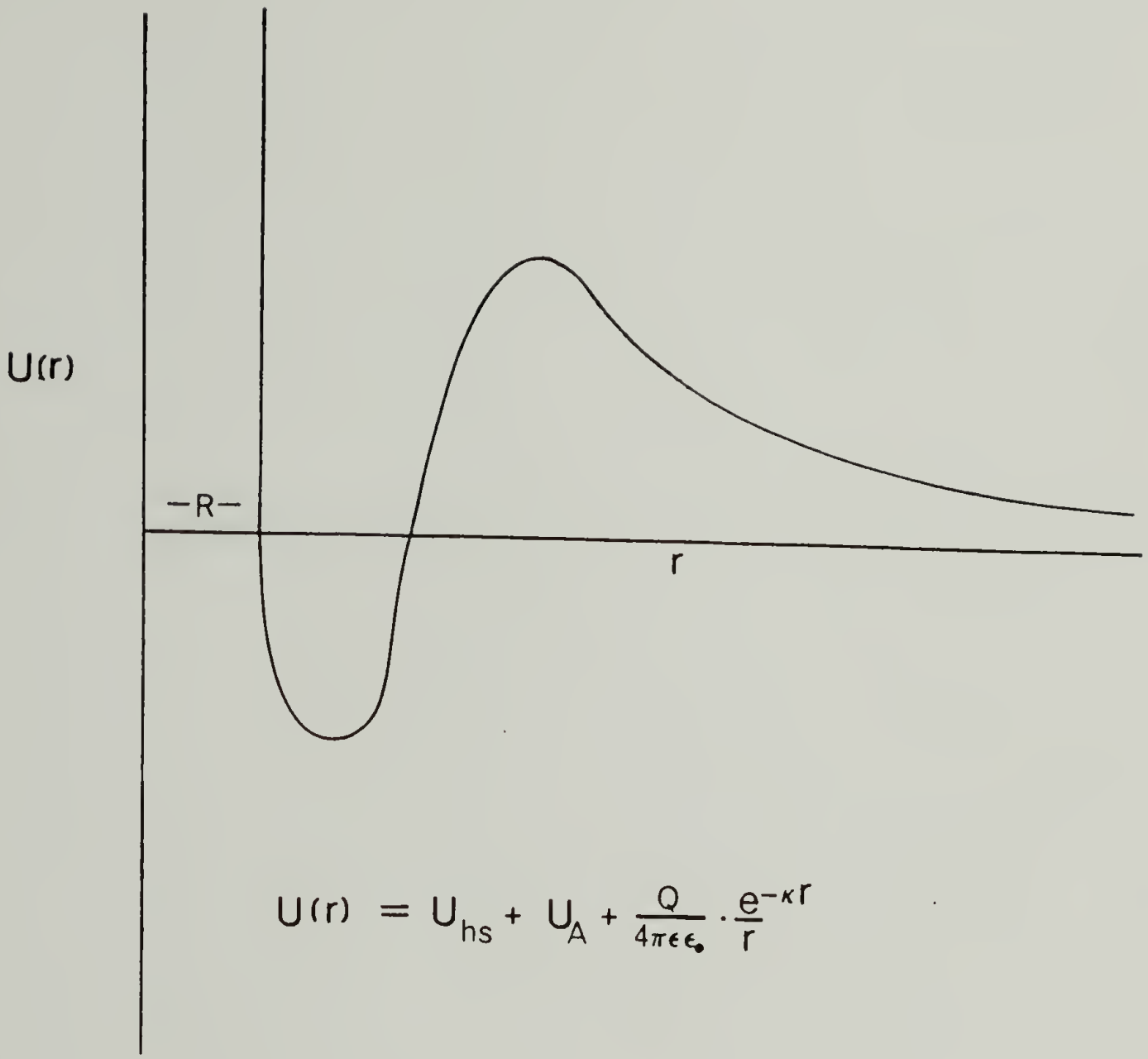

$$U(r) = U_{hs} + U_A + \frac{Q}{4\pi\epsilon\epsilon_0} \cdot \frac{e^{-\kappa r}}{r}$$

Figure 2.1 A schematic of the total DLVO potential.

renormalized inverse Debye screening length, and ψ_o^* is the renormalized surface potential. There is a question[10b] as to whether or not a large static dielectric constant, like those observed in charged latex suspensions, is consistant with the screened Coulomb approximation.

For small Z, renormalization is unnecessary and the surface potential can be written using Gauss' law as:

$$\psi_o = \frac{Ze^-}{4\pi\varepsilon\varepsilon_o R}$$

Remember that eq. II.II is not valid as r→R.

Equation II.II represents the simplest and approximate case of the potential energy between two macroions having only a monopole moment. In general, the higher order anisotropic interactions in the multipole expansion of the charge distribution could be taken into account. In the theory of uncharged dense liquids, the entire static and dynamic behavior is shown to be determined by the hard sphere repulsion and the interaction between these higher moments, i.e., dipole-dipole, dipole-quadropole etc. The effect of these interactions on the translational and rotational motions of liquids has been studied in depth by NMR, NQR, dielectric dispersion, and depolarized light scattering techniques. To date, the effect of these higher moments on the structural or self-dynamical properties of interacting colloidal systems has not been reported although casual

references have questioned whether they might be important. Hastings[10b] and Kirkwood[11a] to date have been the only authors to suggest modifying the interparticle potential to include the anisotropic interactions arising from the large electrical polarizability exhibited by a macroions counterion atmosphere. Indeed, electrolyte solutions including proteins[17] and latex spheres[18] have been observed to display pronounced dielectric increment and dispersive behavior. Although they were not studied as a function of high particle density, they suggest the ease at which a dipole can be induced in the presence of an electric field.

The dielectric properties of macromolecules in solution have been studied for years by dielectric dispersion, relaxation, and Kerr effect measurements to yield information on molecular conformation, shape, dipole moments and reorientational dynamics. Density anomolies observed in these systems have never been specifically documented and attributed to interparticle effects, but instead to sources of unknown origin. In a historic paper, Kirkwood and Schumaker[19a] reported discovering that the large dielectric increments of protein molecules in solution, could not be explained by the presence of a average dipole moment by virtue of symmetry arguments, but could be explained entirely by the presence of a non-zero mean square dipole $\langle \mu^2 \rangle$ and that this could be responsible for long range interparticle forces.[19b] In protein solutions[19a] and in colloidal suspensions,[20] it has been shown that there exists a dynamic equilibrium between the

many ionizable sites on a particle and their counterions. As a result, at any instant a molecule or particle will possess a distribution of charge which will not be centrosymmetric. Among other possible mechanisms tested to explain these observations, the mean square dipole mechanism has prevailed.[18,20] In the absence of an electric field, there exists a dipole and through it an effective polarizability as a result of thermal fluctuations alone which can be given by[21]: $\alpha = <\mu^2>/kT$, so that a dipole induced at low field strength $E \to 0$ would be given by $\vec{\mu} = \vec{E}<\mu^2>/kT$. The magnitude of the polarizability is governed by the size of the fluctuating dipole which in turn is determined by the volume available for the counterion atmosphere to move. The polarizability is also a function of the shape of the macroion as counterions may have a greater or lesser range of motion along different axies of a non-spherical particle, analogous with the optical polarizability. One can now make some statements about the motion of a polarizable macroion in an electric field. When a isotropically polarizable macroion is placed in an electric field, a dipole will be induced in the counterion atmosphere in the direction of the field. As a spherical particle will be coupled isotropically to its counterion atmosphere, by nature of the arguments above, the particle itself will have no preferential orientation with respect to the applied field, however, its rotational motion will be hindered as the particle must track its' counterion atmosphere. The time scale of the relaxation process is determined by the relaxation rate of the fluctuating dipole itself and the rate at which the electric field

changes direction. A non-spherical particle with a tensoral electric polarizability would first experience a dipole induced in its' atmosphere and then this dipole would tend to orient preferentially along the long axis of the particle in the direction of the applied field, the axis with the largest effective volume thus producing a particle torque. Free rotational motion would be hindered, a function of the coupling strength between the macroion and its' atmosphere. For dielectric measurements, the electric field is supplied by an applied electric field. In an interacting colloid system, a significantly large electric field can be supplied through the monopole field of a nearest neighbor. If the field is obviously strong enough to affect a hindrance of translational diffusion and structural ordering, a monopole-induced dipole interaction might be strong enough to produce an effect on rotational diffusion and an interparticle position-orientation correlation.

To calculate the potential energy between two macroions, one must now consider the second term in the multipole expansion of the potential energy. A monopole-induced dipole term can be included in the potential energy for the monopole-monopole term and can be written for an isotropic polarizability to good approximation as:

$$U(r) = \frac{Q^2}{4\pi\epsilon\epsilon_o r} e^{-\kappa r} - \frac{1}{2}\frac{Q^2\alpha}{4\pi\epsilon\epsilon_o r^4} e^{-\kappa r} \qquad (13)$$

where the second term on the right containing the isotropic

polarizability is the monopole-induced dipole interaction. The induced dipole will follow the instantaneous position of the Brownian particle supplying the field. Even though the potential energy given by eq. II.13 is still radial for the isotropic case, this expression does not contain explicitly the effective torque that the polarized atmosphere exerts on its macroion. In the case of a tensoral polarizability, the potential energy would have an explicit anisotropic term, the torque exerted to aline the particle and the coupling force tending to keep the particle alined with the field would be a much more complicated expression, one which is not available at the present time. It remains to be discussed in a later Chapter what the magnitude to the polarizability and the relaxation times might be. The theory of Oosawa will be invoked here.

2. Static Structure

From the discussion of the previous section, interacting particles will tend to take up positions and orient themselves in space so as to minimize their potential energy in the field of their neighbors, this tendency dependent upon the particle density implying the possibility that a phase change can take place. For Coulombically interacting systems, two phases have been identified: the colloidal crystal and the liquidlike phase. The spacial ordering observed in these systems is entirely analogous to the structure of crystalline solids and molecular liquids which has been studied for years by

neutron and x-ray scattering (diffraction). As such, the statistical mechanical methods, formulae and experimental techniques developed for these systems are of value here.

Statistical mechanical methods center around calculating the pair probability or radial distribution function $g_2(r)$. From this quantity, many properties, both structural and thermodynamic may be calculated for a liquid. The pair probability distribution function is related to the radial distribution function by $n^2(\vec{r}_1,\vec{r}_2) = g_2(r)\rho^2$, g(r) having the property that as r gets larger than about 5 molecular diameters (or effective diameters in the case of Coulombically interacting systems), particles become uncorrelated where $g(r)\to 1$ while for shorter distances it oscillates and goes to zero as $r\to R$ due to the hard sphere repulsion. Pertinent to this discussion is the fact that scattering techniques measure interference effects between pairs of particles (see Chapter III) and thus makes $g_2(r)$ experimentally accessible through the measurement of the static structure factor S(q) which is related to $g_2(r)$ by the Fourier transform:

$$S(q) = 1 + 4\pi C\int_0^\infty [g_2(r) - 1]e^{iqr}rdr \qquad (14)$$

The ultimate structure of molecular liquids or macrofluids, is determined by the total N-body interparticle potential energy $\hat{U}(\vec{r}^N,\Omega^N)$ where $\vec{r}^N$ and Ω^N are the position and orientation vector spaces for the N particles respectively. The pair distribution function is related

to $\hat{U}(r^N,\Omega^N)$ by the Boltzmann theorm:

$$g_2(r) = \exp[-\hat{U}(\vec{r}^N,\Omega^N)/kT] \tag{15}$$

For equation II.15 to be useful in any way, the relationship between the N-body potential energy $\hat{U}(\vec{r}^N,\Omega^N)$ and the pairwise potential energy $U(r,\Omega)$ must be specified, this problem being the focus of liquid state theory. For instruction, consider the weak coupling limit commonly used as an approximation on many occasions. This approximation is the same as that used in the DH approximation. If a liquid or macrofluid for that matter is dilute enough so that only pairwise interactions need be considered and at the same time the pairwise potential energy is very much less than kT, then a linearization of the Boltzmann equation can take place, analogous to that performed within the Poisson equation. Under these assumptions, equation II.15 can be written:

$$g_2(r) \tilde{\approx} 1 - U(r,\Omega)/kT \tag{16}$$

If the radially symmetric screened Coulomb potential is used as the pairwise interaction, a radial distribution in the DH level of approximation becomes:

$$g_2(r)_{DH} = 1 - \beta\frac{A}{r}\, e^{-\kappa r}$$

where $\beta = (kT)^{-1}$, and $A = Q^2/4\pi\varepsilon\varepsilon_o$. Putting this form of $g_2(r)$ into eq. II.14 yields an expression for the static structure factor in the DH limit:

$$S(q)_{DH} = 1 - \frac{\kappa_m^2}{q^2 + \kappa^2}$$

where $\kappa_m^2 = CQ^2/\varepsilon\varepsilon_o$, which like κ^2, represents the contribution of the macroions to the screening of the pairwise potential. This form of the structure factor produces a monotonically increasing curve from S(0)(the osmotic compressibility in the DH limit) to the asymtotic high q value of $S(q) = 1$, thus predicting no peak structure and positional correlations as is known to exist in macrofluids and molecular liquids alike. The presence of maximums in $g_2(r)$ or S(q) indicate that the system is strongly ($U(r) \sim kT$) coupled, structure factors for macroionic solution demonstrate the effect of a second nearest neighbor influence and the need to include 3 body interactions in the reduction of $\hat{U}(\vec{r}^N, \Omega^N)$. Inclusion of these higher body interactions effects the shape of $g_2(r)$ at large r and the shape of S(q) at small q. Just as the DH approximation is unable to accurately represent the potential field nearby a large highly charged macroion with finite sized counterions, it is also unable to predict the structure of these solutions for the same reasons. Surprisingly, this form has been invoked in many calculations where a analytic form for S(q) is needed and as such will represent a first order approximation in its use. Its use in predicting the dynamic properties of inter-

acting macroionic solutions is of concern here and calculations along this line are worth discussing.

The central problem in the calculation of liquid state structure at densities where interactions higher than binary are important remains the decomposition of $\hat{U}(\vec{r}^N,\Omega^N)$, conveniently written as the sum of a pairwise component and a component representing the interaction of a particle with all other particles in solution averaged over all possible configurations. In the case of angularly independent interactions, many approximate theories have been developed offering methods to calculate from the pair potential U(r), the radial distribution function $g_2(r)$ and through it S(q). In determining the potential of mean force, $f(\vec{r}_1)$ acting on a particle, one can justify carrying out the interaction to 3-body only and derive an equation:[22]

$$f(\vec{r}_1) = -\frac{\partial U(\vec{r}_1)}{\partial \vec{r}_1} = -\frac{\partial U(\vec{r}_1,\vec{r}_2)}{\partial \vec{r}_1} - \int \left[\frac{n^3(\vec{r}_1,\vec{r}_2,\vec{r}_3)}{\rho^2 g_2(\vec{r}_1)}\right]\left[\frac{\partial U(\vec{r}_1,\vec{r}_2)}{\partial \vec{r}_1}\right] d\vec{r}_1 \quad (19)$$

where $n^3(\vec{r}_1,\vec{r}_2,\vec{r}_3)$ is a triplet correlation function. The force upon a particle at $\vec{r}_1$ becomes the sum of the direct force between it and another particle at $\vec{r}_2$ and a term relating the average force exerted by a third particle at $\vec{r}_3$ through the particle at $\vec{r}_2$. Approximate schemes are required to solve this equation as the triplet correlation function n_3 is not known. In terms of the radial distribution function, equation II.19 can be written as:

$$h(\vec{r}_1,\vec{r}_2) = f(\vec{r}_1,\vec{r}_2) + \rho\int f(\vec{r}_1,\vec{r}_2)h(\vec{r}_2,\vec{r}_3)d\vec{r}_3 \qquad (20)$$

this is the famous Ornstein-Zenike (OZ) equation where $h(\vec{r}_1,\vec{r}_2)$ is defined as $h(\vec{r}_1,\vec{r}_2) = g_2(r) - 1$. Written in this form, the first term on the right (eq. II.20) represents the pairwise interaction between a given particle (1) and another neighboring particle (2) while the second term expresses the average effect of a third particle through the second particle on the first. To simulate the indirect effect of the other neighboring particles on the first, the position of the third particle is treated as a variable whereupon the integral is evaluated over all possible positions, possibly many nearest neighbor distances away. The approximate schemes used in solving the OZ equation involve the development of some closure relation between $h(\vec{r}_1,\vec{r}_2)$ and $h(\vec{r}_2,\vec{r}_3)$. The simplest and therefore least useful relation is that of Kirkwood[23] who used the superposition approximation to reduce $\hat{U}(\vec{r}^N)$, i.e., $\hat{U} = U(r_{ij})$ and therefore $n^3(\vec{r}_1,\vec{r}_2,\vec{r}_3) = \rho^2 g_2(\vec{r}_1,\vec{r}_2)g_2(\vec{r}_2,\vec{r}_3)g_2(\vec{r}_1,\vec{r}_3)$. Born and Green[24] (BG) employed this form and derived an integro-differential equation from the OZ equation for $g_2(r)$ which contains only pair correlations:

$$\ln(g_2(r)) = -\beta U(r) - \beta\rho\int(g_2(r) - 1)\left[\int_\infty^r g_2(r')\left(\frac{\partial U(r')}{\partial r'}\right)dr'\right]dr \qquad (21)$$

As mentioned before, to be of any value higher order interactions, at least 3 body are required thus other researchers Yvon,[25] Bogolivbov,[26]

Percus-Yevick[27] and those involved in the hypernetted chain approximation,[28] etc. attempt to solve the more general analogue of eq. II.21 which is written as a density expansion as:

$$\ln(g_2(r)) = -\beta U(r) + \ln(1 + \rho x_1(r) + \rho^2 x_2(r) + ...) \quad (22)$$

The size of the n th order expansion coefficient represents the influence of higher order n th body interactions. Practicality requires applications of this equation to include up to 3 body interactions. This introduces correction terms linear in concentration, thus characterizing a "linear" theory. Feasibility dictates treating the 3 body interaction in an approximate way under the auspices of the OZ equation. All these techniques employ cluster expansions and graph theory to calculate the coefficients $x_1(r)$, $x_2(r)$ etc., the description of which is unnecessary here. The most successful method has been that of Percus and Yevick who derived a closed analytic expression for $g_2(r)$ for hard spheres. They employ a mean spherical approximation (MSA), a closure relation which for hard spheres states that $g_2(r) = 0$ for $r \leq R$ while $U(r) = 0$ for $r > R$. Hayter and Penfold[29a] and later Hansen and Hayter[29b] adopted and modified the solution of the OZ equation by Palmer and Weeks[30] for unscreened Coulomb systems for application to a screened system. The MSA closure relation for a screened Coulomb system with a hard core repulsion reads:

$$
\begin{aligned}
f(\vec{r}_1,\vec{r}_2) &= \infty & x \leq R \\
f(\vec{r}_1,\vec{r}_2) &= -\beta U(r) & x > R \\
g_2(r) &= 0 & x \leq R
\end{aligned}
\tag{23}
$$

The general theoretical background involved in this calculation and others can be found in a recent review article by Baus and Hansen.[31] Their alogorithm employs a rescaling argument to avoid the failure of the MSA closure relation at low densities where letting $\rho \to 0$ in eq. II.20 and using II.23 yields $g_2(r)$ 1 - $\beta U(r)$ for r>R which is unphysical (negative g(r)) for realistic potential energies as those seen in Coulomb systems. This argument allows the calculation of the particle center structure factor, $S_c(q)$ for colloidal suspensions at low densities through knowledge of ρ , R, and the renormalized screened Coulomb potential parameters ψ_o^* and κ^*. Their approach has gained popularity in applications to liquidlike systems as a fitting procedure to estimate the parameters ψ_o^* and κ^*. Its use in this study will be revealed in a later Chapter.

In systems with pronounced anisotropic interparticle interactions, no theories exist in an analogous calculation for what is called the absolute static structure factor $S_{Hv}(q)$ as this quantity includes particle center correlations, interparticle position-orientation and orientation-orientation correlations. This is a result of introducing angular variables in the potential energy. These types of structure factors are commonplace in the study of molecular liquids. Models of molecular liquids have relied upon

computer and molecular dynamics simulations. Extraction of the particle center and orientational structure factors from $S_{Hv}(q)$ is possible and has been achieved by work carried out in neutron scattering, but it relys upon assumptions such as total or totally uncoupled correlations between particles. The similarity of these neutron scattering analyses to those required in depolarized light scattering from optically anisotropic systems will be invoked and discussed in insuing chapters.

Experimental determination of the static structure factor or diffraction patterns have been carried out on liquidlike dispersions and colloidal crystals[8] respectively by light scattering. The results for liquidlike systems have been addressed in depth by Gruner and Lehman[32] and by Brown, et.al.[33] These measurements were carried out by light scattering from optically isotropic and spherical polystyrene latex spheres. The characteristic of optical isotropy forbids the activity of the effect of orientational correlations arising from anisotropic interparticle interactions on the isotropically scattered light and also forbids the study of rotational diffusion by depolarized light scattering. Thus, the structure factors measured by these authors represent only particle center correlations and were adequately fit by the Hayter and Penfold theory using renormalized DLVO parameters. The observations of these two groups were similar demonstrating liquidlike structure in a concentration dependent structure factor, the peak maximums indicating the presence of the

first (q_{max}), second and sometimes third nearest neighbor shells. The distinguishing characteristics of the absolute static structure factor $S_{Hv}(q)$ as compared to the particle center structure factor $S_c(q)$ will be discussed in a later section.

C. Dynamic Properties

1. The Harmonically Bound Brownian Particle

In modeling the dynamics of Coulombically interacting Brownian particles, consider first a simple model in which a given particle is viewed as being trapped within a potential well created by the repulsive forces of an effectively fixed spherically symmetric configuration of nearest neighbors. The particle can then be considered mathematically as being harmonically bound to a virtual lattic site within this cage. This describes the main features of Pusey's cage model[34a,b] used by him to interpret dynamic data in a system of interacting polystyrene spheres. A Langevin equation describing this situation is written:

$$m\left(\frac{d^2x(t)}{dt^2}\right) + f\left(\frac{dx(t)}{dt}\right) + m\omega^2 x(t) = F(t) \qquad (24)$$

where ω is the harmonic frequency. Assume also that the driving force is again the Brownian force even though a fluctuating force due to the movement of the cage exists. This will be shown later to be related to a memory effect. The harmonic motion described above is strongly

damped by the slovent, i.e., $\beta/\omega >> 1.(\beta = f/m)$ at times much longer than the short lived solvent-particle relaxation time $\tau_B \sim 10^{-8}$s. The interesting behavior occurs as a result of the relative time scales that the Brownian and interparticle forces act on. Although it seems Coulomb forces on the order of kT or lower would not be sufficient to cause spacial ordering and a diffusional retardation, they however, are long range, directional and act over a much longer time scale than the short range delta function Brownian forces. It is as a result of these long lived forces that particle motion over long observation times is directed. In the case of overdamping, the solution to eq. II.24 in terms of the velocity autocorrelation function becomes:[35]

$$\phi(\tau) = \frac{kT}{m}\left[\left(1+\frac{\omega^2}{\beta^2}\right)\exp-\beta\tau\left(1-\frac{\omega^2}{\beta^2}\right) - \frac{\omega^2}{\beta^2}\exp-\frac{\omega^2}{\beta}\tau\right] \qquad (25)$$

In reality, the potential experienced by a particle in a liquidlike colloidal array is not harmonic nor is the particle confined to a virtual lattice site defined by its nearest neighbors. One can write an approimate form to eq. II.25 describing a liquidlike array by rewriting eq. II.25 to lowest order in ω/β as:

$$\phi(\tau) = \left(\frac{kT}{m}\right)\exp-(\tau/\tau_s) + A\exp-(\tau/\tau_I) \qquad (26)$$

where τ_s is the free particle relaxation time (β^{-1}), $A \sim \frac{kT}{m}\left(\frac{\omega}{\beta}\right)^2$ and τ_I for a solidlike array would be β/ω^2. The interparticle collision time τ_I may be defined as being the time it takes a particle to diffuse a

mean interparticle spacing and is approximately the length of time a particle is trapped within this cage. Pusey, in using eq. II.26 to analyze his dynamic data, has estimated τ_I to be 10^{-4} s. The value of τ_I for a liquidlike array would be expected to be less than β/ω^2. From the Green-Kubo relation, one can define a time dependent diffusion constant as:

$$D(t) = \frac{1}{3}\int_o^t \phi(\tau)d\tau \qquad (27)$$

Placing eq. II.26 into II.27 yields:

$$D(t) = D_o[1 - \exp-(t/\tau_s)] - A\tau_I[1 - \exp-(t/\tau_s)] \qquad (28)$$

Equation II.28 shows that at very short times, that is $t >> \tau_s$ but $t << \tau_I$, the particle diffuses freely while at longer times $t \sim \tau_I$, the interactions are strongly felt. For $t >> \tau_I$, $D = D_o - A\tau_I$. The constants A and τ_I are dependent upon concentration, i.e., the size of the cage and are expected to increase with an increase in concentration. Pusey has found that D can be as little as $D_o/3$ in the system investigated in his work. He did not, however, investigate the concentration dependence of the translational diffusion constant for these systems.

Although this approach is simple and can predict trends, a complete theory which can predict not just a hindrance of trans-

lational diffusion but address its complete concentration dependence as well is needed. This theory should be based on first principles using experimental constants and a single set of self-consistent parameters derived from the form of the interaction potential. Major theoretical advances have been made recently in this direction and a brief review of their major features is given in the next section.

2. Recent Theoretical Treatments of Interacting Brownian Particles

From a review by Marqusee and Deutch,[36] previous work on the concentration dependence of self-diffusion (D_s) has centered around three approaches. These approaches treat translational self-diffusion only and assume spherically symmetric potentials. The first type is based on the use of irreversible thermodynamic theory to specify the concentration dependence of D_s through the friction factor f, regarded as a perturbation on the infinite dilution Stokes formula $D_s = kT/f$. For mutual diffusion, a problem addressed more frequently, the same parameter must be specified although it is not necessarily the same as that used for D_s and in addition, the density dependence of the osmotic compressibility S(0) must also be evaluated. The osmotic compressibility, the thermodynamic driving force acting to relax concentration gradients through the mutual diffusive process, is formulated through non-ideal gas laws and partition function calculations of the radial distribution function. This approach has yielded a result which has been used frequently in the analysis of

experimental data.[37] Phillies[38] has obtained a generalization of the Stokes formula as:

$$D_m = \left[\frac{\partial \Pi}{\partial C} \right]_{P,T} \frac{(1 - \phi)}{f} \tag{29}$$

The osmotic pressure of an imperfect gas of Brownian particles, Π is given by:

$$\Pi = kTC - \frac{2\pi C^2}{3} \int_0^\infty \left[\frac{\delta \Pi}{\delta C} \right] g(r) r^3 dr \tag{30}$$

where g(r) is the pair probability of radial distribution function. In the hydrodynamic limit, the friction coefficient is found to increase with particle density due to an increase in the bulk viscosity. These indirect hydrodynamic forces are usually treated in the Oseen approximation. This approach has failed to produce a concentration dependence for self-diffusion due to direct interactions alone. In this approach, the failure seems to be a result of applying oversimplified thermodynamic theory and equating the mutual and self-friction coefficients. This fallacy is a result of neglect of the fact that in the presence of direct interactions, the particles alone suffer from an additional source of friction while the solvent itself is left unaffected. The second approach employs irreversible thermodynamics and a density expansion of the diffusion coefficient in the N-particle Smoluchowski equation. To further confuse matters, this second approach ignores the fluctuating force due to the relative

motion of the other particles on the test particle in an assumption that the configuration of the macroparticles is effectively frozen over the time characterizing the diffusive process. Thus the dynamic coupling of one particle to the others through the direct interaction is neglected thus this approach also fails to produce a concentration dependence due to direct interactions alone.

The third approach, addressed by Marquesse and Deutch[36] and Dieterich and Peschel[39] employ the Mori[40] projection operator technique on the N-particle Smoluchowski equation (SE) while Hess and Klein have treated both the SE and the more complete Fokker-Planck equation (FPE) by the same method. The projection operator technique[41] has enjoyed much popularity in recent times as a very powerful and elegant alternative in the solution of dynamical equations encountered in theoretical physics in contrast to the cumbersome cluster (virial) expansion techniques.[42] A brief review of its rudimentary features is in order to better define the nature of the results yielded by this method.

a. The Projection Operator Formalism

A mechanical property A containing the conserved slow variables Γ which evolves with time through the operator $\Omega(r)$ can be written:

$$\frac{\partial A(\Gamma,t)}{\partial t} = \Omega(\Gamma)A(\Gamma,t) \qquad (24)$$

which is a restatement of all diffusion equations. The formal solution to II.24 reads:

$$A(\Gamma,t) = \exp[i\Omega(\Gamma)t]A(\Gamma,0) \tag{24}$$

where $\exp(i\Omega(\Gamma)t)$ is called the time evolution propagator. Thus, the time evolution propagator takes the initial property $A(\Gamma,0)$ to its value $A(\Gamma,t)$ at a later time. The time dependence of the dynamic variable $A(\Gamma,t)$ is given by

$$\frac{\partial A(\Gamma,t)}{\partial t} = i\Omega(\Gamma)\exp[i\Omega(\Gamma)t]A(\Gamma,0) \tag{26}$$

and a time correlation function may be written (bra-ket notation):

$$C(t) = \langle A(\Gamma,t)A(\Gamma,0)\rangle = \langle A(\Gamma,0)\left|\exp[i\Omega(\Gamma)t]\right|A(\Gamma,0)\rangle$$

$$= \int \rho_o(\Gamma)A^*(\Gamma)\exp[i\Omega(\Gamma)t]A(\Gamma)d\Gamma \tag{27}$$

where $\rho_o(\Gamma)$ is the equilibrium distribution function $\exp(-\beta\Omega(0))$ from which the later distribution will evolve. Inspecting the form of II.27, one might be reminded of equations of similar form found in quantum mechanics where $A(\Gamma)$ may be treated as a wavefunction of vector space while the "Hamiltonian" operator for instance would be $\exp(i\Omega(\Gamma)t)$. Thus the time correlation function $C(t)$ becomes the equilibrium expectation value of the property $A(\Gamma)$ with the time evolution operator. The mathematical techniques used to treat quantum mechanical systems may be invoked to treat classical dynamical systems

when they are written in this form.

The property $A(\Gamma)$ for Brownian systems represents the coordinate and/or momentum space for the N-macroparticles, and the operator $\Omega(\Gamma)$ becomes a diffusion operator taking $A(\Gamma,0)$ into $A(\Gamma,t)$. The diffusion operators derived from Brownian systems are extensions of the Langevin equation with inclusion of the interparticle force field. Two have been derived, one by Smoluchowski and by Fokker-Planck and differ from one another:

$$\Omega(\Gamma)_{SE} = D_o \sum_i \frac{\partial}{\partial r_i} \left[\frac{\partial}{\partial r_i} - \beta \vec{F}_i(\{r\}) \right] , \quad \beta = (kT)^{-1}$$

$$\Omega(\Gamma)_{FPE} = - \sum_i \left[\frac{p_i}{m} \cdot \frac{\partial}{\partial r_i} + \vec{F}_i(\{r\}) \cdot \frac{\partial}{\partial p_i} \right] \tag{28}$$

$$+ \zeta \sum_i \frac{\partial}{\partial p_i} \cdot \left[kT \frac{\partial}{\partial p_i} + \frac{p_i}{m} \right]$$

where $\vec{F}_i(\{r\})$ is the interaction force acting on particle i due to all the other particles ($F_i(\{r\}) = \nabla_i \widehat{U}(\vec{r}^N)$). The difference between the two is the presence of momenta variables as well as position variables in the FPE, while these have been integrated out in the SE which contains only the particle positions. The SE is found to be only an approximate generalization of the more complete FPE. The SE can be derived from the FPE by performing an expansion with respect to the spacial gradients $\partial/\partial r_i$ and with respect to the inverse friction coefficient ζ^{-1}, the expansions being convergent and therefore valid only for certain values of these expansion parameters. In general, if

the momenta are not strongly damped by the media and decay on a drastically different time scale as the positions, then the two equations will not be convergent. This will be discussed in more detail later.

When applied to systems of Brownian macroparticles, the property $A(\Gamma)$ becomes the N-particle position amplitudes which can be written in recipricol space as:

$$c(q) = \sum_{i}^{N} e^{-iqr_i} \tag{29}$$

The N-particle space-time correlation function is then written as:

$$G(q,t) = \langle c(q) | \exp[i\Omega(\Gamma)t] | c(-q) \rangle \tag{30}$$

where the c(-q) term specifies translational invariance. Notice that the static structure factor can be recovered from this dynamic structure factor by setting t=0 in eq. II.30:

$$S(q) = G(q,0) = \langle \sum_{i} e^{-i\vec{q}\vec{r}_i} | \sum_{j} e^{-i\vec{q}\vec{r}_j} \rangle = 1 + \langle \sum_{i \neq j} e^{-i\vec{q}\cdot(\vec{r}_i - \vec{r}_j)} \rangle \tag{31}$$

From G(q,t) a number of collective properties may be calculated such as the mutual diffusion coefficient or pressure. Following Mori's procedures, a "memory" equation can be derived for G(q,t) written in the form of a diffusion equation as:

$$\frac{\partial G(q,t)}{\partial t} = -D(q)q^2 G(q,t) + \frac{1}{S(q)} \int_o^t M(q,t-t')G(q,t-t')dt' \qquad (32)$$

where $M(q,t-t')$ is the memory function and in the absence of hydrodynamic interactions $D(q) = D_o/S(q)$. In the absence of memory (interparticle interactions) eq. II.32 reduces to a simple Fickian diffusion equation. Equation II.32 represents a formal rewriting of the diffusion equation II.24. The effect of the interactions on the dynamic structure factor may be seen by calculating the deviation from single exponential decay as would be expected if the second term on the right of II.32 were absent. Forming the short time cumulant expansion of II.32:

$$G(q,t) = G(q,0)\exp[\, -a_1(q)t - \tfrac{1}{2}\, a_2(q)t^2 + ...] \qquad (33)$$

we have $a_1(q) = D_o q^2/S(q)$

and $a_2(q) = M(q,0)/S(q)$

These cumulants may be compared with the values obtained by the harmonically bound Brownian particle model.[2]

$$a_1(q) = D_o q^2 \quad , \quad a_2(q) = A/D_o^2 q^2$$

Thus the deviations from single exponentiality (a_2) results from the

memory the particles experience relative to the surrounding particles through the term $M(q,0)/S(q)$ and this memory effect manifests itself at longer times as it occurs with the factor t^2. In the low $q,t\to 0$ limit, the collective diffusion constant is recovered: $D_c = D_o/S(0)$. In terms of the cage or harmonically bound Brownian particle model, the memory term replaces the $A\tau_I$ term. A particle will be correlated or remember its cage for a time τ_I and will then become free of it. In actuality, there is not one relaxation time for this process but a spectrum of relaxation times. Thus the memory function cannot be given by a single exponential with decay rate τ_I, this being a restatement of eq. III.58.

Expressing the memory function or the effective diffusion constant in terms of the time evolution operator and $S(q)$ is the principal task for theroticians. One can Laplace transform II.32 to give:

$$G(q,z) = S(q)[z + \Omega(q) + M(q,z)]^{-1} \qquad (34)$$

where $\Omega(q) = D_o q^2/S(q)$

and $M(q,z) = - < \tilde{c}(q)|z - \hat{Q}\Omega(\Gamma)\hat{Q}|\tilde{c}(-q)>/S(q)$

Written in this form, the memory function contains the interparticle dynamic coupling embodied in what can be thought of as the overlap integral between interacting particles measured by the length of the

projection of their vector spaces onto each other through the projection operator $\widehat{Q}$ which is defined as:

$$\widehat{Q} = 1 - \widehat{P}$$

$$\widehat{P} = |c(q)><c(q)|/S(q)$$

$$\widetilde{c}(q) = \widehat{Q}\Omega(\Gamma)c(q)$$

To apply to self-diffusion, the single particle position amplitude must replace the N-particle function and be used along with a single particle projection operator:

$$c_1(q) = e^{-iqr_1}$$

$$\widehat{Q}_s + \widehat{P}_s = 1$$

$$\widehat{P}_s = |c_1(q)><c_1(q)|$$

The self-diffusion constant can be expressed as:

$$D_s = -\int_o^\infty \lim_{q\to 0} \frac{\partial^2}{\partial t^2} \frac{G_s(q,t)}{q^2} dt \qquad (35)$$

$$G_s(q,t) = <c_1(q)|\exp[i\Omega(\Gamma)t]|c_1(-q)> \qquad (36)$$

Laplace transformation of eq. II.36 gives:

$$G_s(q,z) = \frac{1}{z + D_s(q,z)q^2} \qquad (37)$$

Notice that unlike eq. II.34, $G_s(q,z)$ does not contain $S(q)$ explicitly as no cross particle terms may occur explicitly in a "self" calculation. This is as a result of the normalization condition t=0 in eq. 36. The generalized self-diffusion coefficient is given by:

$$D_s(q,z) = D_o - M_s(q,z)/q^2 \tag{38}$$

The value of D_s measured from the dynamic structure factor from light scattering depends on evaluation of $M_s(q,z)$ at certain limiting values.

b. Results for Self-Diffusion Using the Projection Operator Formalism

The formalism used to calculate the memory functions are quite complicated and readers interested in details should consult the references. For the purposes intended here, an evaluation of the procedures and approximations used in solving for $M_s(q,t)$ in specific cases is necessary and can be done briefly.

In compact form, $M_s(q,t)$ can be written:[1]

$$M_s(q,t) = \langle f_s(q,0)^* | f_s(q,t) \rangle \tag{39}$$

where $$f_s(q,t) = \exp[\hat{Q}\Omega(\Gamma)t]\hat{Q}\Omega(\Gamma)e^{-iqr_1}$$

These expressions are so complicated they can only be estimated or evaluated at extreme limits or in various levels of approximation. Experimental determination[33] of $M_s(q,t)$ indicate a maximum value at q_{max} and a decay rate on the order of τ_I as predicted.[43] Also in the limit $q \to \infty$, $M_s(q,t) \to 0$, falling off as $1/q$. At $q \to 0$, $M_s(q,t)$ does not

approach zero even though M(q,t) does. This is because if one lets q = 0 in eq. II.39, the memory function becomes equal to q^2 times the total force acting on a single particle due to all others, this total force being non-vanishing due to symmetry considerations with respect to nearest neighbors and their arrangement in dilute solution. At $q<<q_{max}$, collective properties represented by M(q,t) are measured where M(q,t) is quadratic in q while at $q\sim q_{max}$ it becomes linear in q.

Marqusee[36] calculated $D_s(q,z)$ based on the SE operator employing a weak coupling approximation (WCA), this having the same meaning as that employed for the reduction of S(q) in the DH approximation. His technique states that $P_s G_s(q,0) = 0$ as there are no concentration gradients present in dilute solution at equilibrium. Employing the WCA, the N-particle potential $\hat{U}(\underset{\sim}{r}^N)$ in the SE operator is first reduced in the Kirkwood superposition approximation then the equilibrium static distribution $P(\underset{\sim}{r}^N) = \exp(-\beta\hat{U}(r))$ is linearized to first order and the concentration considered dilute enough so that pairwise interactions need be considered. One can see from eq. II.32 that the memory term consists of the memory function in convolution with the true dynamic structure factor which in turn is determined by the memory function itself which embodies the effect of interparticle interactions. Equation II.32 resembles the OZ equation (II.20) which was solved approximately by the development of a closure relation. In principal, eq. II.32, just like the OZ equation should be solved

iteratively, however mathematical complexity requires that in this case instead of developing a closure relation, the true dynamic structure factor occuring in the integral be approximated by another form. One such approximation is to replace the time evolution of the fluctuating force by the free diffusion propagator $G_s(q,t) = e^{D_o q^2 t}$ which is accurate if D_o is not hindered too much by the interparticle forces. The expression for $D_s(q,z)$ becomes:

$$D_s(q',z) = D_o[1 - \frac{\beta^2 D_o C}{(2\pi)^3}\int \frac{(qq'U(q))^2}{(z + D_o(q'^2-(q'-q)^2)} dq'] \qquad (40)$$

where the second term on the right is related to the memory function. In the zero q and zero z limit, the self-diffusion constant becomes:

$$D_s = D_o[1 - \frac{\beta^2 C}{(2\pi)^3} \frac{1}{6}\int_o^\infty U(q)^2 dq] \qquad (41)$$

Once placing the expression for the Fourier transformed screened Coulomb potential into II.41, the integral can be evaluated analytically to yield:

$$\frac{D_s}{D_o} = [1 - \frac{C}{3(kT\varepsilon)^3} \cdot \frac{Q^4}{\kappa}] \qquad (42)$$

where κ is the inverse screening length. Thus the self-diffusion constant calculated from the SE in the WCA is yielded an expression linear in C. As spoken of before, the linearization of the Boltzmann equation for the equilibrium distribution is unable to reproduce

trends observed in strongly interacting colloidal systems which display peak structure. Thus this equation would be valid only for weakly interacting systems which were sufficiently dilute so that only pair interactions are important and where the potential energy is much much less than kT. Hess and Klein,[1] using a linear response formalism have calculated the self-memory function in terms of the dynamic friction factor based on the FPE. In the WCA, however, an identical result is obtained.

In a modification of this approach which in some cases can improve the results of the WCA is to apply a mode-mode coupling approximation (MMCA). In the general treatment thus far, the slow variable considered important was the position and/or the momenta of the Brownian macroions. The MMCA assumes that the next most important slow variables are the products of the first order slow variables. For the self-diffusion process, this implies that the single particle fluctuations are coupled to the fluctuations of the other particles. The tagged particle, which before was labeled $c_1(q)$, may then scatter off the randomly fluctuating internal field created by the Coulomb potential field of the other particles. In the approach of Hess and Klein,[1] this internal field is treated self-consistently within the confines of Poisson's equation using the linear response formalism to calculate the perturbation affect of the interaction. The memory function, (eq. II.34) for the N-particle system must be reduced to treat self-diffusion but this time within a MMCA. This is

accomplished by approximating the operator $\hat{Q}$ by an operator which projects products of the single particle position amplitudes onto each other. Thus $c_1(q)$ is replaced by $b(q^N)$ which represents the sum of the bilinear products and can be written:

$$b(q^N) = c_1(q_1)\sum_{i=2}^{N} c_i(-q_i) \tag{43}$$

The resulting N point correlation function is factorized into the products of two point correlation functions. In principal, the sum is represented by a single product of the type q_i, q_{i+1} which is then integrated over all pairs. For instance for $i=2$, $b(q_1,q_2) = c_1(q_1)c_2(q_2)$. The projection operator becomes:

$$\hat{Q} \approx \frac{V}{(2\pi)^6}\int d^3q_1 d^3q_2 \frac{|b(q_1,q_2)><b(-q_1,-q_2)|}{CS(q)} \tag{44}$$

This is the lowest order MMCA where higher order correlations, i.e., i,i+2 etc. are neglected. In this way, the N-body problem is solved to first order in concentration to second order in interaction. The memory function in the MMCA is written:

$$M_s(q,t) = \frac{C}{(2\pi)^3}\int d^3q' [D_o qq' h_D(q')]^2 G_s(q-q',t)G(q,t) \tag{45}$$

where $h_D(q') = \frac{(1-S(q'))}{CS(q)}$

In principal, the interactions between a particle and its surroundings

would be given by the N-particle interaction potential. The MMCA replaces this with h_D, the effective two particle potential and thus introduces the structure factor back into the memory function which is usually absent in a self-particle calculation. This expression (eq. II.45) can be described as representing the motion of a single particle, $G_s(q,t)$, moving in the fluctuating surroundings of the other particles given by $G(q,t)$. This approach better approximates the actual physics of strongly interacting Brownian particles. In terms of the simple harmonically bound Brownian particle model, the Coulomb repulsive cage surrounding each lattice site can now be treated mathematically as being in dynamic fluctuation, this fluctuation driven by the diffusion process itself.

Employing the SE operator and some assumptions, the self-diffusion coefficient may be calculated as before. Although eq. II.45 is exact for a second order interaction approximation, to be solved, further approximations must be introduced similar to those used in the simple WCA. Again, if the free particle motion is not hindered to drastically by the surrounding repulsive cage of particles, the single particle propagator $G_s(q,t)$ can be replaced by its free particle expression. Also, another approximation must be employed for the dynamic structure factor describing the surrounding particles. From eq. II.10 in the short time limit, an expression for the N-particle dynamic structure factor was calculated as a simple single exponential of the form:

$$G(q,t) = G(q,0)\exp(-\frac{D_o q^2 t}{S(q)}) = S(q)\exp(-\frac{D_o q^2 t}{S(q)}) \qquad (46)$$

Applying this short time form, which is exact for short enough times, to longer times represents an approximation as the memory function becomes active at longer times through the second cumulant. This is called the mean field approximation. Again, if the hindrance of free translational diffusion is not too great, a single exponential form with a decay rate given by $D_o q^2/S(q)$ will be accurate for all time regimes. Next, for eq. II.46 to be evaluated analytically, an expression for S(q) must be used as it relates to the direct correlation function h_D. The simplest form which enables an analytical integration is the DH structure factor (eq. II.18). Using $S_{DH}(q)$ yields the relation:

$$\frac{D_s}{D_o} = [1 - .346C^{1/2}\frac{Q^3}{(kT\varepsilon)^{3/2}}] \qquad (47)$$

this result to be compared with the non-MMCA, WCA result having only a C dependence. Apparently, this more accurate representation tends to reduce the rate of decrease of self-diffusion due to concentration as compared to the less accurate WCA approach. This result has also been obtained by Onsager[44] for diffusion in polyelectrolytes in which the friction coefficient of one kind of ion becomes much larger than all others. This result was also obtained by Harris[45] by a different method. The MMCA-WCA approach when applied to the FPE gives the same

result. In an attempt to estimate the value of D_s/D_o for a strongly interacting system, Hess and Klein[46] in deriving this result used an experimentally determined S(q) and performed the integration in eq. II.45 numerically. They found the value to be about $D_0/3$, a value much smaller than if based on the FPE as will be described next.

In the WCA, analytic expressions for S(q) were used for the analytic evaluation of the memory function integral, ones which do not reproduce trends or represent the actual physics found in strongly interacting systems. The liquidlike form found in colloidal systems exhibiting peak structure indicates that such a system is strongly coupled. Using an actual structure factor or a semi-analytic form which can accurately reproduce real ones would result in a relation valid for strongly interacting systems.

Within the confines of the MMCA, and again approximating the self-diffusion propagator by its free particle expression and the dynamic structure factor by its mean field form, Hess and Klein[1,47] have derived an integral equation for self-diffusion but this time through the Fokker-Planck equation without reducing S(q) within a WCA. They obtain:

$$\frac{D_s}{D_o} = \left[1 - \frac{C}{6\pi^2}\int_0^\infty \frac{(qh(q))^2}{(1 + S(q))}\, dq\right]^{-1} \tag{48}$$

where S(q) is the particle center static structure factor and h(q) is the direct correlation function such that $S(q) = 1 + Ch(q)$. The

concentration dependent self-diffusion constant can now be evaluated by replacing the integral in eq. II.48 by a summation and performing a numerical integration once an expression for the structure factor is available. The algorithm of Hayter and Penfold has been shown to provide a reasonably accurate model for the structure of strongly interacting suspensions, although it does have some shortcomings when applied to ultra high dilutions where interparticle interactions become weak. The concentration dependent structure factor obtained by their algorithm can now be used in eq. II.48, the parameters of which (D_K* and ψ_o^*) floated until a best fit to experimental data is obtained by iteration. By inspection, it is obvious that the concentration dependence predicted by eq. II.48 is entirely different from the C or $C^{1/2}$ forms of eqs. II.42 or 47. Equation II.48 represents the most complete and physically accurate approach available and therefore it will be used primarily in the discussion of the observations presented in this study. The ramifications of the predictions embodied in eq. II.48 as well as eqs. II.42 and 47 and their physical foundations are the topic of the concluding chapter of this work.

C H A P T E R III

LIGHT SCATTERING: THEORY AND PRACTICE

A. Background

The theory of light scattering crystallized with the work of Rayleigh[48] who formulated the mathematics applicable to a dilute non-interacting gas where the particles can be treated in a point dipole approximation in what is called the molecular scattering theory. Concurrently, development of x-ray scattering from crystalline materials created a necessity for a mathematical technology relating a complex scattering pattern to the order and physical characteristics of the material. In this regard, Fourier space analysis arose as did the form (particle) and structure factor functions. Light scattering from condensed non-crystalline substances began taking form with the work of Debye[49], Smoluchowski[50], Einstein[51], etc. who corrected the failure of the molecular theory introduced by Rayleigh which seriously overestimated the total scattered intensity of a condensed phase as a result of neglecting interference effects. In a completely homogeneous medium, there would be no scattered light as a given scattering center could always be combined with another destructively netting a zero intensity. When the scattering is modelled as arising from the statistical density fluctuations, the correct scattered intensity is predicted and the information contained in the scattering may then be related to static

and dynamic properties of the solution through statistical mechanics. The molecular approach still acts as the basis for the more complete theory when interference effects are included. Over the years, a great body of work has been compiled in an effort to characterize the nature and structure of the liquid state. Recently, this labor has been adopted and applied in the study of interacting colloidal systems. Here, in dealing with dilute suspensions the interparticle distances encountered places these systems in the regime where the use of visible light is most expedient. Beginning with a brief review of the molecular approach, the static and dynamic structure factors are derived for an N-body system. Relations applicable to the anisotropic bodies studied in this work are presented and the mathematical procedures involved in extracting relevant data described.

For instruction, consider the simplest case. Place at a position P a pointlike particle with a position vector $\vec{r}$ with respect to an arbitrary origin. Let an incoming plan wave emanating from a laser source for instance be given by $\vec{E}_i(r,t) = \hat{y}\vec{E}_0 \exp i(\vec{k}_i \cdot \vec{r} - wt)$ where the light is y polarized having a wavevector $\vec{k}_i$. If a particle is emersed in an electric field of strength E_0, its electrons will be displaced away from their unperturbed positions enveloping the nuclei of the atoms comprising the particle. The magnitude of the separation of positive and negative charge determines the effective dipole moment M such that $\vec{M} = \alpha\vec{E}_i$ where α is the proportionality constant, possibly a tensor quantity, describing the electronic elasticity of the

material. Under the alternating electric field, the electrons are accelerated at the frequency of the forcing function which can be written in terms of a forced differential equation. From classical electromagnetic theory, this accelerating charge and oscillating dipole will act as a source of secondary electromagnetic radiation and this scattered light can be measured by light detection techniques. For convenience, let the particle have an isotropic and therefore scalar polarizability such that the incoming plane wave induces a dipole only in the direction of its polarization. In the more general case where the particle is optically anisotropic, a tensor polarizability is required. This more complicated case will be presented in a later section. The scattered electric field becomes proportional to the incident electric field such that $E_s \propto \alpha E_i$. From figure 3.1, it can be seen that the scattered radiation will suffer a phase difference relative to the origin. The phase difference is related to the path length difference d_1+d_2 by $\Delta\phi = \frac{2\pi}{\lambda}(d_1+d_2)$ and from figure 3.1, $\Delta\phi = \vec{r}\cdot(\vec{k}_i-\vec{k}_s)$. In the situation considered here, the scattering process is nearly elastic, a massive particle interacting with a photon. A small degree of inelasticity results from the doppler shift suffered by the photon due to the Brownian motion. If only a change in momentum occurs with little change in energy, $|\vec{k}_i| \sim |\vec{k}_s|$. From the figure and using the law of cosines:

$$q^2 = k_i^2 + k_s^2 - 2k_i k_s \cos(\theta)$$

$$q^2 = 2k_i^2[1 - \cos(\theta)]$$

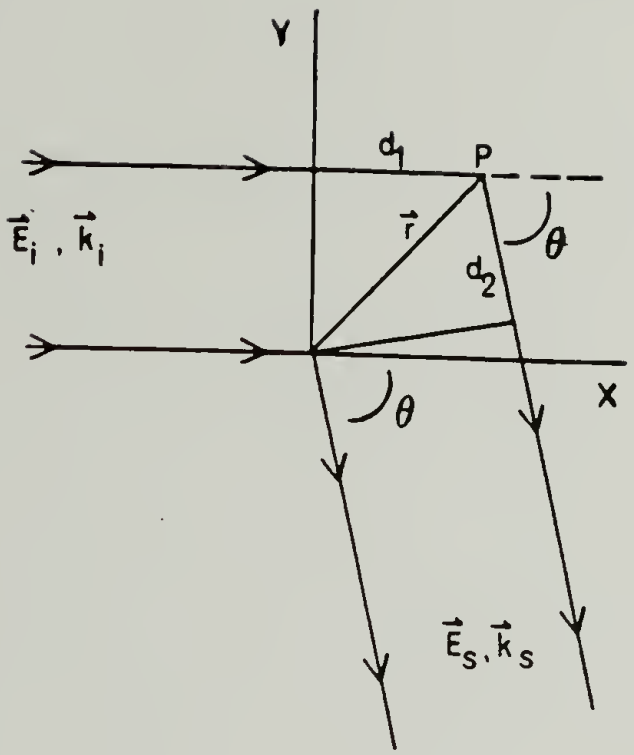

$$\vec{E}_s(q) = \alpha \vec{E}_i e^{i(\vec{q}\cdot\vec{r})}$$

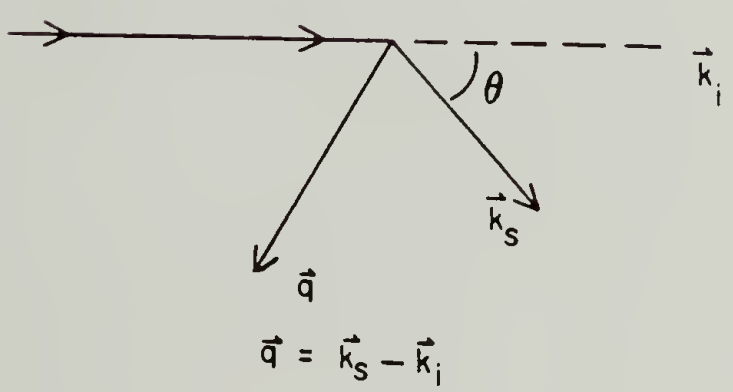

Figure 3.1 The vectoral convention used to describe the scattering process.

implies

$$q = \frac{4\pi}{\lambda}\sin(\theta/2)$$

The direction of q bisects the incident and scattered beams. Just as in rigid body kinematics q, as defined by the scattering angle θ, measures the amount of momentum transferred. The phase difference between the light scattered from the particle relative to a path taken through the origin is $\vec{q}\cdot\vec{r}$. The component of the scattered light in phase relative to the path through the origin is $\cos(\vec{q}\cdot\vec{r})$ and the out of phase component is $\sin(\vec{q}\cdot\vec{r})$. In the complex representation one writes

$$E_s(q) \propto \alpha E_i e^{i(q\cdot r)}$$

Placing the origin at the particle (r=0) or observing forward scattering (q=0), one gets $\vec{q}\cdot\vec{r}=0$, the phase factor equals 1 and no interference effects can be observed. A reciprocal relationship exists between q and r in how large the phase factor can become. This can be visualized by placing another scattering particle at the origin. The scattered intensity will now vary through the phase factor, between twice the intensity of one to zero for a given $\vec{q}$ depending upon $\vec{r}$. For a given $\vec{r}$, the wavevector can be varied through θ so that the product $\vec{q}\cdot\vec{r}$ can span ranges where observation of the angular dependence of the scattered intensity can yield information

about the interparticle spacing.

Next, consider a number (N) of identical pointlike particles with polarizability α placed in an arbitrary coordinate system (see figure 3.2). The scattered field reaching the detector placed in the far field will be a superposition of the scattered fields emanating from all the particles. From the concepts introduced above, each particle will contribute a different phase relation to the total field reaching the detector due to its position relative to the origin. The total field can be written:

$$E_s(q) \propto \sum_{i=1}^{N} \alpha \exp -i(\hat{q}\cdot\hat{r}_i) \qquad (1)$$

The intensity measured at the detector is written:

$$I_s(q) = E_s^*(q)E_s(q) \propto \sum_{i,j}^{N} \alpha^2 \exp -i\vec{q}\cdot(\vec{r}_i-\vec{r}_j) \qquad (2)$$

Thus, the major contribution to the total scattered intensity at a given q is made by those particles whose pairwise interparticle distances r_i-r_j is such that $\exp -i\vec{q}(\vec{r}_i-\vec{r}_j)$ is large. At different q values, different length scales within the scattering array are probed. A study of the q dependence of $I_s(q)$ at a low q allows evaluation of the structure of a scattering array where distant scattering centers contribute a larger portion to the total scattering while scattering centers occurring at short distances will contribute

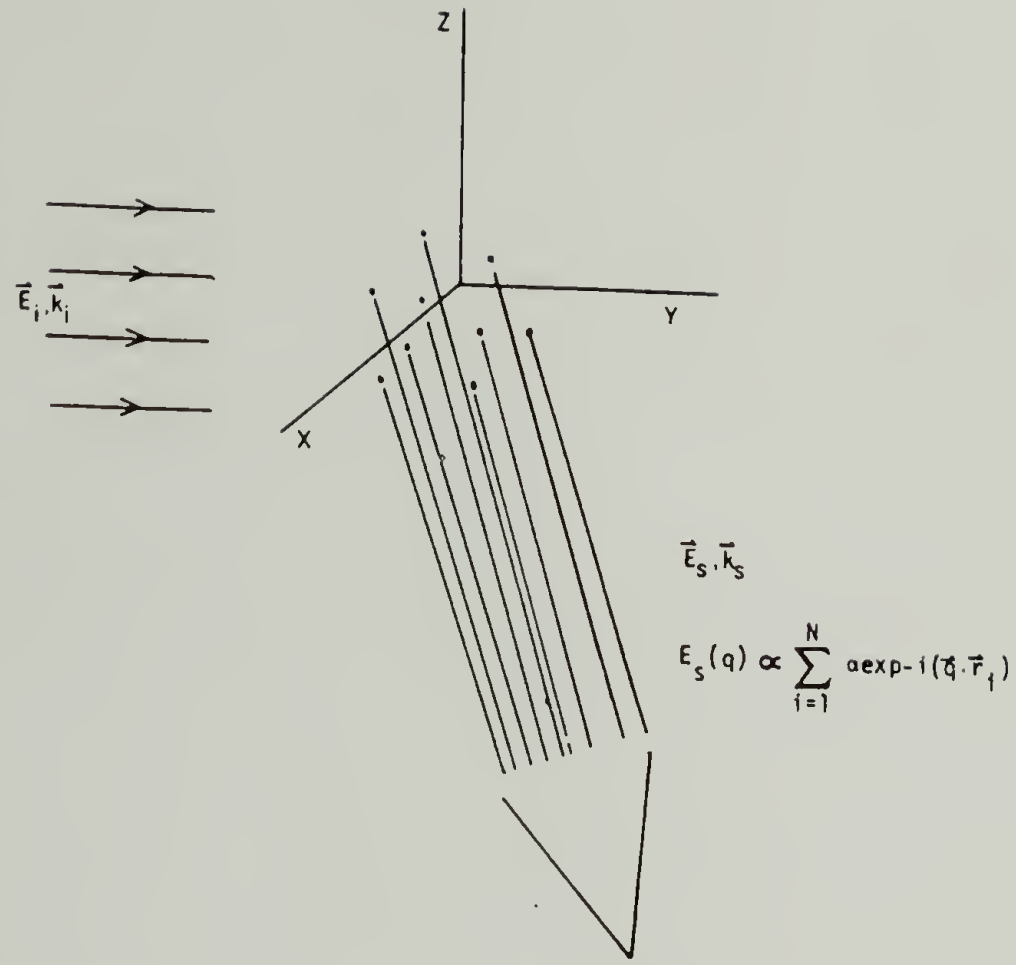

Figure 3.2 In scattering from an array of pointlike particles, the scattered electric field from each particle is determined in part by its phase relation, the total scattered field is then a summation over all illuminated particles.

more at large q. The same kind of interference effects can arise if the particle is large enough whereby interference between scattering centers on the same particle occurs (see fig. 3.3). This has important implications in the scattering from large bodies where if L is a characteristic length qL is greater than $1/20\lambda$. In this case, the q dependence of the total scattered intensity can result in the measurement of the radius of gyration of the particle which is related to the size and shape of the particle. This is detailed in the next section.

B. Dynamic Structure Factor: Autocorrelation Methods

Unlike Bragg scattering from crystals where a discontinuous set of sharp peaks are observed, the diffraction pattern from a random arrangement of scattering centers will be continuous in q, a Fourier superposition of all the particles taken pairwise which fulfill the Bragg condition. In a random array where all interparticle spacings have equal probability, a constant intensity with $\vec{q}$ is expected. In systems with only hard core repulsions for example, excluded volume effects become pronounced at high concentrations and the diffraction pattern encountered will resemble that for a "liquid like" array which is dominated by short range order. Here, interference between nearest, next nearest neighbors are responsible for the strength and position of the diffraction peaks. In a true solution such as colloidal suspension however, the particle positions are not

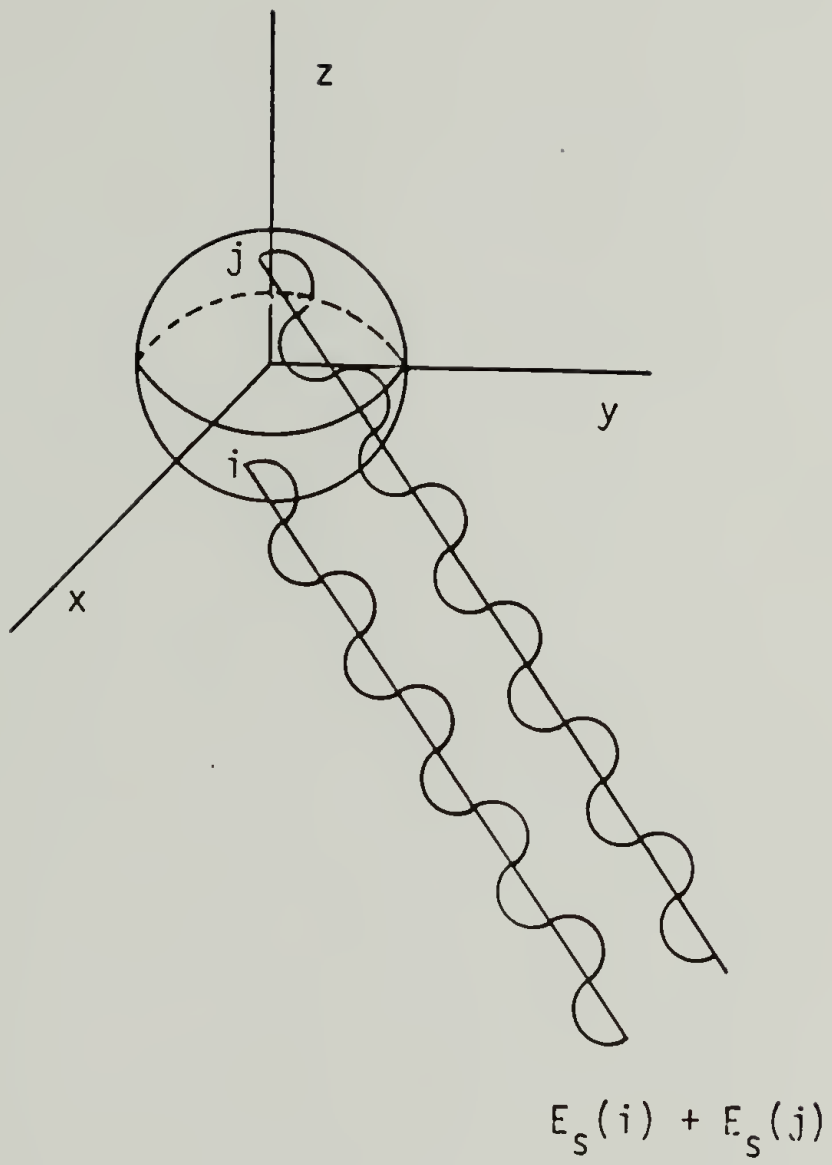

Figure 3.3 Intraparticle interference can occur if path length differences between scattering centers eminating from a particle approaches an appreciable fraction(1/20λ) of the wavelength of the incident light.

stationary with time but fluctuate as a result of Brownian forces. At a given $\hat{q}$, the scattered intensity will fluctuate in time in a way shown in figure 3.4. What is needed is a mathematical formulation which can characterize the statistical nature of this intensity fluctuation, one which can be easily related to the parameters characterizing the movement of the particles themselves. The simplest function by which a fluctuating quantity can be characterized is by its first order correlation function. An intensity autocorrelation function is written:

$$I(q,t)I(q,t+\tau)$$

where is the delay time. For an ensemble or time average, we define the intensity autocorrelation function $g^{(2)}(q,\tau)$ as:

$$g^{(2)}(q,\tau) = \langle I(q,0)I(q,\tau)\rangle = 1/2T\int_{-T}^{T} I(q,t)I(q,t+\tau)dt$$

The initial ensemble $\{r_N(0)\}$ evolves with time through the diffusion process but any configuration chosen at any time could be treated as an initial ensamble. Thus the time and ensemble averages are equivalent measurements, this being a requirement for a system to be statistically independent. This definition is exactly true only when a configuration is history independent, i.e., the system displays no memory. In general, the presence of interparticle forces results in long lived correlations between particles in their relative motions and positions where the methods of Chapter II apply. The intensity autocorrelation function is related to the electric field correlation

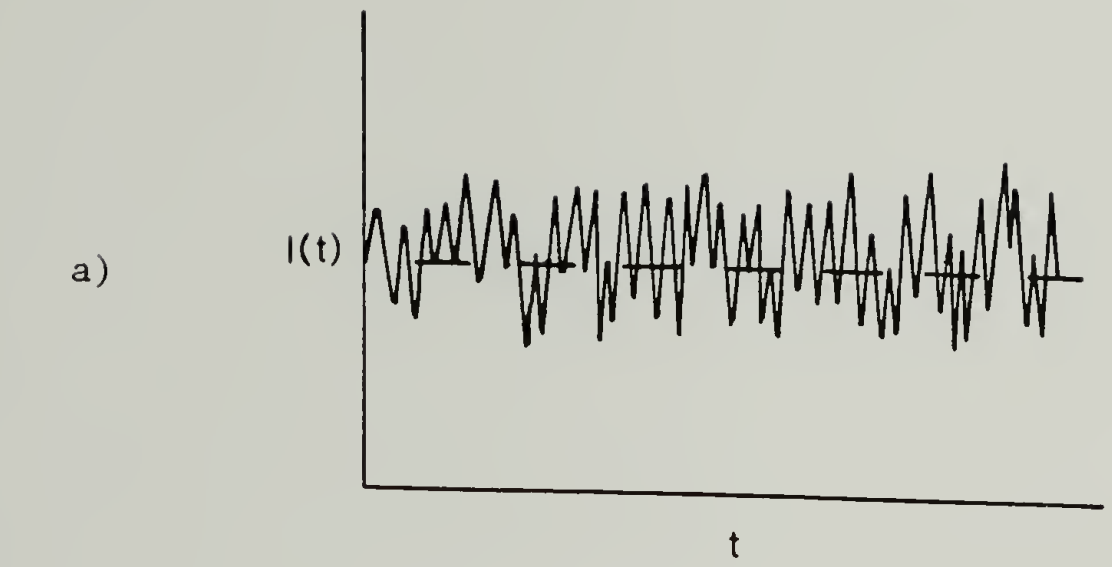

Figure 3.4 The relative motion of a large ensemble of scattering particles causes the scattered light to fluctuate in time(a). This fluctuation may best be represented by a time correlation function(b).

function which in turn is a function of the motion of the ensamble of particles through their relative change in phase. If the number of particles in the scattering volume is large enough, the scattered electric field becomes a randomly fluctuating gaussian variable as the mechanism driving the fluctuation is the Brownian process itself. This allows rewriting the intensity autocorrelation function in terms of a normalized electric field autocorrelation function $g^{(1)}$ using the positive square root function:

$$g^{(1)}(q,\tau) = < \frac{E_s(q,0)E_s^*(q,\tau)}{E_s^2(q,0)} > \tag{3}$$

so that

$$g^{(2)}(q,\tau) = 1 + |g^{(1)}(q,\tau)|^2 \tag{4}$$

Substitution of III.1 into III.3 gives:

$$g^{(1)}(q,\tau) = F(q,\tau)/S(q) \tag{5}$$

where

$$F(q,\tau) = \frac{1}{N} \sum_{i,j}^{N} <\exp i\vec{q}\cdot(\vec{r}_i(0)-\vec{r}_j(\tau))> \tag{6}$$

is the self-intermediate scattering function and

$$S(q) = F(q,0) = 1/N \sum_{i,j}^{N} <\exp i\vec{q}\cdot(\vec{r}_i(0)-\vec{r}_j(0))> \tag{7}$$

is the static structure factor which measures the spatial or time averaged correlations amongst the particles. Here, the indices i and j refer to the coordinates of the different pointlike scattering centers. If the particles are large enough ($L \sim \lambda$) so that intraparticle interference effects arise, this sum must include the coordinates of the intraparticle scattering segments $\vec{b}_i$ away from the particles center of mass position $\vec{R}_i$. Rewriting $F(q,\tau)$ and $S(q)$ by replacement of III.8 into III.6 and 7:

$$\vec{r}_i(t) = \vec{R}_i(t) + \vec{b}_i(t) \tag{8}$$

yields a modified scattering function $F'(q,\tau)$ written as:

$$F'(q,\tau)=1/N \sum_{i,j}^{N} \langle \exp i\vec{q}\cdot(\vec{R}_i(0)+\vec{b}_i(0)-\vec{R}_j(\tau)-\vec{b}_j(\tau))\rangle \tag{9}$$

With neglection of scattering between segments on different particles, i.e.,

$$\langle(\exp i\vec{q}\cdot(\vec{R}_i(0)-\vec{R}_j(\tau))(\exp i\vec{q}\cdot(\vec{b}_i(0)-\vec{b}_j(\tau))\rangle$$

$$=\langle\exp i\vec{q}\cdot(\vec{R}_i(0)-\vec{R}_j(\tau))\rangle\langle\exp i\vec{q}\cdot(\vec{b}_i(0)-\vec{b}_j(\tau))\rangle$$

gives

$$F'(q,\tau) = F(q,\tau)P(q,\tau) \tag{10a}$$

while

$$S'(q) = F'(q,0) = S(q)P(q) \tag{10b}$$

$F(q,\tau)$ has its previous definition based on a center of mass position. The form factor has the definition:

$$P(q,\tau) = 1/N \sum_{i,j}^{N} \langle \exp i\vec{q}\cdot(\vec{b}_i(0)-\vec{b}_j(\tau))\rangle \qquad (11)$$

With small particles ($L<\lambda$), $\vec{q}\cdot(\vec{b}_i(0)-\vec{b}_j(\tau))<<1$ intraparticle interference is negligible, $P(q)=1.$, and the result for pointlike particles is recovered (eqs. III.6+7). In general, a model for the distribution of particle scattering segments about its center of mass is needed for the reduction of equation III.11. The form factor for many different particle shapes has been calculated[52,53]. In the low q region where $\vec{q}\cdot(\vec{b}_i(0)-\vec{b}_j(\tau))<1.$, however, the exponential can be expanded to second order to yield a form dependent upon the second moment of the radius of gyration, R_g, which is independent of particle shape. The zero time form gives:

$$P(q) \simeq 1 - \frac{R_g^2 q^2}{3} \qquad (12)$$

and can be conveniently used to determine the radius of gyration experimentally. The form factor for large anisotropic bodies, its q dependence, and the influence of its time dependence on the self-intermediate scattering function will be discussed in a later section.

In a non-interacting system of particles, the cross terms in the double sums of eqs. III.6+7 vanish to give at all q:

$$S(q) = 1., \tag{13a}$$

$$F(q,\tau) = 1/N\langle \exp i\vec{q}\cdot(\vec{r}(0)-\vec{r}(\tau))\rangle \tag{13b}$$

This reduced form is an ideal self-intermediate dynamic structure factor describing individual particle motions. In a system of interacting particles, this result may also apply only if measurements of $F(q,\tau)$ are made where $S(q)=1.$, a situation which always occurs at high q. The scope of this work concerns the application of eq. III.13 in the high q region. Analysis of the dependence of $F(q,\tau)$ combined with a mathematical model describing the evolution of r(0) into $r(\tau)$ will yield the single particle dynamics and self diffusion constant characterizing the interacting system studied here.

As to the model describing the evolution of r(0) into r(t), consider simple Fickian diffusion. In Chapter II, it was described how the probability density function G(r,t) evolved with time under the influence of Brownian diffusion. By inspection, it should be obvious that the functions G(r,t) and F(q,t) are Fourier transform pairs and therefore F(q,t) must be subject to the same criterion. If G(r,t) is a solution to Ficks diffusion equation, F(q,t) must also be satisfied. Writing:

$$\frac{\partial G(r,t)}{\partial t} = D\nabla^2 G(r,t) \tag{14}$$

and Fourier transforming:

$$\int_{\infty}^{\infty} e^{i\vec{q}\cdot\vec{r}}\left[\frac{\partial G(r,t)}{\partial t}\right]d^3r = D\int_{\infty}^{\infty}\nabla^2 e^{i\vec{q}\cdot\vec{r}}\left[\frac{\partial G(r,t)}{\partial t}\right]d^3r$$

reduces to:

$$\frac{\partial F(q,t)}{\partial t} = -Dq^2F(q,t) \tag{15a}$$

where

$$F(q,t) = \int_{-\infty}^{\infty} G(r,t)e^{i\vec{q}\cdot\vec{r}}d^3r \tag{15b}$$

The solution to equation III.15a is trivial. The self-intermediate scattering function or dynamic structure factor may be written for non-interacting systems or for interacting systems in the $S(q)=1$ regime as:

$$F(q,t) = e^{-Dq^2t} \tag{16}$$

therefore

$$g^{(1)}(q,t) = e^{-Dq^2t} \tag{17}$$

and

$$g^{(2)}(q,t) = 1 + e^{-2Dq^2t} \tag{18}$$

As mentioned earlier D in the dilute non-interacting case can be identified as D_0, the free diffusion constant. As measurement of the dynamic structure factor using quasi-elastic light scattering probes the $t>>\tau_B$ regime, single exponential decay is expected (eq. III.16). In general, the presence of interparticle interaction causes the mechanism of evolution of r(0) into r(t) is not a simple Frickian process anymore. Particles become correlated in their positions and motions and follow non-Gaussian statistics. From the discussion of Chapter II, this complex dynamical problem encountered in interacting systems does reduce to single exponential behavior at sufficiently long times and high wavevectors, the process then described by a single diffusion constant. A strict definition as to what kind of diffusive process is being measured will be required, however.

C. Small Anisotropic Particles

In the example in the previous section, it was assumed that the scattering particles were pointlike, much smaller than the wavelength of the incident light; optically isotropic where the scattered light has the same polarization as the incident light. In general particles may have many different shapes and optical properties so that this light scattering theory must be extended in application. First,

consider the influence of optical anisotropy on the light scattered from a small particle. Without specifying a particular geometrical shape, particle fixed coordinate axes must be assigned from which the nine unique elements of the complete second rank Cartesian tensor can be described. For particles possessing a plane of symmetry or an inversion center, the tensor becomes symmetric specified by a maximum of six tensor elements. Both convenience and applicability dictate working in a principal coordinate system in which only three diagonal elements are required. For particles with cylindrical symmetry, the three elements reduce to only two, a value describing properties parallel and two equal elements describing properties perpendicular to the symmetry axis. This situation may be visualized as a polarizability ellipsoid whose principal axes do not necessarily coincide with the coordinate axes usually assigned on the basis of the symmetry of the geometrical structure. In the case of an isotropic particle with a scalar polarizability α, only polarized Vv scattered light is allowed, the static intensity given by[53] $I = Nk^4\alpha^2$. Relaxing the restriction of optical isotropy forces one to consider the tensoral nature of the polarizability. The electric field polarized in the j th direction now will induce two orthogonally polarized dipoles such that $\vec{M}_i = \alpha_{ij}\vec{E}_j$ where α_{ij} is the diagonal polarizability tensor. The value of the total scattered intensity from an ensamble and orientational averaged collection of N particles for the polarized and depolarized components are respectively:[53]

$$I_{Vv} = Nk^4[\bar{\alpha}^2 + \frac{4}{45}\beta^2] \tag{19a}$$

$$I_{Hv} = \frac{Nk^4}{15}\beta^2 \tag{19b}$$

Hv refers to the component scattered horizontally or parallel to the scattering plane. Here, $\bar{\alpha}$ is the first invariant of the polarizability tensor called the mean polarizability and β the polarizability anisotropy. These two parameters determine the static intensities of the polarized and depolarlized light scattered from a small anisotropic particle. Most particles studied in the literature are completely isotropic (β=0) or weakly anisotropic. A convenient estimate of the degree of anisotropy may be found in measuring the depolarization ratio ρ_v defined as I_{Hv}/I_{Vv}. From the relationship between α and β, it is easy to find the limiting values of ρ_v for model systems. For an isotropic particle β=0 and ρ_v=0. As the value of the anisotropy increases, ρ_v will increase from 0 to a value of 1/3 for a completely anisotropic particle.

In the isotropic case, intensity fluctuations result from relative translational motion of the particles through the phase relation $\sum_{i=1}^{N} e^{i\vec{q}\cdot\vec{r}_i(t)}$. Dynamics applicable to isotropic bodies was given in part B. As a scalar, an isotropic polarizability has the same value in any frame of reference. An anisotropic particle with a tensoral polarizability continually translates and rotates and thereby the magnitude and direction of the orthogonally polarized dipoles induced by polarized light in a fixed laboratory coordinate system

will fluctuate with time accordingly. Inclusion of a variable amplitude in eq . III.1 is required i.e.: $\alpha(t)e^{-i\vec{q}\cdot\vec{r}_i(t)}$. A correlation function will then be related to the form: $\alpha(0)\alpha(t)e^{i\vec{q}\cdot(\vec{r}(0)-\vec{r}(t))}$. The intensity may fluctuate due to two different mechanisms when optical anisotropy is involved, particle translation through the exponential factor and particle rotation through a time dependence in the amplitude factor. Each particle in the ensamble will contribute a different amount of light to the polarized and depolarized components in an amount exactly determined by the orientation of the particle fixed polarizability with respect to the laboratory coordinate system in which the incident and scattered polarizations are defined.

Expressing the magnitude of the projection on the particle fixed Cartesian tensor components onto the laboratory axies which specify the Vv and Hv scattering configurations is achieved by direct tensor transformation using the time dependent Eulerian angles ($\Omega(t) = \alpha(t),\beta(t),\gamma(t)$) and the Wigner rotation functions. Following the formalism of Berne and Pecora,[53] a generalization of eq. III.2 can be derived for the polarized and depolarized scattering from small anisotropic particles which are written:

$$g^{(1)}_{Vv}(q,t) = \langle N\rangle\langle\sum_{i}^{N}\alpha^{i}_{zz}(t)\alpha^{i}_{zz}(0)\exp i\vec{q}\cdot(\vec{r}_i(t)-\vec{r}_i(0))\rangle$$
$$g^{(1)}_{Hv}(q,t) = \langle N\rangle\langle\sum_{i}^{N}\alpha^{i}_{yz}(t)\alpha^{i}_{yz}(0)\exp i\vec{q}\cdot(\vec{r}_i(t)-\vec{r}_i(0))\rangle \qquad (20)$$

where $\alpha_{zz}(t)$ and $\alpha_{yz}(t)$ are the time dependent values of the particle fixed polarizability components of the i or j th particle surviving after projection onto the laboratory axies specifying Vv and Hv scattering respectively. Employing the spherical tensor formalism and assuming cylindrical optical symmetry, their values may be written in terms of the zeroth and second order spherical harmonics:

$$\alpha_{zz}(t) = \bar{\alpha} + \beta Y_{2,0}(\Omega(t))$$

$$\alpha_{yz}(t) = i\beta[Y_{2,1}(\Omega(t)) + Y_{2,-1}(\Omega(t))] \qquad (21)$$

where the zeroth order spherical harmonic reduces to the mean polarizability, which is independent of $\Omega(t)$ and $Y_{2,m}$ are the second order unnormalized spherical harmonics. These equations reduce to those derived for isotropic scattering when $\beta=0$. The presence of optical anisotropy causes additional correlations through these amplitude factors and an "anisotropic broadening" of the correlation functions.

For instruction, consider drawing an analogy with translational diffusion and write a Fickian law for independent particle rotational motion without rotational-translational (RT) couplings. This may be done by specifying a orientational distribution function whose argument is the Eulerian angle space $\Omega(t)$.

Defining $U(\Omega(t))$, the Fickian law is written:

$$\frac{\partial U(\Omega(t))}{\partial t} = \Theta \nabla^2 U(\Omega(t)) \tag{22}$$

where Θ is a rotational diffusion constant, a scalar for a geometrically spherical particle. Neglecting particle translation amounts to ignoring the radial part of the Laplacian operator. Equation III.22 reduces to:

$$\frac{\partial U(\Omega(t))}{\partial t} = \Theta \hat{I}^2 U(\Omega(t)) \tag{23}$$

where $\hat{I}^2$ is the angular momentum operator acting only on $\Omega(t)$. The formal solution to eq. III.23 may be written:

$$U(\Omega(t)) = \exp[t\Theta \hat{I}^2] U(\Omega(t)) \tag{24}$$

From quantum mechanical applications it is known that the spherical harmonics are eigenfunctions of the angular momentum operator. Thus eq. III.24 may be written:

$$U(\Omega(t)) = \sum_{L,M} \exp[-L(L+1)\Theta t] Y^*_{LM}(\Omega(t)) Y_{LM}(\Omega(t)) \tag{25}$$

The time correlation functions of the polarizability projections present in eq. III.20 will be related to averages of the form

$$< Y^*_{LM}(\Omega(t)) Y_{LM}(\Omega(t)) > = \exp[-L(L+1)\Theta t] \delta_{LL'} \delta_{MM'} \tag{26}$$

Replacing eq. III.26 into 21 and 20 and assuming the particles are small and display no RT coupling is yielded the expressions for the unnormalized correlation functions:

$$g_{Vv}^{(1)}(q,t) = \langle N \rangle [\bar{\alpha}^2 \exp -Dq^2 t + \frac{4}{45} \beta^2 \exp -(Dq^2 + 6\Theta)t] \qquad (27a)$$

$$g_{Hv}^{(1)}(q,t) = \langle N \rangle \frac{\beta^2}{15} \exp -[6\Theta + Dq^2]t \qquad (27b)$$

where $\bar{\alpha} = \frac{1}{3}(\alpha_{\parallel} + 2\alpha_{\perp})$

and $\beta = (\alpha_{\parallel} - \alpha_{\perp})$

If the optical anisotropy is large, $g_{Vv}^{(1)}(q,t)$ will consist of a sum of two exponentials, the relative amplitude between the two, with decay rates q^2D and $q^2D+6\Theta$, being $\frac{4}{45}(\beta/\bar{\alpha})^2$. A particles anisotropy can be weak enough so that the second order exponential in $g_{Vv}^{(1)}$ is negligible yet will depolarize enough light to allow measurement of rotational diffusion through eq. III.27b. In this case, eq. III.27a can be approximated by its single exponential isotropic component given by:

$$g_{Vv}^{(1)}(q,t) \; < N > \bar{\alpha}^2 \exp -Dq^2 t \qquad (27c)$$

This approximation will be justified in the results section of Chapter V. Analysis of the polarized dynamic structure factor easily allows for a measurement of a translational diffusion constant while

extraction of decay rates from the depolarized scattering extrapolated to zero q yields a rotational diffusion constant.

The analysis above was based on a geometrically spherical particle whose rotational diffusion constant may be described by a scalar Θ , and one whose polarizability has cylindrical optical symmetry. In general, a particles optical and geometrical symmetry may be quite complex requiring, in any particular particle fixed reference frame, all six elements of polarizability and the six possible elements of the rotational diffusion tensor. All aspects of this most general case have been revealed by Berne and Pecora.[53] In the situation encountered here, the cylindrical particle symmetry allows a particle fixed coordinate system to be chosen in which the optical polarizability and moment of inertia tensors are diagonal simultaneously (figure 3.5). The mean polarizability and anisotropy defined in eqs. III.27 are retained while the rotational diffusion tensor becomes:

$$\overset{\Theta}{\approx}_{ij} = \begin{bmatrix} \Theta_{\parallel} & 0 & 0 \\ 0 & \Theta_{\perp} & 0 \\ 0 & 0 & \Theta_{\perp} \end{bmatrix}$$

where $\Theta_{\parallel}$ describes a spinning or spiral motion about the long axis and $\Theta_{\perp}$ describes a tumbling motion of this axis. The particles studied here are not geometrically anisotropic enough to require anything but a scalar translational diffusion constant. In this

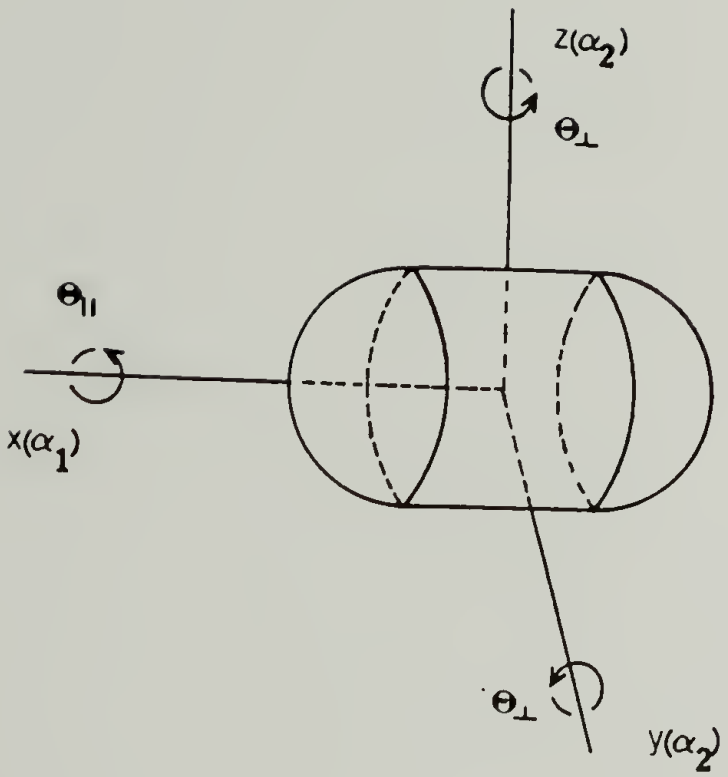

Figure 3.5 A cylindrically symmetric principal coordinate system assigned to the geometrical structure of these particles from which the coordinate axes(x,y,z), optical properties (α_1, α_2), and the rigid body rotatory motions($\Theta_{\parallel}$, $\Theta_{\perp}$) may be described.

case[53], the scalar Θ in eqs. III.27.a,b is replaced by $\Theta_{\perp}$. Symmetry considerations forbid the activity of $\Theta_{\parallel}$ in the spectral distribution. These ideal equations will serve as the basis for the interpretation of the dynamic light scattering data for this system. Due to the presence of both large size and anisotropy, qualifications in their use are needed.

1. Large Anisotropic Particles

The previous equations (III.27a&b) are valid for non-interacting weakly anisotropic small particles, or large ones viewed in the low q region ($qL<<1$) where intraparticle segmental interference and its time dependence may be neglected. In this case, eqs. III.27b&c may be justifiably and have been universally used for the interpretation of dynamic light scattering data for small anisotropic particles. These simple forms are characterized by a constant amplitude with q and decay rates linear in q^2 for all q. The principal task for theroticians is the reduction of eqs. III.20 when modified to include the effect of large particle size. the effect of particle size is introduced by defining a coordinate transformation from segment-origin position $\vec{r}$ to be defined in terms of the center of mass (CM) position $\vec{R}$ and the CM-segment position $\vec{b}$, i.e., $\vec{r} = \vec{R} + \vec{b}$. Assuming independent particles we have (and reverting to a single sum double index notation):

$$g_{Vv}^{(1)}(q,t) = \langle N\rangle\langle \exp i\vec{q}\cdot(\vec{R}(t)-\vec{R}(0))\sum \alpha_{zz}(t)\alpha_{zz}(0)\exp i\vec{q}\cdot(\vec{b}_i(t)-\vec{b}_j(0))\rangle \quad (28a)$$

$$g_{Hv}^{(1)}(q,t) = \langle N\rangle\langle \exp i\vec{q}\cdot(\vec{R}(t)-\vec{R}(0))\sum \alpha_{yz}(t)\alpha_{yz}(0)\exp i\vec{q}\cdot(\vec{b}_i(t)-\vec{b}_j(0))\rangle \quad (28b)$$

where the sums are over all the segments in a particle. The problem with reducing eqs. III.28a&b concern the exponential factors containing the argument $b_i(t)-b_j(0)$. For there reduction, approximations center around the size of this quantity or its time dependence and whether it can be separated from appearing as a product with the polarizability. Of course, this term is set equal to zero, i.e., small particles or large ones viewed at low q where these equations reduce to eqs. III.27. Unfortunately, the mathematical complications involved in introducing intraparticle interference exactly makes the writing of simple correlation functions such as eqs. III.27 impossible. The treatment of Saito[54] for large anisotropic, non-spherical (rodlike) particles if for instance worthless in its use as a tool here as it deals with unpolarized scattering and is written in the frequency domain. Furthermore, their solution is written in a undeciferable series formalism requiring evaluation of complicated sums. For instruction, consider the case of a large isotropic particle. Letting $\beta = 0$ and using eqs. III.21 and expanding $\exp iq.(b_i(t)-b_j(0))$ in terms of spherical Bessel functions one obtains:

$$g^{(1)}_{iso}(q,t) = S(x)\exp-Dq^2t + S_1(x)\exp-(Dq^2 + 6\Theta)t + ... \quad (29)$$

where $S(x)$ and $S_1(x)$ are amplitude factors dependent on q and the size and shape of the particle. The coefficient $S_1(x)$ becomes significant at higher $q(qR \sim 1.73)$ where $g^{(1)}_{iso}(q,t)$ becomes the sum of two single exponentials, the higher order exponential introducing a dependence on the rotational motion of the particle. Measurement of the decay rate of the second order exponential at high q allows measurement of the rotational diffusion constant[55] through the effect of intraparticle interference on the scattered light. Usually this quantity can only be extracted through depolarized scattering a difficult procedure if one is dealing with an optically isotropic system. Thus one may therefore state that the effect of large size introduces multi-exponentiality at high q and the decay rate extracted would be larger than q^2D as based on analysis using the ideal equations III.27a&b. This behavior would complicate the interpretation of results observable in interacting systems where a q dependent diffusion constant is also observed.

Convenience dictates recasting eqs. III.28 in a form like III.27 which include higher order terms of increasing importance at higher q. The applicability of these forms could be questioned only when necessitated by experimental observations of non-conformity. This can be facilitated by expansion on the exponentials of the argument

$\vec{q}\cdot(\vec{b}_i(t)-\vec{b}_j(0))$ for small q or small $b_i(t)-b_j(0)$. The leading term in this expansion is 1 and equations III.27 are recovered as the leading terms in the corresponding correlation functions. In another approximation the argument may be replaced by its t=0 value if the decay times of the CM and internal motions are well enough separated. Pecora[56] has restated this by letting $\vec{b}_i(t) = \vec{b}_i(0) + \vec{l}(t)$ so that if $\vec{q}\cdot\vec{l}(t) \ll 1$ over the time range studied, then $b_i(t)-b_j(0) = b_i(0)-b_j(0)$. This exponential factor may then be taken out of the summation where it occurs as a product with the time dependent polarizabilities. In this case, it will become an amplitude factor for both the Vv and Hv scattering function dependent on q and independent of time. Whichever assumption, if either, is valid will be borne out by experimental results.

In general, because the time dependent segmental positions $b_i(t)$ in fact determine the time dependence of the polarizability factors $\alpha_{zz}(t)$ or $\alpha_{yz}(t)$, separation of this factor from occuring as a product with the polarizability is unfeasible. As an exception, consider the polarized scattering from a weakly anisotropic system. Under the assumption of $\alpha_{zz}(t) \sim \bar{\alpha}$ and in the absence of RT coupling, the polarized spectrum becomes identical with that calculated for large isotropic particles which in series form is given by eq. III.29. the general form is written:

$$g_{Vv}^{(1)}(q,t) = P(q,t)e^{-Dq^2t}$$

while $$S_{Vv}(q) = g_{Vv}^{(1)}(q,0) = P(q,0) \qquad (30)$$

where P(q,t) is the dynamic form factor given by:

$$P(q,t) = \frac{1}{N} \left\langle \sum_{i,j}^{n} \exp i\vec{q}\cdot(\vec{b}_i(t)-\vec{b}_j(0)) \right\rangle \qquad (31)$$

The zero time form, just like S(x) in eq. III.29, is easily calculated from knowledge of the particles shape, i.e., rods, discs, coils, etc. The first term in an exponential expansion is related to the radius of gyration of the particle. Again, for a rigid particle of arbitrary shape the exponential argument in eq. III.31 may be expanded and rewritten in a series of spherical Bessel functions, these reducing to even simpler forms for systems of high symmetry. If the anisotropy is not negligible compared to $\bar{\alpha}$, eq. III.28a cannot be reduced beyond:

$$g_{Vv}^{(1)}(q,t) = \langle N \rangle \; e^{-Dq^2t} \left\langle \sum_{i,j}^{n} \alpha_{zz}(t)\alpha_{zz}(0)\exp i\vec{q}\cdot(\vec{b}_i(t)-\vec{b}_j(0)) \right\rangle \qquad (32)$$

As eq. III.31 will be modulated by the time dependence of $\alpha_{zz}(t)$. At low q, the result for small molecules is recovered (eq. III.27a). Deviations from this two exponential form are expected at higher q due to this exponential factor. Likewise, $g_{Hv}^{(1)}(q,t)$ cannot be reduced any further due to the coupling between $\alpha_{yz}(t)$ and the $(b_i(t)-b_j(0))$ term. Performing an expansion of the exponential would give a form:

$$g_{Hv}^{(1)}(q,t) = N\frac{\beta^2}{15}e^{-(Dq^2+6\Theta)t} + \mathcal{O}(\beta,q,t) \qquad (33)$$

where the first term on the right is the ideal form obtained by neglecting the argument $(b_i(t)-b_j(0))$, this single exponential part representing the low q dynamic spectra. The second term on the right, $\mathcal{O}(\beta,q,t)$ represents the higher order large q correction terms expressing the effect of intraparticle interference. The first term in $\mathcal{O}(\beta,q,t)$ is written:

$$<N>e^{-Dq^2t}<\alpha_{yz}(t)\alpha_{yz}(0)\sum_{i,j}^{n}i\vec{q}\cdot(\vec{b}_i(t)-\vec{b}_j(0))> \qquad (34)$$

Concerning the static properties, Van Aartsen[51] has calculated the static form factors for the polarized and depolarized scattered light for cylindrically symmetric particles of arbitrary thickness. Their forms are essentially the t = 0 values of eqs. III.32&33. Different angular dependencies are found as would be suggested by inspection of the difference between $\alpha_{zz}(t)$ and $\alpha_{yz}(t)$. Pertinent to this discussion is the form of the static and dynamic correlation functions for interacting systems. This requires further generalizations, these being the subject of the next section.

2. Large Anisotropic Interacting Particles

Deriving correlation functions for large anisotropic interacting

particles requires retention of the sums in eqs. III.20 running over different particles. Generalizing these equations for non-independent particles one obtains:

$$g_{Vv}^{(1)}(q,t) = \langle N\rangle\langle\sum_{i,j}^{N} \exp i\vec{q}\cdot(\vec{R}_i(t)-\vec{R}_j(0))\sum_{l,m}^{n}\alpha_{zz}^{i}(t)\alpha_{zz}^{j}(0)\exp i\vec{q}\cdot(\vec{b}_l^{\,i}(t)-\vec{b}_m^{\,j}(0))\rangle \quad (35a)$$

$$g_{Hv}^{(1)}(q,t) = \langle N\rangle\langle\sum_{i,j}^{N} \exp i\vec{q}\cdot(\vec{R}_i(t)-\vec{R}_j(0)\sum_{l,m}^{n}\alpha_{yz}^{i}(\underline{t})\alpha_{yz}^{j}(0)\exp i\vec{q}\cdot(\vec{b}_l^{\,i}(t)-\vec{b}_m^{\,j}(0))\rangle \quad (35b)$$

where i and j refer to the CM positions of different particles while and m refer to the segmental positions within a particle. Before considering these equations specifically with regard to large interacting anisotropic particles at arbitrary q, it is worth mentioning how other workers have dealt with equations of this type in other circumstances. A bulk of subject matter in which these scattering functions are encountered can be found in applications concerning dielectric relaxation,[58] NMR,[59] and depolarized dynamic light scattering[58] of molecular fluids. Because the authors have addressed the collective anisotropic reorientations of small molecules, they have addressed the $q \to 0$ regime for dynamic light scattering where the exponential factors in eqs. III.35a&b may be set equal to 1, while dielectric relaxation and NMR events are identically q=0 measurements. In the limit of weakly anisotopic particles, $\alpha_{zz}(t) \sim \bar{\alpha}$ to give $g_{Vv}^{(1)}(q,t) = N\bar{\alpha}^2$, thus no information concerning pair correlations of any kind can be gathered from the polarized scattering in the $q \to 0$ limit. Depolarized light scattering, on the other hand, allows measurement of the two particle correlation function $g_2(t)$ associated

with the decay of the product of the two particle second rank spherical harmonics. It is given by::

$$g_2(t) = <\sum_{i,j}^{N} \alpha_{yz}^{i}(t)\,\alpha_{yz}^{j}(0)> \;=\; 1 + <\sum_{i\neq j}^{N} \alpha_{yz}^{i}(t)\,\alpha_{yz}^{j}(0)> \qquad (36)$$

which is exactly $g_{Hv}^{(1)}(q,t)$ evaluated at zero q. It was shown earlier that the rotational diffusion constant for free rotational relaxation is related to eq. III.36's "self" particle (i = j) analogue. In the free rotation case, the decay rate is given by $6\Theta_o$. Authors involved in studying the reorientational dynamics of molecular fluids have calculated the decay rate of the orientational correlation function based on two different formats.

Schurr[58] and Keyes[60] calculate the correlation function assuming particles are Brownian diffusers, i.e., the rotational motion of particles occurs within a hydrodynamic continumm of small pointlike particles. These authors have calculated the decay rate in the short time limit and give an expression for the rotational diffusion constant of a particle interacting with its surroundings as $6\Theta_o/g_2(0)$. This result is in analogy with the short time result for translational diffusion of interacting isotropic particles given by $D_o q^2/S_c(q)$. The effect of interparticle interactions on rotational diffusion in the $q\to 0$, short time limit is given by $g_2(0)$, a parameter acting as a correction factor measuring pairwise orientational order. The long time behavior of the rotational diffusion constant of inter-

acting Brownian systems has not been investigated theoretically nor experimentally as has been the long time translational diffusive behavior of interacting particles (see Chapter II). Experimental observations of the rotational dynamics of molecular fluids have shown g_2 to be much different from 1 and to be density dependent.[61]

In a second more detailed but less useful application, Steel[62] has advanced a theory of molecular reorientation of non-Brownian diffusers. Here, the supporting background medium are particles (or a vacuum in the case of a gas) as large as the diffusing particles in question. Thus a diffusing particle undergoes great changes in orientation with few collisions with nearest neighbors. Where intermolecular forces are spherically symmetric or not important, the correlation function $g_2(t)$ decays on the time scale $\tau_o = (I/kT)^{1/2}$ where I is the moment of inertia about the axis reorienting and τ_o is a rigid rotor rotational period. Steele introduced the effect of the total intermolecular potential interaction given by $V(R^N)$ on the rotational reorientational time for cylindrically symmetric particles. The effect of the interparticle interactions are felt at longer times where the decay rate is given by $(\frac{I}{3kT}<\frac{\partial^2 V(R^N)}{\partial\psi^2}>)^{1/2}$ where ψ is the orientation angle of the molecular symmetry axis with respect to another particle and the average is over all particle encounters. The correction factor for rotational diffusion in this limit is written in terms of the angular gradients of the intermolecular potential. Steele has mentioned that the potential energy can be

decomposed and written as the sum of pairwise interactions and then the ensemble average calculated using the same g_2 factor used in the other approach. Unfortunately, the parallel between the two approaches stops here due to incompatible differences regarding application of the results to Brownian systems.

It should be pointed out at this time with regard to static behavior that a mathematical extrapolation of eq. III.35b to $q \to 0$ does yield the zero time form of eq. III.36 but in practice this is invalid. The static particle center factor $\sum_{i \neq j}^{N} \exp i\vec{q}\cdot(\vec{R}_i(0)-\vec{R}_j(0))$ itself extrapolated zero q yields the osmotic compressibility $S_c(0)$, a thermodynamic quantity which for strongly interacting Coulombic systems has a value on the order of .1. Thus extrapolation of actual data for a Coulomb system with orientational correlations to zero q would yield neither the osmotic compressibility nor the factor $g_2(0)$ but a composite of both. This observation has never been addressed in the literature so it is mentioned only as a warning.

Dielectric relaxation techniques on the other hand measure the reorientational relaxation time of a single dipole or a collection of dipoles, this dipole moment vector described by the first order spherical harmonics, the analogous correlation function given the name the Kirkwood factor g_1. This is in contrast to the description of a second rank symmetric tensor, like that encountered in anisotropic light scattering, by the second order spherical harmonics. In this case, the reorientational relaxation rate is given by $6\,\Theta_o/g_1(0)$.

Applications in static x-ray and neutron scattering from molecular liquids also employ scattering functions like eqs. III.35 evaluated at t=o but for arbitrary q. X-ray and unpolarized neutron scattering are isotropic events therefore the scattering function of interest here becomes either eq. III.35a or b without the time dependent polarizabilities. These functions can be evaluated at arbitrary q to yield the very simple form:

$$S_m(q) = P(q) + P'(q)(S_c(q) - 1) \tag{37}$$

where $S_m(q)$ is an absolute static correlation function, $S_c(q)$ the molecular center correlation function, P(q) the single particle form factor (eq. III.31) and P'(q) is an interparticle intersegmental form factor given by:

$$P'(q) = \frac{1}{N}\sum_{i,j}^{N}\sum_{1,m}^{n} \exp iq\cdot(b_1^i(0)-b_m^j(0))> \tag{38}$$

This function will differ from P(q) in that it embodies information on pairwise orientational correlations. It is related to the function g_2 but unfortunately, the relationship has never been revealed as it could bridge a gap between x-ray and neutron scattering at finite q and depolarized light scattering measurements. Employing eq. III.38, authors[63] calculate model correlation functions for various pair orientations, these predictions then compared with experimental observations. Built into the derivation of eq. III.37 is an

assumption of statistical independence between the orientation and position of a pair of particles. The effect of this is that at high q, $S_m(q)$ becomes P(q) only. Although P′(q) has significant structure and magnitude at high q, its presence is rendered negligible because it occurs as a product with $(S_c(q) - 1)$ which is zero at $q>>q_{max}$.

The presence or orientational order or a concentration dependent rotational diffusion constant is an indication of the influence of anisotropic interparticle forces. The nature of the interparticle forces encountered in uncharged molecular fluids allows the employment of assumptions such as the statistical independence between the orientation and position (O-P) of a pair of particles while position-position (P-P) and orientation-orientation (O-O) correlations are presumably present. The corresponding correlation functions in the qR<<1 limit have the form:

$$\text{O-P} = \langle \alpha^i_{yz} \exp i\vec{q}\cdot\vec{R}_j \rangle$$

$$\text{O-O} = \langle \alpha^i_{yz} \alpha^j_{yz} \rangle$$

$$\text{P-P} = \langle \exp i\vec{q}\cdot(\vec{R}_i - \vec{R}_j) \rangle$$

Unfortunately, assumptions of O-P independence is not justified for long range Coulomb forces, thus the approaches employed for neutron scattering etc., are not useful for interacting Coulomb systems. From the discussion of Chapter II section 2.1, a monopole-induced dipole

interaction would forbid O-P independence and at the very least cause a coupling of the time dependence of reorientational relaxation with the position of a nearest neighbor. It does seem reasonable that O-O correlations are absent based on arguments of the radial symmetry of the Coulomb potential in the far field. Because equations III.35 cannot be written in terms of eqs. III.39 and reduced they cannot be simplified without making unjustifiable assumptions. The presence of P-P correlations is easily identified by peaks in the absolute structure factor S_{Hv} measured from $I_{Hv}(q)$ or in the particle center structure factor measured from $I_{Vv}(q)$, just as they are seen in interacting optically isotropic systems.

To extract data from interacting anisotropic systems at arbitrary q requires writing down the static and dynamic scattering functions in forms containing principal functions and parameters of interest. At low q, QR<<1, the polarized scattering function may be reduced in the $\alpha_{zz}(t) \sim \tilde{\alpha}$ approximation to give:

$$g^{(1)}_{Vv}(q,t) = N\alpha^2 e^{-Dq^2 t}$$

$$S_{Vv}(q) = g^{(1)}_{Vv}(q,0) = 1 + \frac{1}{N}\left\langle \sum_{i,j}^{N} \exp i\vec{q}\cdot(\vec{R}_i(0)-\vec{R}_j(0)) \right\rangle \tag{40a}$$

Thus, $S_{Vv}(q)$ equals the particle center static structure factor $S_c(q)$ while the diffusion constant, D. measured from the dynamic correlation function becomes the "interacting" diffusion constant defined in Chapter II. not D_o the free diffusion constant. From Chapter II, $g^{(1)}_{Vv}(q,t)$ for $q>>q_{max}$ but qR<<1 will be a simple single exponential with a decay rate linear in q^2. In the same limit, the depolarized

scattering function becomes:

$$g^{(1)}_{Hv}(q,t) = N\frac{\beta^2}{15}e^{-(Dq^2+6\Theta)t}$$

$$S_{Hv}(q) = g^{(1)}_{Hv}(q,0) = 1 + N\sum_{i\neq j}^{N}<\alpha^i_{yz}(0)\alpha^j_{yz}(0)\exp i\vec{q}\cdot(\vec{R}_i(0)-\vec{R}_j(0))> \quad (40b)$$

where both D and Θ are the diffusion constants of the interacting particles not D_o and Θ_o respectively. One can see that in this limit, $S_{Vv}(q)$ measures the spacial correlations between particle centers while $S_{Hv}(q)$ measures a convolution related to O-P, O-O, and P-P correlations. Notice also that at $q\to 0$, $S_{Hv}(q)$ does not measure the same type of osmotic compressibility that $S_c(q)$ does. Thus at $0<q<q_{max}$ $S_{Hv}(q)$ will differ from $S_c(q)$ as a result of O-O and/or O-P correlations, the influence easily seen by comparing $S_{Hv}(q)$ with $S_c(q)$.

To generalize these results for applications at higher q, $qR\sim 1$ cannot be done without making invalid assumptions concerning the behavior of the $\hat{q}\cdot(\vec{b}^i_l(t)-\vec{b}^j_m(0))$ terms with regard to Coulomb systems. For example, one could follow the neutron scattering approach and assume the polarized scattering is isotropic and that O-P correlations are absent and obtain:

$$g^{(1)}_{Vv}(q,t) = P(q,t)e^{-Dq^2t} \quad (41)$$

and if the time dependence of translation and rotation are separated sufficiently:

$$g_{Vv}^{(1)}(q,t) = P(q)e^{-Dq^2t}$$

while

$$S_{Vv}(q) = P(q)S_c(q) \tag{42}$$

Simultaneously:

$$\begin{aligned} g_{Hv}^{(1)}(q,t) &= e^{-Dq^2t}\sum_{i,j}\sum_{l,m}\alpha_{yz}^{i}(t)\alpha_{yz}^{j}(0)\ \exp i\vec{q}\cdot(\vec{b}_l^{\,i}(t)-\vec{b}_m^{\,j}(0))> \\ &= e^{-Dq^2t}\sum_{i,j}\alpha_{yz}^{i}(t)\alpha_{yz}^{j}(0)\sum_{l,m}\exp i\vec{q}\cdot(\vec{b}_l^{\,i}(t)-\vec{b}_m^{\,j}(0))> \end{aligned} \tag{43}$$

Assuming that the polarizabilities and the segmental distribution that defines them are independent (an impossible assumption):

$$g_{Hv}^{(1)}(q,t) = e^{-Dq^2t}\sum_{i,j}\alpha_{yz}^{i}(t)\alpha_{yz}^{j}(0)>\sum_{i,j}\sum_{l,m}\exp i\vec{q}\cdot(\vec{b}_l^{\,i}(t)-\vec{b}_m^{\,j}(0))> \tag{44}$$

Employing the 0-0 term in eqs. III.39 and setting it equal to zero

$$g_{Hv}^{(1)}(q,t) = e^{-(Dq^2+6\Theta)t}\sum_{i,j}\sum_{l,m}\exp i\vec{q}\cdot(\vec{b}_l^{\,i}(t)-\vec{b}_m^{\,j}(0))> \tag{45}$$

and likewise:

$$S_{Hv}(q) = S_c(q)g_2(0)[P(q) + \sum_{i\neq j}\sum_{l\neq m}\exp i\vec{q}\cdot(\vec{b}_l^{\,i}(0)-\vec{b}_m^{\,j}(0))>] \tag{46}$$

These equations are indeed quite complicated to interpret even with the maximum number of assumptions, most of which are unjustifiable. Obviously, this is possibly a reason why authors treat the $q \to 0$ limit when doing experiments. As such, the interesting structure measured by the cross segmental or cross polarizability correlation functions have not been addressed, their presence subdued by working with either isotropic Coulomb systems or small optically anisotropic molecular fluids. Instead of pursuing this subject any further, it seems best to wait and discover what approximate procedure, if any, is best to follow once these functions are actually measured. In this way, equations can be judged with regard to their conformity with actual observations.

1. Cumulant Analysis

Dynamic light scattering data taking the form of equation III.5b can be conveniently analyzed and the decay rates extracted by the method of cumulants[40]. Dynamic structure factors are accumulated by taking the time-autocorrelation function of the photocounts reaching the detector. In the homodyne (self-beat) method, the un-normalized second order field correlation function $g^{(2)}(\tau)$ takes the form:

$$g^{(2)}(\tau) = \langle n \rangle^2 (1 + f(a)|g^{(1)}|^2(\tau)) \qquad (47)$$

where $g^{(1)}$ may represent a polarized or depolarized correlation function given by eqs. III.27c. The correlation function, for

purposes of fitting the data may take the form:

$$g^{(2)}(\tau) = A + Bg^{(1)2}(\tau) \tag{48}$$

where A and B are constants determined experimentally. In the presence of a size and shape distribution where a particles scattering power is dependent upon its size through its polarizability, a modified expression for $g^{(1)}$ is written:

$$g^{(1)}(\tau) = \int_0^\infty G(\Gamma)e^{\Gamma\tau}d\Gamma \tag{49}$$

where $G(\Gamma)$ is a continuous function expressing the light scattered by a particle with decay rate Γ. For anisotropic particles, $G(\Gamma)$ is given by:

$$G(\Gamma) \propto N(\Gamma)\alpha^2 \tag{50a}$$

or

$$G(\Gamma) \propto N(\Gamma)\beta^2 \tag{50b}$$

for polarized and depolarized spectrums respectively. For modelling purposes, the polarizability and anisotropy are proportional to the particle volume. This has precedent in the literature from light scattering studies at polymeric films of a spherulitic morphology and macromolecular polarizability/anisotropy calculations based on bond-atom polarizability/anisotropy tensor addition models. In this method, the effect of non-single exponentiality resulting from poly-dispersity or interparticle interactions are expressed by the size of

the power series expansion coefficients in the delay time of the function $g^{(1)}(\tau)$ using eq. III.49. Expansion to second order is warranted for small deviations from linearity. The expression for the intensity autocorrelation function after baseline subtraction and normalization is written:

$$\ln\left[\frac{g^{(2)}(\tau)-g^{(2)}(\infty)}{g^{(2)}(\Delta\tau)-g^{(2)}(\infty)}\right] = C_o - 2\langle\Gamma\rangle + \mu_2\tau^2 \qquad (51)$$

where $g^{(2)}(\tau)$ represents the infinite time value or baseline and $\langle\Gamma\rangle$, μ_2 are the first and second cumulants respectively. In the absence of interparticle interactions, the second cumulant expresses the degree of sample polydispersity through the second moment of the decay rate distribution. The mean value of the decay rate, $\langle\Gamma\rangle$, representing the first cumulant of eq.III.5 is:

$$\langle\Gamma\rangle = \bar{\Gamma} = \int_{-\infty}^{\infty} G(\Gamma)\,\Gamma d\Gamma \qquad (52)$$

while the second cumulant is the second moment of $G(\Gamma)$:

$$\mu_2 = \int_{-\infty}^{\infty} (\Gamma-\bar{\Gamma})^2 G(\Gamma) d\Gamma \,. \qquad (53)$$

$\bar{\Gamma}$ can be calculated exactly is the distribution of particle sizes and shapes is known. In that the distribution takes the form of a histogram, eq.III.51 must be written in terms of a summation. Specifically, from equations III.27c, the first cumulant yields the

decay rates $\bar{\Gamma}_{Vv} = Dq^2$ and $\bar{\Gamma}_{Hv} = Dq^2 + 6\Theta$ respectively. The average values of the free diffusion constants based on the equations of Perrin are given by[5]:

$$\Gamma_{Vv} = D_o q^2 \propto \frac{\sum_i N_i a_i^{-1} \alpha_i^2 G(\rho_i)}{\sum_i N_i \alpha_i^2} \tag{54a}$$

and

$$6\Theta = \lim_{q \to 0} \Gamma_{Hv} \propto \frac{\sum_i N_i a_i^{-3} \beta_i^2 G'(\rho_i)}{\sum_i N_i \beta_i^2} .$$

Here, a_i is the half length of the i th particle and $G(\rho_i)$, $G'(\rho_i)$ are functions related to the particles ellipticity. The polarizability and polarizability anisotropy are proportional to the particle volume. In the absence of interparticle interactions, it has been found[65] that quasielastic light scattering is quite insensitive to small sample polydispersity as a single exponential with a properly defined average decay rate can fit the data as well as a multi-exponential fit. From this point on, the effect of polydispersity will not be considered or discussed theoretically as the significant character of the data can be appropriately interpreted by following the behavior of an average diffusion constant.

No complete theory for $g^{(1)}(q,t)$ exists at the present which can at the same time embody all dynamical behavior of interacting particles throughout the high/low q and short/long time regimes. From

the standpoint of the cumulant analysis, the behavior occurring in these intermediate regimes would be represented by multiexponentiality. However, at the limits of these regimes, $g^{(1)}(q,t)$ reduces to a simple single exponential form lending itself to a cumulant analysis based on ideal models. A discussion of the limiting forms of $g^{(1)}(q,t)$ and the type of process being measured in the regimes to which it is applied is in order for a proper definition of extracted parameters.

In Chapter II, it was stated that quasielastic light scattering always probes the Brownian, $t>>\tau_B$ regime where $g^{(1)}(q,t)$ is always a single exponential for non-interacting particles at any q for any time:

$$g^{(1)}_{Vv}(q,t) = e^{-D_o q^2 t} \tag{55a}$$

$$g^{(1)}_{Hv}(q,t) = e^{-(D_o q^2 + 6\Theta)t} \tag{55b}$$

where D_o and Θ_o are the free or infinite dilution values of the diffusion constants dependent only on the size and shape of the particles. Unfortunately, no theory exists describing the time, q or concentration dependence of rotational diffusion therefore discussion of $g^{(1)}_{Hv}(q,t)$ will be neglected here and only experimental results presented in a later section with attempts at plausible explanations. In the presence of direct interactions a third time scale can be identified τ_I where in $\tau_B << t << \tau_I$ a particle moves as a free diffuser as the interactions are felt only at longer times approaching τ_I. This allows equating the short time behavior expansion of eq.

III.13 with that of eq. III.49:

$$g^{(1)}_{Vv}(q,t)\Big|_{t<<\tau_I} = S_c(q) - D_o q^2 t + \mathcal{O}(t^2)$$

where S(q) is again the static structure factor and $\mathcal{O}(\tau^2)$ characterizes the departure from single exponential behavior like the second cumulant due to polydispersity and/or interparticle effects. Remembering that the interparticle effects become important at longer times and that we are following the average first cumulant at these longer times, this term may be dropped from the discussion. After normalization, eq. III.56 becomes:

$$g^{(1)}_{Vv}(q,t)\Big|_{t<<\tau_I} = 1 - D_e q^2 t \qquad (57)$$

where $D_e = D_o/S(q)$. Again, in the absence of interactions, S(q)=1. and eq. III.54a is recovered. In the presence of interactions, D_e, the effective diffusion constant will have, for all q, a dependence mirroring that of S(q). This has been shown by Pusey[34] experimentally, thus, the free diffusion constant may be measured in an interacting system without the necessity of an infinite dilution extrapolation by making a short time dynamic measurement and a measurement of S(q).

More interesting is the long time, $t>\tau_I$ behavior of $g^{(1)}_{Vv}(q,t)$ and what kind of diffusive process is being observed as the particles interact. In the $q>>q_{max}$ regime where S(q)=1., self-diffusive single

particle properties are being observed however the diffusion constant is no longer given by its free value in the short time limit and the value of S(q). When $t>\tau_I$, the long lived interparticle forces begin to hinder free motion. It is in this regime and time range where the interesting concentration dependent behavior occurs. This problem was solved in Chapter II through application of a velocity autocorrelation function for a harmonically bound Brownian particle and also in the procedure by Hess and Klein. It was found that in the long time ($t>\tau_I$) and large q ($q>>q_{max}$, S(q)=1.) range, the diffusion constant D_L, based on the bound particle model is given by $D_L = D_o - A\tau_I$ and the self-intermediate scattering function takes a single exponential form:

$$g^{(1)}_{Vv}(q,t) = e^{-D_L q^2 t} \tag{58}$$

where the concentration dependence comes in through the term $A\tau_I$, a result to be contrasted with the more sophisticated result eq. III.49 of Chapter II. In the intermediate time regimes ($t\sim\tau_I$), $g^{(1)}_{Vv}(q,t)$ can be written as a weighted sum of the short time and long time forms:

$$g^{(1)}_{Vv}(q,t) = (1-A)e^{-D_o q^2 t} + Ae^{-D_L q^2 t} \tag{59}$$

and has been successfully applied to interacting systems[33]. A simple cumulant analysis in this time regime will result in a decay rate related to a weighted average of D_o and D_L and yield a large second cumulant in spite of low polydispersity. A collective diffusion constant is defined in a similar way. This kind of diffusion is a long wavelength ($q<<q_{max}$) phenomenon involving many particle

collective motions. Observed at long times, it is given by $D_c = D_o/S(0)$, where S(0) is the osmotic compressibility thus relating diffusion to the macroscopic thermodynamics of the system. Considerable discussion can be found in the literature concerning the difference between the self and collective (mutual) diffusion constants in interacting systems. As self diffusive behavior is of concern here, and has been defined previously, interested readers are referred to the references[1,2].

C H A P T E R IV

MATERIAL CHARACTERIZATION AND PREPARATION

A. Physical Characterization of This Teflon Colloid

1. Internal Structure

The contemporary way of synthesizing large quantities of polymer from vinyl monomers having low boiling points and high heats of reaction such as tetrafluoroethylene is by the emulsion polymerization process[66]. The monomer is pressurized to liquification in the presence of a non-solvent. Monomer globules form and these micelles must be stabilized against coagulation with the aid of a surface active agent. The monomer within the micelles initiated by a solvent soluble peroxide fragment, polymerizes and subsequently crystallizes, a characteristic distinguishing Teflon from most other amorphous polymers made by this technique. Initially, a rigid fluorocarbon chain deforms the liquid micelle and becomes a nucleation site along which other chains crystallize. At high monomer conversion, the particle shape becomes set and at the end of the polymerization, a rigid prolate ellipsoidal structure results, the internal structure of which consists of 90% crystalline material. The internal morphology[67] consists of pleated or folded ribbonlike crystallites and the polymer chains within them are all parallel to the long axis of the ellipsoid as shown in figures 4.1a,b. The folding of the ribbonlike crystallites is believed to be a result of agitation of the aqueous phase during

a

(I)

(II)

b

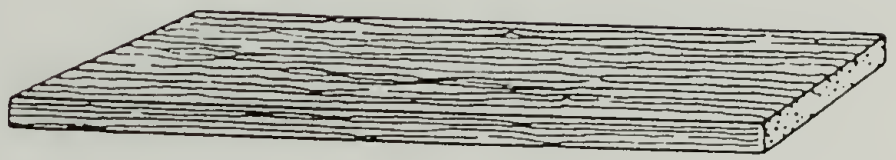

Figure 4.1 (a) Reproduction of a drawing from reference 67 showing the genesis of a Teflon particle. (b) The internal architecture of the unfolded crystallites taken from reference 67.

polymerization. The coincidence of this internal structural orientation and external geometrical symmetry makes it convenient to assign a particle fixed coordinate system about which optical properties and rigid body motions may be described (see figure 3.5). The internal anisotropy resulting from uniaxial cylindrically symmetric chain orientation is responsible for the large overall optical anisotropy. This symmetry dictates specification of only two polarizability parameters, α_1, and α_2 needed to describe the tensoral polarizability; α_1 being the polarizability along the long axis (x) and α_2 the polarizability along the other two equivalent axes (y,z) orthogonal to it. The amount of depolarized light resulting from the anisotropy ($\beta = \alpha_1 - \alpha_2$), is sufficient to allow measurement of a rotational diffusion constant characterizing rigid body rotations of these particles. Methods in this regard will be explained in a later section.

2. Size and Shape Analysis

The emulsion polymerization process always produces particles with a variable size distribution due to the nature of the globule formation[66,67]. In this case, a shape variation is present as well partly as a result of a distribution of initiation-termination step sequences which each particle experiences and local differences in agitation of the suspending fluid. This tends to direct growth rates of the spontaneously formed crystallites and their capacity for greater unidirectional orientation.

Particle diffusion and the angular distribution of scattered light are both fundamentally related to the particles geometrical size and shape. It is important, therefore, to evaluate as exactly as possible the geometrical characteristics of the particles studied here. A particle size and shape analysis was done on the bulk polymerized material through electron microscopy by Ottewill and Rance[68]. Their histogram is reproduced in figure 4.2, displayed as a long and short axis length versus number plot. The particles are shown to be quite disperse with respect to size and shape, the standard deviation in long axis length being 45% of the mean. Sizes and shapes are left uncorrelated in this analysis making it a poor way of characterizing the distribution from a light scattering/Brownian dynamics standpoint. Polydispersity effects have been shown to complicate the interpretation of the parameters characterizing measured dynamic structure factors, however, if the polydispersity is low enough, interpretation may proceed if based on expression of these physical characteristics through appropriately defined moments and averages of the distribution. In dealing with a distribution as broad and complex as that found in the bulk material, only general statements concerning bulk diffusive behavior could be made. Instructive as they may be, they might not be specific enough for purposes of a definitive, quantitative analysis. In an attempt to reach the ideal situation of a monodisperse system of particles all having the same shape, a size fractionation was undertaken to reduce the polydispersity to as narrow a range as possible. In the modifi-

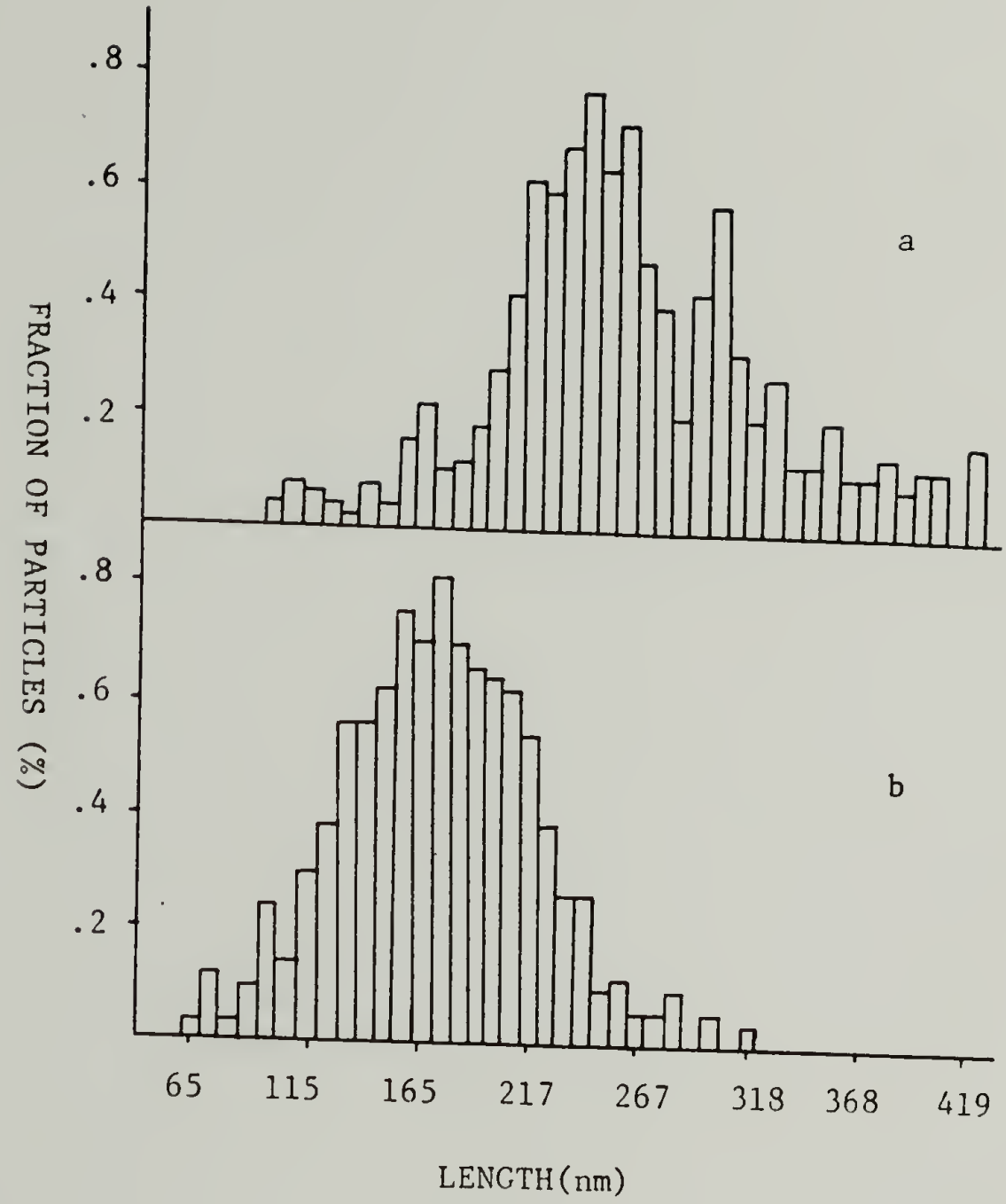

Figure 4.2 The results of a particle size analysis done on the bulk material by Ottewill and Rance taken from reference 68. a) long axis lengths, b) short axis lengths.

cation, the technique to be described later, it can be assumed that sizes greater than 3000 Å were excluded. A new size and shape analysis was then carried out on this derived material used in the actual experiment. The analysis was carried out in a way similar to that of Ottewill and Rance by performing transmission electron microscopy (JEOL model 100CS) on particles shadowed with Chromium at 60 deg. Unprotected samples were found to be extremely sensitive to radiation damage characterized by swelling, observed at the lowest intensities for times of ca. 15 seconds making the search/focus/photograph process impossible. Figure 4.3 shows a TEM micrograph of some particles used in the analysis. The particle shape is best represented by a hemispherically capped right circular cylinder instead of an ellipsoid. Shadow lengths are related to particle height and are recorded in pairwise fashion with the particle length. A histogram based on analysis of 444 , plotted as the radius of the equivalent sphere versus particle number is shown in Figure 4.4.

From a particle radius standpoint, the radius distribution of the equivalent sphere is rather narrow, the standard deviation being about 15% of the mean indicating a significant reduction of the poly-dispersity from that of the bulk material. Appropriate averages or moments must be extracted from this distribution to calculate the free values of the translational and rotational diffusion constants. Neglecting the form factor, these averages were defined in eqs. III.53a&b and are easily calculated from the length and ellipticity

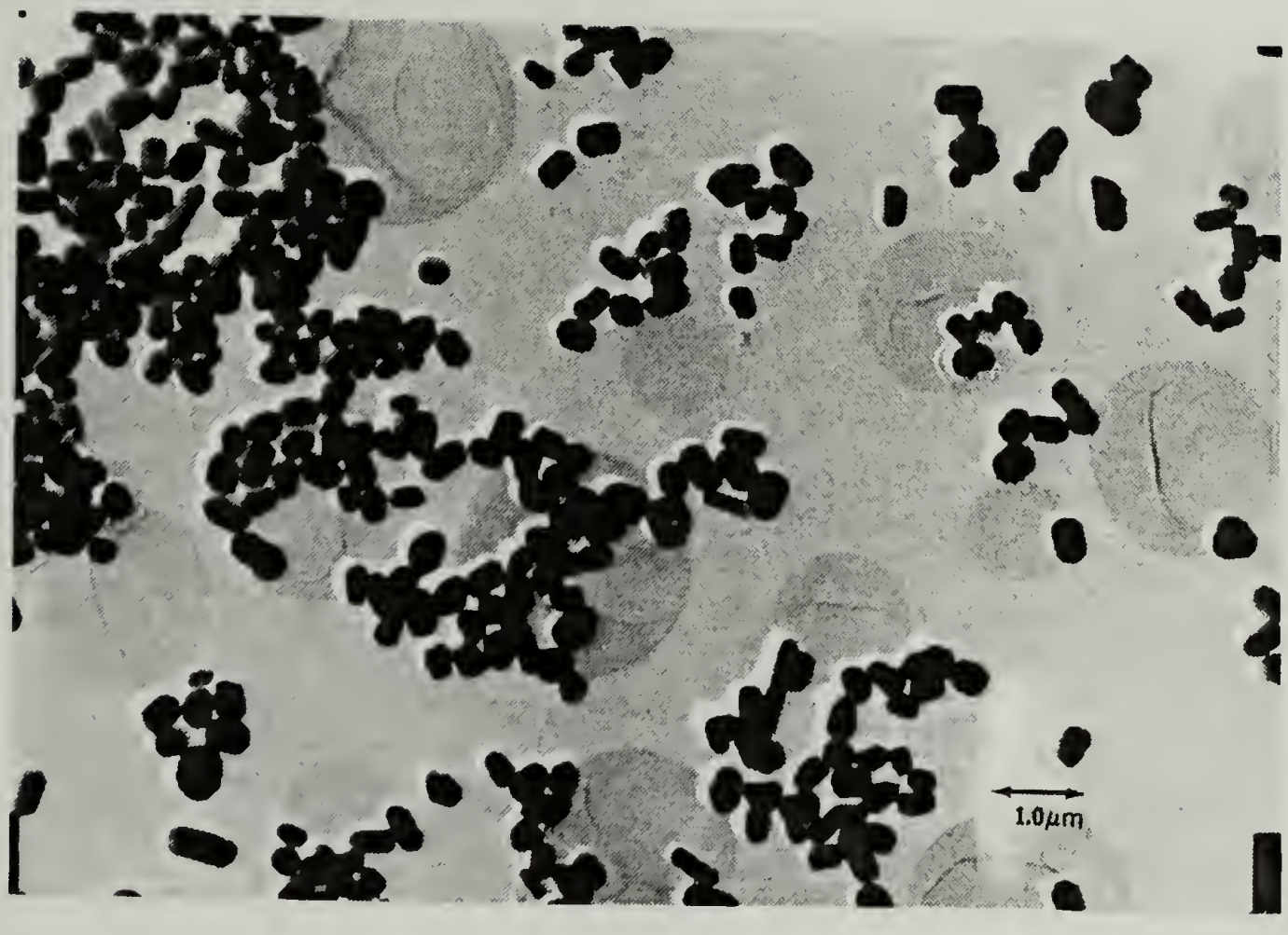

Figure 4.3 An electron micrograph of some of the Teflon particles used in the histogram analysis.

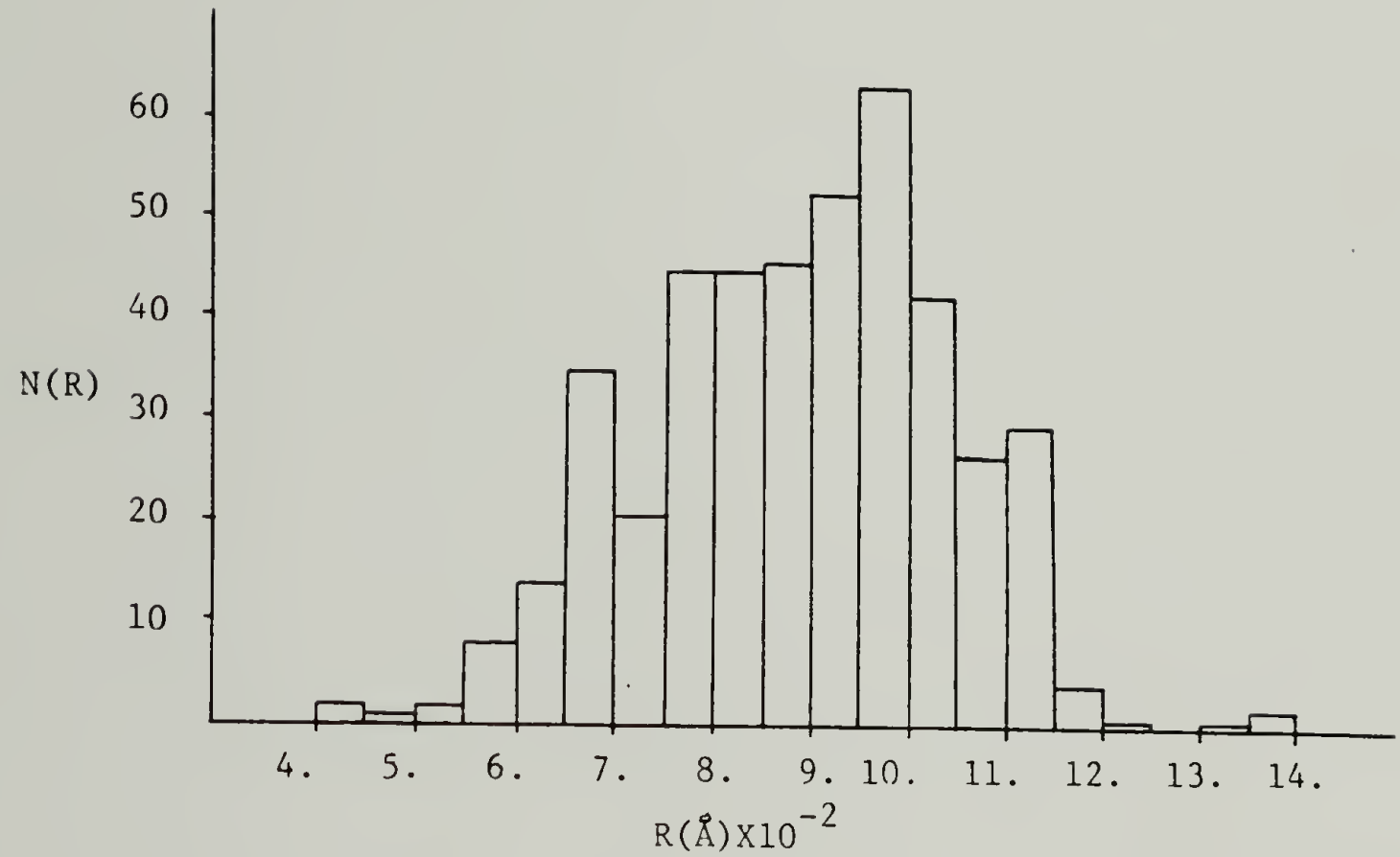

Figure 4.4 The results of the particle size analysis done on the material modified from the bulk and used in the study here. The plot is one of particle equivalent radius versus number.

data collected from the histogram analysis. The volume, which occurs as a weighting parameter, is that based on the capped right circular cylinder. The pertinent values based on the Perrin equations[5] applicable to non-spherical particles are as follows:

$$\langle D_o \rangle = 2.51 \times 10^{8} \text{Å}^2/s$$

$$6\langle \Theta_o \rangle = 1131.4\ s^{-1}$$

$$\langle V \rangle = 3.21 \times 10^{9} \text{Å}^3$$

$$\langle V^2 \rangle^{1/2} = 4.0 \times 10^{9} \text{Å}^3$$

$$\langle R_o^2 \rangle^{1/2} = 985.\text{Å}$$

These are to be compared with the values calculated with the simple Stokes-Einstein relations based on the second moment radius of the equivalent average sphere; $\langle D_o \rangle_{Stokes} = 2.48 \times 10^{8} \text{Å}^2/s$, $6\langle \Theta_o \rangle_{Stokes} = 1151.s^{-1}$. These values must be considered approximate due to the nature of performing an average over a complex distribution of shapes and sizes and in this light, the values of $\langle D_o \rangle = 2.48 \times 10^{8} \text{Å}^2/s$ and $6\langle \Theta_o \rangle = 1151.\ s^{-1}$ will henceforth be used as the calculated values of the free diffusion constants.

3. Surface Charge

In the emulsion polymerization process it is necessary to use a solvent soluble radical initiator capable of diffusing and implanting

itself into the monomer globule surface. This phenomenon causes a diffusion controlled chain termination reaction rate which is responsible for the ultra high molecular weights and narrow molecular weight distributions obtained by this method. The initiator is made soluble for use in this aqueous dispersing medium by attaching a carboxylic acid group to a peroxide fragment. To prevent aglomeration of the monomer globules into larger ones, surface active agents are commonly added into the dispersing medium to charge up the globules making them stable against decomposition. In the case of this Teflon colloid, the surface active agent used to stabilize the pre and post polymerized material was ammonium perfluorooctanate, chosen for its ability to completely wet the high critical surface tension Teflon surface. This surfactant can be removed by dialysis. The surface concentration of the permanently fixed ionizable groups which are excluded from the interior of the particle was measured by Ottewill and Rance on a dialyzed sample of the bulk colloid by conductometric titration of the hydrogen ions. It was found to be 1 particle/ 4200 $\mathring{A}^2$, about 2500e- per particle. Ottewill and Rance performed an exhaustive inquiry into the stability of the dialyized and undialyized latex. The dialyized latex, reported as reasonably stable, suffered yet from instability towards mechanical agitation and coagulation catalyized by contact with the air-water-glass interface. Any coagulated material in a sample is unacceptable for quality light scattering measurements while sensitivity towards mechanical agitation would render a sample unfilterable. Because this could not be

avoided, a .01 molar potassium perfluorooctanate (KPFO) solution was used in this experiment as the macroparticle diluent. This surfactant increases the stability of the colloid by increasing the effective valence of the macroparticles, its presence protecting the colloid from surface catalyzed coagulation and stabilizing them against coagulation during filtration. At this concentration, approximately 1/3 the critical micelle concentration (CMC), a vertically oriented monolayer at the particle surface is formed with a surface density of 1 particle/ 43 $\mathring{A}^2$, the surfactant particle physically absorbed to the surface with an energy per particle of about 15kT. This characteristic was determined previously through surface tension versus concentration studies by Shinoda.[69] This surface density was determined at an air-water interface. Documentation has shown that this property may be translated to solid surface interfaces and even a higher energy of adhesion to a Teflon surface might be expected.

The physical chemistry of surfactant solutions themselves have been studied in depth[70] both above and below the CMC, their behavior found to be very non-ideal. Non-ideal behavior below the CMC is observed even in short chain non-fluoronated surfactants, characterized by formation of dimers,[71] trimers and tight ion binding resulting in a disassociation factor of 1/2 in the case of KPFO. An unusually large disproportionality between the mobilities and sizes of the ions and coions, the differential microscopic solubilities between the carboxylate group and the 15 $\mathring{A}$ long fluoronated chain and the large

delocalization of charge along this backbone due to the electronegative fluoroenes adjacent to the carboxylate group are also other sources of non-ideality. In this regard, the charge distribution surrounding each colloidal particle is therefore expected to be non-ideal, the DH theory unable to predict the Coulomb potential. Knowing the average surface area per particle ($4\pi R_o^2$) and the surface charge density, a potential particle valence of 2.4×10^5 e- is calculated, the charge density itself being some 30 times greater, the particle valence some 10K greater than what has been reported for the well known charged polystyrene latex systems. Thus it is expected that the discussion of Chapter II Section B.1 would apply for the determination of the Coulomb potential around a large macroparticle, highly charged by a surrounding atmosphere of large sized, chemically non-ideal surfactant molecules. Again, the effect of using the full Poisson equation for the calculation of the Coulomb potential surrounding a highly charged macroparticle is the simultaneous reduction of the effective valence of the macroparticle and an increase in the effective Debye screening length. The renormalized DLVO parameters κ^* and ψ^* will describe the potential at large r, the tail end where the potential field of one macroion interacts with the atmosphere of another. Evidence of the resulting interparticle interaction is found in the observation of structure in a colloidal suspension and lowered diffusion constants, this being the main feature of this work. Parameters specifying the magnitude of the renormalized DLVO potential parameters will be discussed in a later

section.

Measurement of the bulk viscosity of the surfactant solution was carried out and demonstrated the absence of an electroviscous effect[72] as the solvent viscosity had nearly the same value as that of pure water (η_o = .008904P). Only a 3% increase over the solvent viscosity is observed in a concentrated suspension some 1000 times (ϕ = .013) larger than the highest concentration used in the light scattering experiment. This is expected as hydrodynamic effects between macroparticles in colloidal suspensions are expected to scale with the volume fraction of the macroparticles through the Einstein relation[4]; $\eta = \eta_o(1 + 2.5\phi)$. The usual assumption therefore, common in the treatment of particle solutions at low density, is to neglect hydrodynamic effects in the discussion and interpretation of dynamic and static properties.

B. Sample Preparation

1. Samples

The concentrated bulk Teflon sample was diluted and twice filtered with a .3μm Millipore filter. This was then centrifuged down twice, not long enough to settle out all the colloid but long enough to collect a good portion at the bottom of the centrifuge tube, the supernatant then discarded. This procedure describes the attempt at modifying the polydispersity by excluding sizes over 3000 Å and

discarding small sizes within the supernatant after centrifugation. The material collected after centrifugation was redispersed with doubly distilled water (superwater) and placed in dialysis tubing (MW cutoff 12K). This solution was dialyzed against a 70X excess of a concentrated NaOH solution (pH $\sim$11), exchanged about every 5 hours 8 different times, then dialyzed against 1 Meg ohm singly distilled water 3 times (70X excess) whereupon the water had resistance greater than 200 K ohm. At this point, the fractionated material was void of surface active agent. Different quantities of this dialyzed colloid were immediately placed into 10 ml. volumetric flasks and diluted with .01 molar KPFO.

Five ml test tubes were used as sample containers and were precleaned in the regular way with superwater until no dust or bright scatterers (sparklers) were seen scattering strong laser light at an angle of 30 deg. for intervals of less than 30 sec. Filters of pore size .3μm were also cleaned with superwater until no dust was seen in the effluent. The colloidal solutions were then filtered with these cleaned filters once again into the cleaned test tubes to remove any residual dust or coagulated material. These samples were capped with parafilm. Solutions remained stable, remaining dispersed for up to 1 year.

2. Concentration Measurements

Due to the non-quantitative method of sample preparation and the very low concentrations being used, sample concentrations were determined via turbidity measurements after the dynamic light scattering experiment. This was the only feasible method in its determination as the sample volumes were only about 2 ml. and were present at high dilution. A turbidity versus concentration curve was made from data collected on a Beckman Acta MIV spectrophotometer at a wavelength of 514.5 nm and was found to be linear throughout a large range of concentrations. Linearity is important in evaluating the importance of multiple scattering phenomenon. Linearity was observed at concentrations much greater than the largest one used in the light scattering experiment. The extinction coefficient was found to be ε_o = .08577 ml/mg. Turbidity and relative scattered intensity measurements were actually taken on a number of prepared samples only some of which were used in the dynamic experiment. The presence of dust or coagulated material in some of the samples was indicated by visual inspection of sparklers in the scattering volume or a jumpy photocount rate. In a final screening of bad samples, these were discarded. A number of the samples used, the three lowest in concentration were too low in concentration to obtain values accurately through absorbance. For these, concentration was determined by their relative scattered intensity with respect to samples of higher concentration which were analyzed through turbidity. A total of eight samples of increasing

concentration were used these values tabulated in Table41. In Table 4.1, the concentrations are expressed in weight conc. (mg/ml), number conc. or volume faction related to weight conc. through the particle density (ρ=2.275 g/cm^3) and the volume of the average equivalent sphere (R_o = 915. $\mathring{A}$).

C. Multiple Scattering

The theories presented earlier describing the light scattering process were based on the simplest case of strictly first order scattering called the Born approximation. In this approximation, light is scattered only once on its way through the sample to the detector. The presence of higher order scattering has been shown to seriously distort the normal shape of the dynamic structure factor and the angular distribution of the static intensity. Multiple scattering and collision induced (interparticle) scattering cause a depolarization of the normally completely polarized scattered light which if present in a system of anisotropic particles may interfere with the interpretation of information contained in the depolarized component arising from anisotropy alone. Addressing the validity of the Born approximation is in order as multiple scattering has been shown to be of considerable importance in systems of concentrated, large interacting particles. Recently, studies[73] have revealed certain characteristics of multiple scattering which make it easy to identify if present. Pusey[34] has stated that the probability of a

Table 4.1

A list of the weight concentrations(C_m), number concentrations(C), and volume fractions(ϕ) for the eight samples analyzed in this study.

Sample	C_m (mg/ml)	$C \times 10^{15}$ (n/A^{o3})	$\phi \times 10^4$
1	.00533	.729	.0234
2	.0101	1.38	.0444
3	.0235	3.22	.1033
4	.0310	4.24	.136
5	.0364	4.98	.160
6	.1120	15.20	.490
7	.227	31.10	.998
8	.310	42.38	1.360

doubly scattered event (the largest portion of the multiply scattered hierarchy) is roughly $(1-T)^2$ where T is the transmittance. The highest concentration used here has a transmittance of 94% implying the effect is small. Traditionally, a test for multiple scattering is the onset of visual turbidity in a solution. In all samples used here this did not occur even though the particle size is quite large. Linearity in the absorbance and relative intensity versus concentration data is additional evidence suggesting the absence of multiple scattering. Sorenson[73a] and Herpigny[73b] have discovered that the decay rate of the multiply scattered component is independent of wavevector suggesting that the depolarized component (arising from anisotropy alone in this case) if it consisted entirely or in large proportion of multiply scattered light, should exhibit no q dependence. This is not observed here (fig. 5.4). The different time dependence of the multiply scattered component comes into the dynamic structure factor as a non-single exponentiality in both the polarized and depolarized components. Combined with the measured second cumulants, reflecting particle size polydispersity and the effect of a time dependent diffusion, they do not suggest any influence of multiple scattered light by virtue of the size or q dependence. It has been shown[34] that the effect is minimal in the long time, $q>>q_{max}$ regime, this being the regime of concern here. Lastly, it has been observed that the decay rate of the multiply scattered component usually extracted in isotropic systems from the depolarized scattered light increases with concentration. To the extent that multiple

scattering is present in the depolarized component of this anisotropic system, the strongly decreasing trend of 6Θ with concentration combined with the other evidence allows us to discount the effect of multiple scattering entirely from the interpretation of the dynamic structure factors.

In the measurement of the static intensity, excess intensity due to multiple scattering is found at the lower, $q<q_{max}$ wavevectors. The presence of this excess intensity can change the shape of the structure factor and certain aspects of the information contained therein. This possibility will be discussed in the next chapter.

C H A P T E R V

DATA ACCUMULATION AND RESULTS

A. Static and Dynamic Data Acquisition

Measurement of the structure factor, S(q), of this colloidal system was undertaken in an effort to discover the extent and nature of the interparticle interaction. The measurement of the total intensity was made on a spectrometer capable of making both static and dynamic measurements. This apparatus has been described in detail elsewhere[74]. The laser source was the 5145Å line of a Spectra-Physics Model 165 Ar laser. The vertically polarized beam was passed through a Glan-Thompson polarizer to insure complete extinction of the residual horizontal component. The photon counting signal from the phototube was passed as input to a Langley-Ford Instruments DC-64 (64 point) correlator interfaced to a Tektronix 4051 microcomputer, facilitating easy access to the data. This instrument is not designed to make measurements of absolute intensity below angles of 20 deg. due to the presence of stray light effects. This stray light however, is mostly vertically polarized and much of it can be eliminated in the Hv configuration. Precision measurements of the depolarized absolute intensity may then be made in the low q region to angles of 1.5 deg. It is in this low q region where particle center correlations are reflected by peaks in the absolute static structure factor and where the inter-intra segmental factor $\vec{q}\cdot(\vec{b}_l^{\,i}(0)-\vec{b}_m^{\,j}(0))$ may be small enough

to neglect. The background Hv intensity, which includes a small amount of depolarized stray light and a dark count, is only a small percentage of the depolarized scattered light arising from the anisotropic particles in solution so and it can be subtracted out with the use of a blank, clean H_2O. The index matching fluid (H_2O) bath in which the sample tube is emersed, helps to reduce the amount of stray light. The bath was cleaned and adjusted so that the laser beam focused to a diameter of 75μm transverses its diameter being careful to avoid defects in the glass container. After preparing a dust free blank, absolute intensity measurements were carried out on samples 5 and 7 at 25 ^{o}C. Starting at 1.5 deg., successive angular measurements were made of the absolute intensity of the blank and sample up to 80 deg. For each data point, seven measurements of the intensity were taken for a 5 second duration. This process was repeated when required to remove occasional spurious data.

Dynamic homodyne correlation functions associated with the I_{Vv} and I_{Hv} intensities were measured in the $q>q_{max}(20^{o} < \theta < 130^{o})$ range, usually equally spaced in q^2. Each correlation function is constructed from 64 data points, the first 56 of which are consecutive, separated by $\Delta\tau$ while the last eight are delayed from the 56 th by $70\Delta\tau$ whose average represents the measured baseline. The measured baseline never differed from the baseline calculated from the photocount rate by more than 1%, indicating the correlation function had decayed completely for the sample time chosen. The first channel

is customarily discarded from analysis due to the presence of photomultiplier after pulsing. In the measurement of a long time correlation function, sample times ($\Delta\tau$) were used such that the function decayed to e^{-1} in about the first 15 channels. This insured that the function had decayed entirely in times shorter than those covered by the last eight. A few short time measurements were made in order to probe dynamics in the $t < \tau_I$ regime. Pusey[13] estimates τ_I to be approximately 10^{-4} sec. so that this region is covered by only the first 5 channels in a long time measurement. To measure the correlation function in this short time region, sample times were chosen such that these early times are spanned by all 64 channels. Most of the time, 19 correlation functions were taken at each angle and were collected for a length of time such that the runs when summed had a baseline of around $1.X10^8$ counts. For the Vv and Hv measurements, the polarization was selected accurately by adjusting the analyzer at each angle to the proper extinction using isotropic polystyrene latex spheres, minimizing the intensity for Hv and minimizing the Vv intensity as viewed through the analyzer (Vv) and then through crossed polaroid film. Analyzer misadjustments would allow a leakage of the orthogonally polarized component of the intensity and could cause a distortion of the correlation function through introduction of a second decay rate with small amplitude. A double exponential decay would result, the decay rates differing by 6Θ. This possibility was tested for and found to be negligible as first and second cumulant values were unchanged with slight changes in

the position of the analyzer away from its ideal position.

A constant temperature bath was used throughout the entire experiment set a 25 ^{o}C. Angles were measured to high precision, approximately .3 ^{o} at a maximum.

B. The Structure and Form Factor

Measurements of the depolarized static intensity were carried out for samples 5 and 7 between 1.5 and 80 deg. The standard deviation of the total count rate of both the sample and blank were mostly below 2.5%. The difference between the count rates of the blank and sample, corrected for photomultiplier saturation, was calculated and multiplied by sin(θ) to normalize the data with respect to scattering volume. The stray light effect was significant in the depolarized spectra to the extent that the background intensity was less than 2.5% of that of the sample at 6^{o} tending to zero above while below 6^{o} it varied between 2.5% up to 17% (only a few angles) at lower angles. This stray light, however, was subtracted out by the use of a blank. In figure 5.1 is shown the absolute static structure factors $S_{Hv}(q)$ for sample 5 and 7, displayed as a plot of $S_{Hv}(q) = I_{Hv}(q)/I_{Hv}(q_{max})$. The solid curves displayed with them are the particle center structure factors, $S_c(q)/S_c(q_{max})$, calculated from the Hayter-Penfold algorithm using the actual particle densities for samples 5 and 7 and the average particle radius (R_o = 915. Å). This facilitates easy comparison between the measured absolute static structure factors,

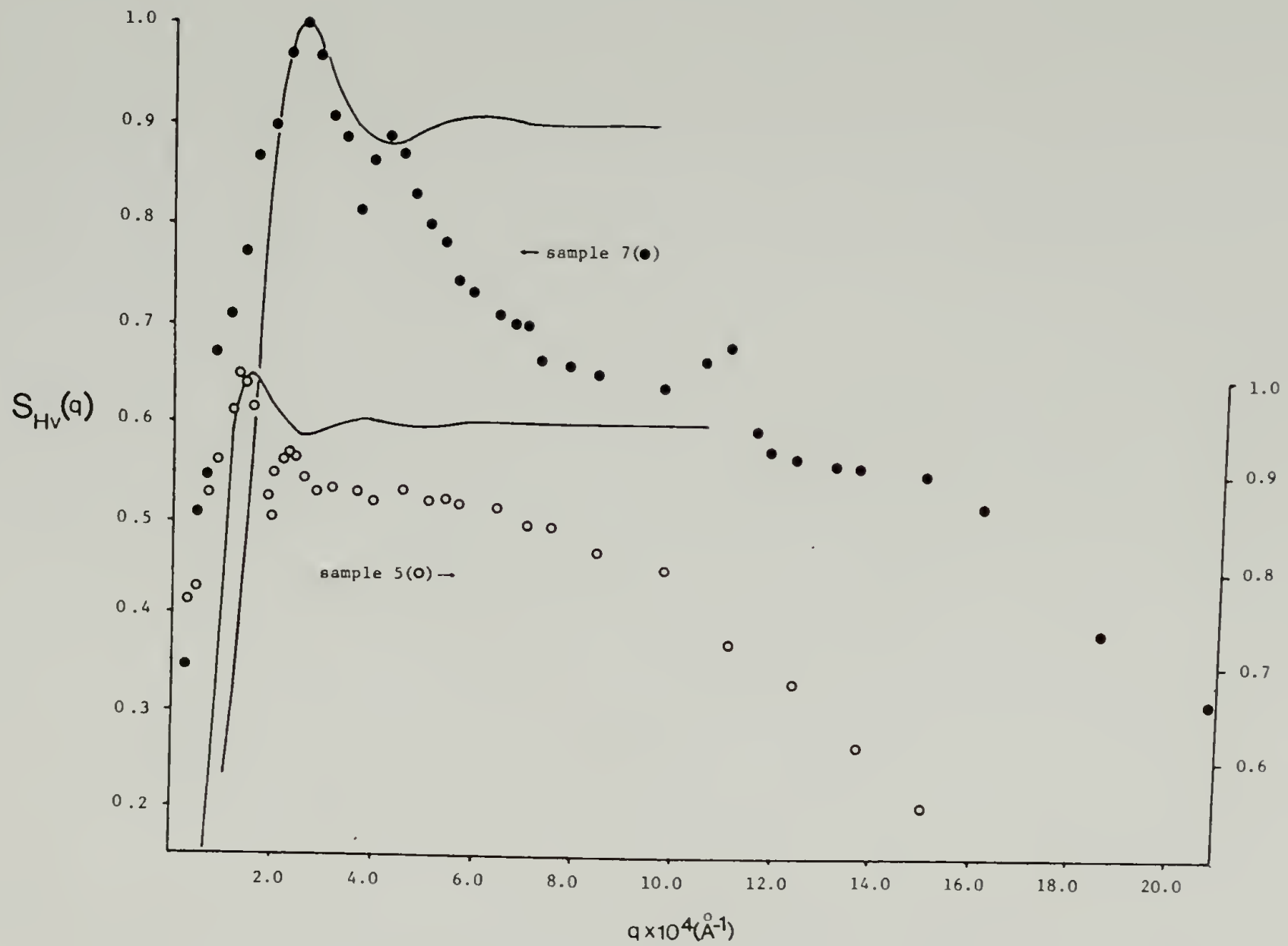

Figure 5.1 Plots of the absolute static structure factor for samples 7(●) and 5(o) plotted as $S_{Hv}(q)/S_{Hv}(q_{max})$. The smooth curves superimposed with them are the particle center structure factors calculated by the method of Hayter and Penfold using the actual particle densities and the best fit DLVO parameters($D\kappa^* = .03$, $\psi_o^* = 29.$ mV).

$S_{Hv}(q)$, measured at different particle densities and comparison of $S_{Hv}(q)$ which contains all interparticle correlations with what would be observed if only particle center correlations were present $S_c(q)$. The same DLVO parameters for both samples were used to calculate $S_c(q)$ by the Hayter-Penfold algorithm. These parameters were chosen by best fit iteration to match the shape and magnitude of the D_s/D_o versus concentration curve, the form predicted by the Hess and Klein theory (eq. II.48). This procedure is described in more detail in the section concerned with dynamic properties.

To interpret the data in Figure 5.1, two observations must be addressed. The difference between the two curves indicates the density dependence of the interparticle correlations while the difference between $S_{Hv}(q)$ and the structure factor containing only correlations between particle centers, $S_c(q)$ indicates the presence of correlations of the O-P and O-O type superimposed with P-P correlations.

Firstly, it should be recognized that the peak structure in $S_{Hv}(q)$ indicates correlations in the positions of the macroions, the main maximum (q_{max}) indicative of the first nearest neighbor shell. A weaker second nearest neighbor shell is also observed. The main maximums occur at q_{max}(sample 5) = 1.27×10^{4} $\mathring{A}^{-1}$ and q_{max}(sample 7) = 2.55×10^{-4} $\mathring{A}^{-1}$, indicating radial symmetric interparticle forces strong enough to affect a weak short range ordering of the particles at spacings as large as 30 particle diameters. The behavior of these

peak maximums with regard to their position in q with concentration is no different than that observed in the polystyrene latex systems.[32,33] The three dimensional random close packed structure simply expands in 3 dimensions upon dilution. However, at ultrahigh dilutions, a looser structure than the random close packed form exists. The mean interparticle spacing, r_{max}, is related to the position of q_{max} for a random close packed structure by the relation[74] $r_{max} = 1.22(2\pi)/q_{max}$, where the constant 1.22 is that calculated theoretically for a random close packed structure. The r_{max} values calculated from the q_{max} peak positions are 60358. and 30060.Å for samples 5 and 7 respectively, to be compared with the average interparticle spacings calculated from $C^{-1/3}$ of 59405 and 29075 Å, these representing average values expected for a simple cubic lattice. This close match is very pleasing considering the system displays a hard sphere radius and therefore particle charge polydispersity. The agreement with the position of q_{max} as calculated from the Hayter-Penfold algorithm for the particle center static structure correlation function is very good for the sample of higher concentration (sample 7). The agreement with sample 5 is not quite as good, however, the Hayter-Penfold algorithm even with its low density rescaling correction has been shown[75] to overestimate the amplitude of the peak structure in isotropic monodisperse systems and to overestimate the position of q_{max}, the agreement found to be poorer for lower concentrations. This observation has also been recognized for other structure factor algorithms.

For the interpretation of the absolute static structure factors, $S_{Hv}(q)$, convenience requires identifying three different q regimes and addressing each one separately, following the outline of the theoretical section.

For $q<q_{max}$, $qR<<1$ and as such the argument $\vec{q}\cdot(\vec{b}_l^i-\vec{b}_m^j)$ may be neglected in the equation for $S_{Hv}(q)$ at low q. In this case, $S_{Hv}(q)$ takes the form of eq. III.40b. The absolute static structure factor now differs from the particle center analouge, $S_c(q)$, by the presence of the cross interparticle polarizability terms. In comparing $S_{Hv}(q)$ with $S_c(q)$, an indication of significant excess intensity in the $q<q_{max}$ region. This deviation due to the cross polarizability terms is evidence of pairwise orientational correlations. As these terms occur as a inseparable product with the particle position factor, it cannot be concluded through this data alone if the correlations are O-P and/or O-O in nature. Measurement of $S_{Hv}(0)$ could not be done directly due to the presence of an unrectifiable small amount of residual intensity which leaks through the analyizer at perfect forward scattering (zero q). Extrapolation of $S_{Hv}(q)$ to zero q would apparently yield the values .6 and .3 for sample 5 and 7 respectively. As mentioned earlier, $S_{Hv}(0)$ is a composite quantity without a clear definition, therefore it will be addressed no further. The presence of the cross poalrizability terms is certainly responsible for the excess intensity at $q<q_{max}$ and causes the $q\to 0$ intercept of $S_{Hv}(q)$ to be much larger than what would be predicted in

the absence of these terms by $S_c(0)$.

With regards to the introduction of charge polydispersity into the system, documentation has shown [76] the shape of the curve in the $q<q_{max}$ region to be virtually unchanged. Introduction of charge polydispersity, as modelled by an equivalent polydisperse hard sphere fluid reduces the height of q_{max} while at the same time washes out the higher order maxima and minima.

Consider next the $q\sim q_{max}$ region of these curves. It is readily apparent that $S_{Hv}(q)$ begins to decrease monotonically at q values just greater than q_{max}, signaling the manifestation of the form factor argument for both concentrations. Furthermore, this onset occurs at q values lower than required for the particle center argument expiq $(R_i(0)-R_j(0))$ to reach its high q asymtotic value of 1. This complicates an easy interpretation of the remaining portions of the curves. In addition, the cross interparticle polarizability terms which are independent of q, undoubtably have some effect on $S_{Hv}(q)$ over the entire q range, although the presence is revealed clearly only at $q<q_{max}$. Invoking x-ray and neutron scattering results, studies have shown that $P'(q)$ has a much stronger q dependence than $P(q)$ in strongly correlated systems and therefore one can expect that they both manifest themselves simultaneously precluding any separation between the two which might facilitate an easier analysis. This also precludes any possibility of deconvoluting $P(q)$ from $P'(q)$, knowing that $P(q)$ could be modeled if necessary from Van Aartsens theory.

Considering other possible explanations regarding the origins of the peak structure observed in the $S_{Hv}(q)$ spectra, Van Aartsen[57] has determined that there are no maximums in the Hv scattered intensity as a function of scattering angle for a random collection of anisotropic cylinders, in contrast with what is observed in the Hv scattering from anisotropic spherulitic structures (polymer films, etc.). This eliminates any possible ambiguity between the peak structure observed in $S_{Hv}(q)$ due to particle center correlations instead of one due to the functionality of $P_{Hv}(q)$.

From recent work,[77] it has been discovered that a random collection of spherical isotropic Mie scatters display a depolarized scattered component and this component has a maximum with q much like that observed in anisotropic spherulitic systems. The previous light scattering theory has been based on the Rayleigh-Debye approximation (the electric field does not change its relative phase upon scattering) stated mathematically as $\frac{4\pi}{\lambda}R[m-1]<<1$, where λ is the wavelength, R is a characteristic particle dimension (radius) of the particle and m is the ratio of the particle and solvent refractive indices. For this system, the term on the left is about .06 placing this system well away from the need to invoke a Mie scattering interpretation.

Addressing next the differences in $S_{Hv}(q)$ for different concentrations, both curves parallel each other in q quite nicely until the position of the second maximum of the sample of higher

concentration. Here, a significant difference between the two curves is observed which can be ascribed to a concentration dependence. In the total scattering function given by eq. III.35b, concentration dependencies will arise from the factors containing the cross interparticle correlations as well as through the particle center correlation factor. At high q, where the particle center part of the function, $S_c(q)$ will be equal to L, differences due to concentration will be a result of the cross terms in the form factor part $\exp iq\,(b_l^i - b_m^j)$ $i \neq j$. The sample of higher concentration obviously has a different curvature and a different structure in this $q >> q_{max}$ region than the sample of higher concentration. The high q portion of the curve of lower concentration decreases with q in a smooth consistent manner. The sample of higher concentration apparently matches its lower concentration counterpart only at very high q, $q > 1.4 \times 10^{-4} \text{Å}^{-1}$. As the functionality of the cross form factor is unknown and because its effect is cloaked by other factors in this high q region, further analysis would be less than speculative.

Figure 5.2 shows a plot of $P_{Vv}^{-1}(q^2)$ obtained from $I_{Vv}(q)$ measurements in the q range where stray light was absent. The limiting $q \to 0$ form of $P_{Vv}(q^2)$ is that of eq. III.12 which yields a radius of gyration from the linear region of $I_{Vv}(q^2)$ versus q^2, its value being 798. Å. The dashed curve also plotted in Figure 5.2 represents the shape of the best fit curve based on eq. III.12 using this value for the radius of gyration. Deviations at high $q (q > 9. \times 10^{-7} \text{Å}^{-2})$ are

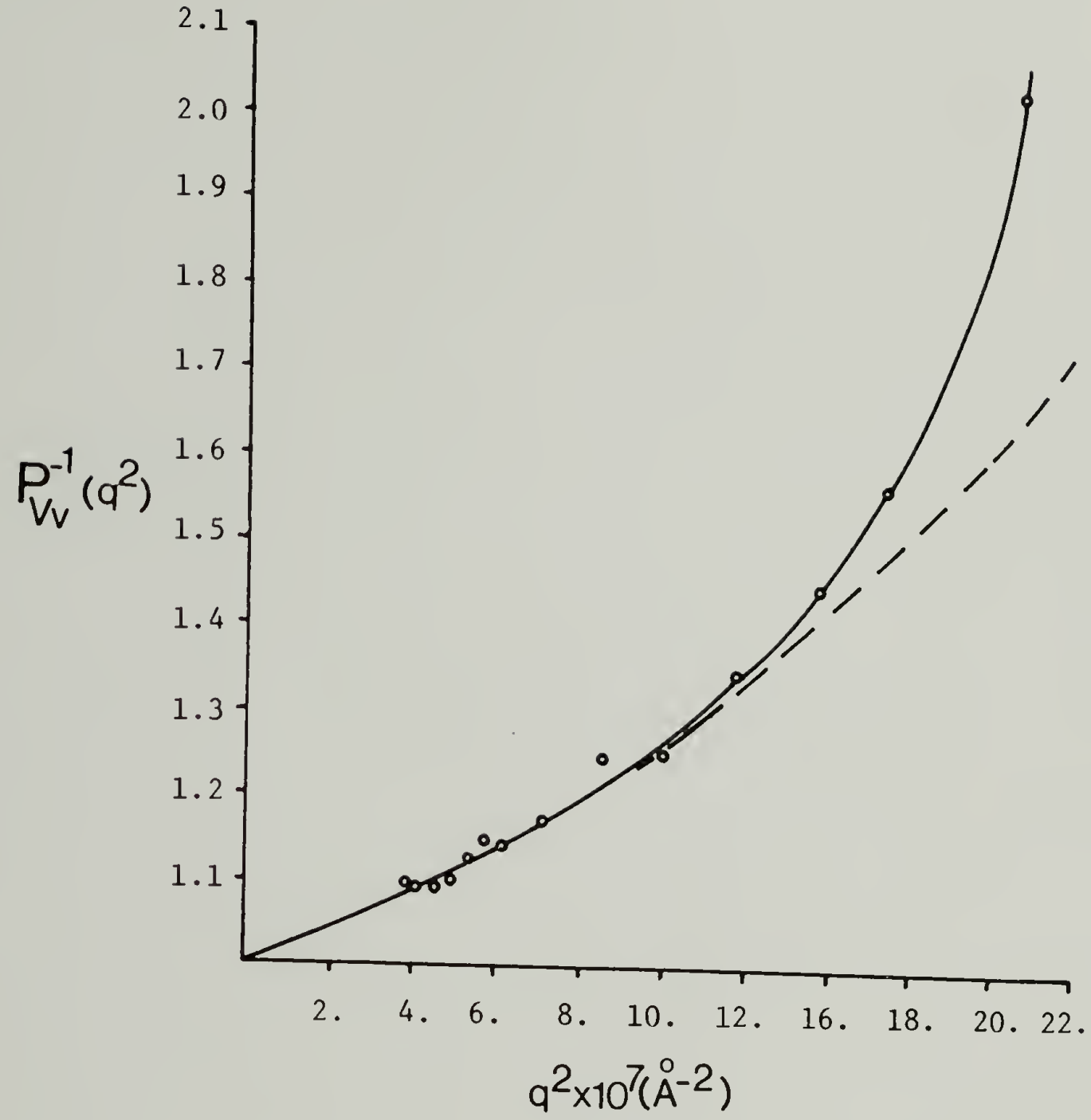

Figure 5.2 A plot of the experimentally determined polarized form factor plotted as $P_{Vv}(q^2)^{-1}$. The dashed curve represents the best fit result using equation II.12. The best fit radius of gyration obtained is 798. Å.

believed to be a result of a number of factors all of which have been discussed earlier. Possible explanations are polydispersity, inclusion of the higher moments of the mass distribution corresponding to each particles small shape anisotropy, particle optical anisotropy, and cross form factor correlations. Van Aartsen has calculated $P_{Vv}(q)$ for anisotropic cylinders, but the shape of the curve predicted was not analyzed beyond that necessary to extract a radius of gyration. The calculated radius of gyration extrated from the low angle polarized scattering, 798. Å, compares quite nicely with the value calculated from the measured histogram using a hard sphere radius based on the second moment of the radius distribution. This value is $R_g = \sqrt{\frac{3}{5}}\langle R^2\rangle^{1/2} = 763.$ Å. All estimations of the particle size, those from the measured histogram, static low angle light scattering are in good agreement. These will be shown to be in good agreement with two other estimations, namely the C = 0 extrapolated value of the translational diffusion constant and the D_o value obtained by making a short time measurement of the polarized dynamic correlation function in accordance with eq. III.56. This is the topic of the next section.

C. I_{Vv} and I_{Hv} Dynamic Measurements

1. I_{Vv} Correlation Functions and Decay Rates

Ideally, measurement of a I_{Vv} decay rate at one angle is sufficient to extract a translational diffusion constant. To test

this, a search for non-linearity of $\bar{\Gamma}_{Vv}$ in q was undertaken. For the eight solutions of different concentrations, $\bar{\Gamma}_{Vv}$ versus q^2 plots were made. These decay rates were extracted from the correlation functions by the method of cumulants. Correlation functions from a few solutions, Samples 2, 3, 4 and 8, are displayed in figure 5.3 where the natural log of the Vv field correlation functions collected at 50 deg. are plotted. In the absence of interparticle interactions, all curves would lie on the solid curve, the curve expected for free diffusion ($D_o = 2.48X10^8$ $\mathring{A}^2/s$). Figure 5.4 shows a plot of the decay rate ($\bar{\Gamma}_{Vv}$) versus q^2 for samples 3(o) and 5(•) as an example. Linearity is observed to 80-90 deg. whereupon a gradual increase in the decay rate is observed for all samples. This deviation from linearity is expected at higher q due to the combined and inseparable effects of interparticle interference and particle anisotropy which bring in higher order correlations and therefore a larger effective decay rate. Intraparticle interference, of the kind described in section III.C.1, becomes significant, as far as the dynamic properties are concerned, for values of q such that $qR_g \sim 1.73$ ($\theta \sim 90^\circ$) where the second order term (eq. III.29) contributes a second exponential with a decay rate larger than the first order term by 6Θ.

The relationship between the non-linearity and the effect of particle anisotropy can be estimated as follows. Figure 5.5 shows a plot of the depolarization ratio ρ_v (P_{Hv}/P_{Vv}) versus q^2. Its non-constant functionality with q^2 indicates that P_{Hv} gets stronger

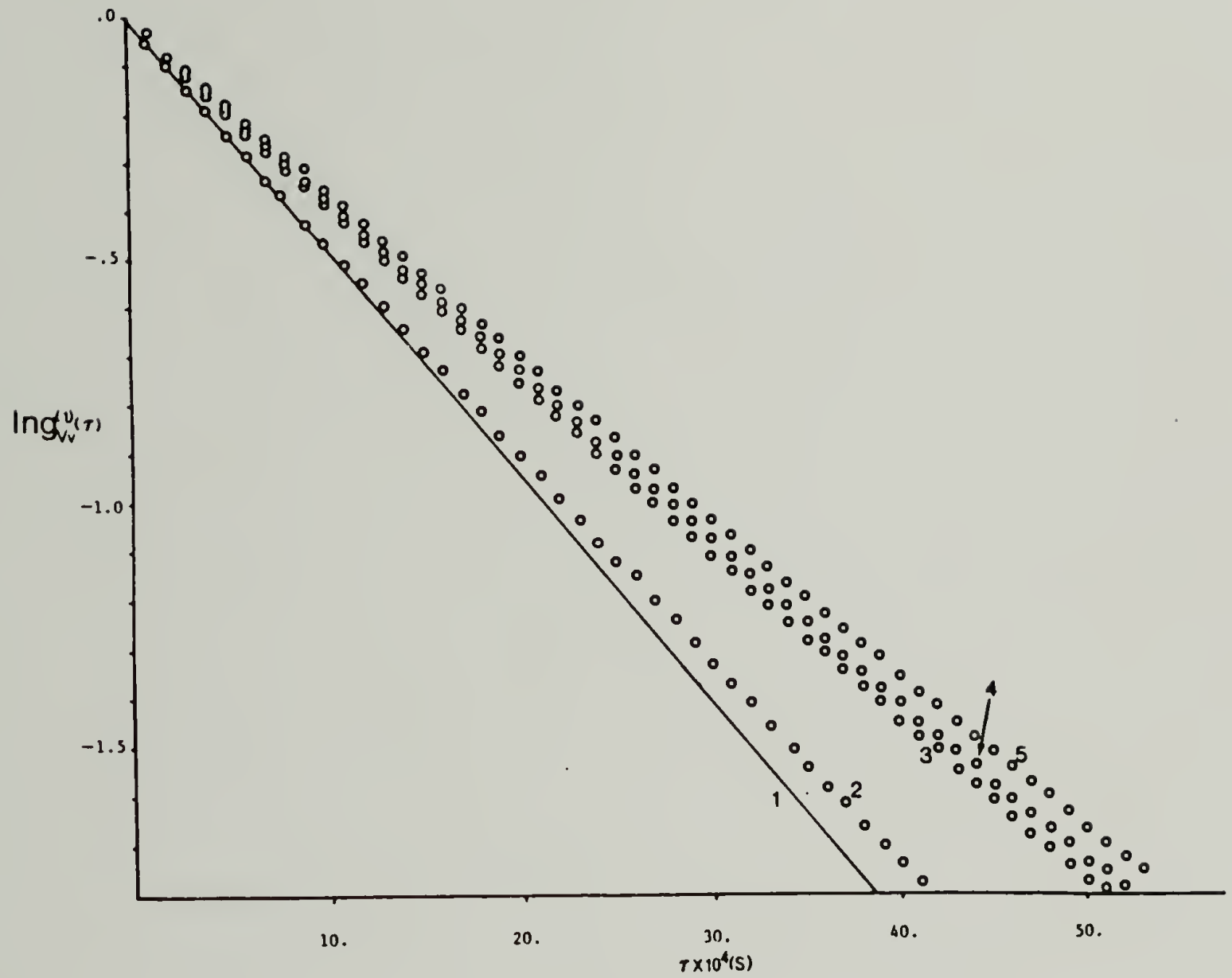

Figure 5.3 The natural log of the Vv correlation functions measured at 50 deg. for samples 2, 3, 4 and 8 as examples. The solid curve is what would be expected for free diffusion.

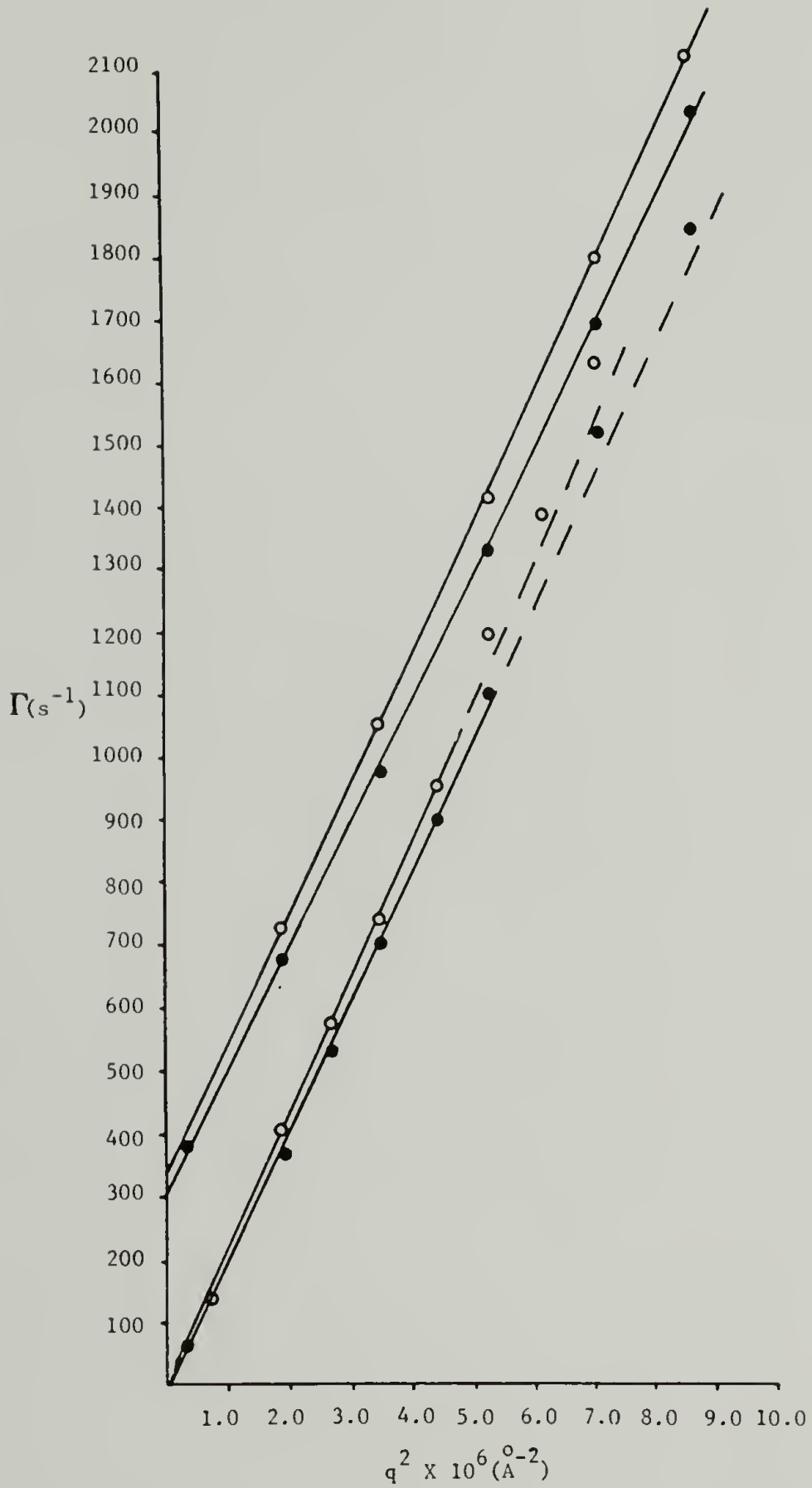

Figure 5.4 The q^2 dependent decay rates obtained from the analysis of the polarized(lower lines with zero intercept) and depolarized (upper lines with intercept 6Θ) correlation functions for samples 3(o) and 5(•).

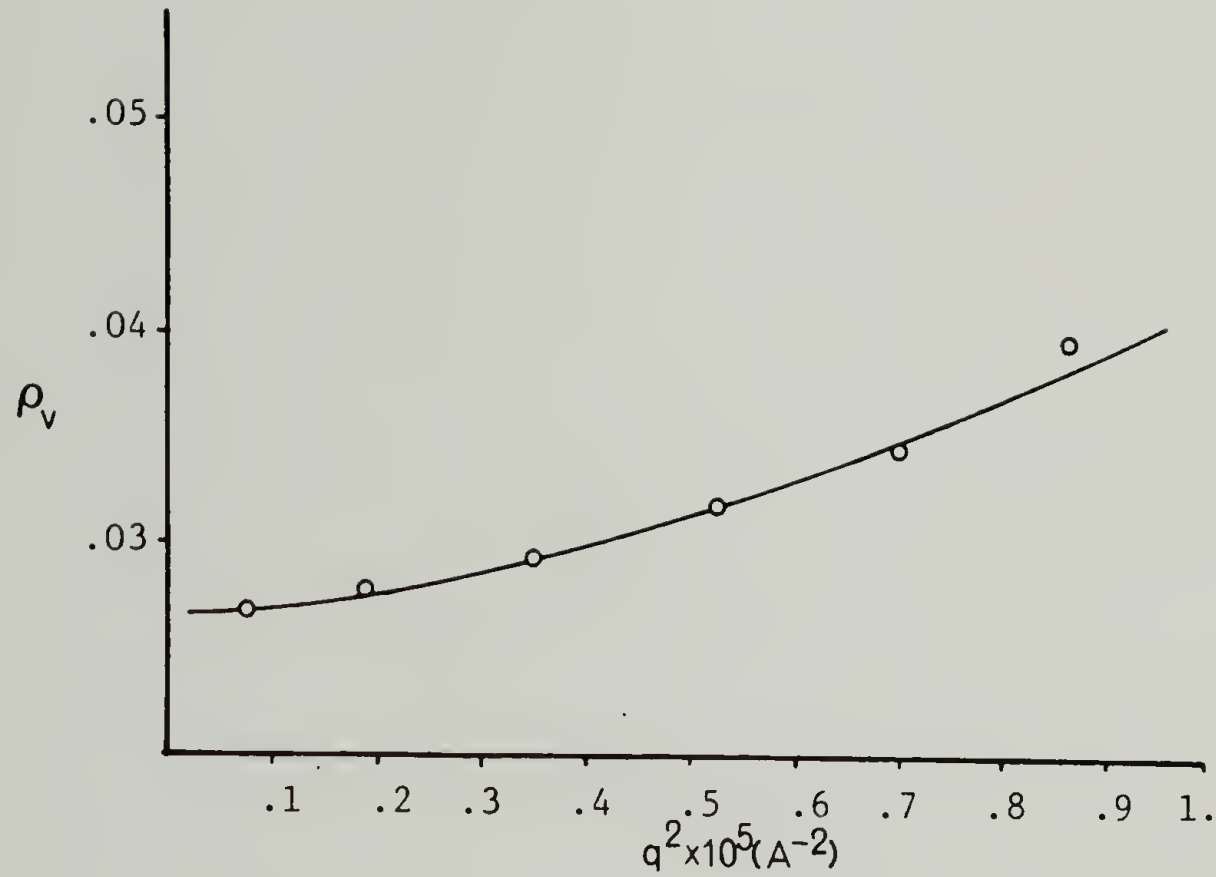

Figure 5.5 A plot of the experimentally determined $\rho_v (P_{Hv}/P_{Vv})$ versus q^2 for this system of anisotropic particles.

relative to P_{Vv} as q increases. The depolarization ratio, ρ_v, can be related to the relative amplitudes between the isotropic and anisotropic components of the polarized correlation function eq. III.27.a. by using equations III.19 such that:

$$\rho_v = \frac{3\beta^2}{45\bar{\alpha}^2 + 4\beta^2}$$

and the relative amplitude factor becomes

$$\frac{4}{45}\left(\frac{\beta}{\bar{\alpha}}\right)^2 = \left(\frac{4}{45}\right)\frac{45\rho_v}{3 - 4\rho_v}$$

In taking from figure 5.5 the $q^2 \to 0$ value of ρ_v of .026, one obtains for the relative amplitude of the second term in III.27a of 3.4%, indicating its contribution to be small at low q and justifying writing an approximation to III.27a by its isotropic component III.27c. Due to the different angular dependencies of P_{Vv} and P_{Hv}, the relative amplitude of the second order exponential term increases from 4.5% at 90° to about 5.6% at 110°. Thus, application of eq. III.27c in the analysis of the polarized correlation function at high q would yield a larger effective decay rate due to this anisotropic contribution. Additionally, it is possible that free diffusion may be observed[2] at very high q due to the very short length scales over which the diffusion process is being measured. At 90 deg., using the sample times employed in the measurement of the dynamic structure factors (100-10μs), a particle translates only a fraction of its total

length during the time the correlation function is being measured. In this case, the additional contribution of free diffusion would cause a gradual increase in the effective long time decay rate with q. This process has a theoretical justification as a result of a recent calculation by Hess and Klein[43] in which a memory function approach is applied to a Brownian one component plasma. They found that the memory function decays to zero at high q where the free diffusion result is recovered regardless of the strength of the interaction. Therefore only the linear, low q portion of the Vv data was used in the calculation of the slope and diffusion constant. A least squares analysis was done on no fewer than 4 points in this region and the correlation coefficients recovered were all greater than .999 indicating linearity and consistency. The diffusion constants extracted from the slopes of the eight samples are listed in Table 5.1. From Figure 5.3, it can be seen that the decay is a single exponential for the long times and this linear region is pushed to earlier times for the samples of higher concentration. Thus, the mean free path traveled before a nearest neighbor encounter gets smaller, or the time τ_I gets smaller as the average interparticle distance becomes smaller. In the measurement of a long time correlation function, this linear region is weighted heavily in the calculation of the effective decay rate from which the long time diffusion constant D_L is recovered. The chi squares of the cumulant fits varied as usual but were mostly less than 5., although some at low angles were around 15. This is due in part to the presence of an angularly dependent

Table 5.1

A list of the long time values of the translational and rotational diffusion constants measured for the eight samples of different concentration.

Sample	$D_s \times 10^{-8}$ ($\AA^2/s$)	6Θ (s^{-1})
1	2.40	434.4
2	2.338	366.6
3	2.19	322.2
4	2.1	314.4
5	2.07	301.7
6	1.977	283.9
7	1.94	272.8
8	1.922	268.4

second cumulant. The normalized second cumulants showed a descending trend with q^2 although it was not consistent. The normalized second cumulants were about .12 and less for 30 deg. measurements and between .04 and .08 for higher angles. These values were approximately a factor of two less than those observed in the bulk unfractionated material. The values at the lowest angles are slightly underestimated as compared to the normalized second cumulant calculated from the measured histogram of .137. The angular dependence of the second cumulant is due in part to the polydispersity where the influence of each particles form factors angular dependence weights smaller particles at larger angles and vice-versa. In the absence of the other factors tending to influence the second cumulant, a reduced polydispersity index at higher angles is a result of observing a more narrow distribution via differential weighting factors. This reduced polydispersity index should be accompanied by an increased first cumulant with q as these smaller particles, which are weighted more heavily at larger angles would exhibit larger diffusion constants. Thus, one would expect the measured value of the polydispersity of a polydisperse sample would decrease with q due to the decreased scattering of the larger particles at the higher angles. This illustrates the relative insensitivity of quasielastic light scattering toward sample polydispersity and the difficulty of quantitative analyses based on the second cumulants which contain the inseparable effects of polydispersity, particle anisotropy, inter-particle interference along with a frequency dependent diffusion

constant arising from the interparticle interactions. The presence of the narrowing effective polydispersity index with q, if exhibited in its pure form would be undoubtedly cloaked by the presence of these other influences. It is expected that the integrity of the diffusion constant calculation is protected by using Vv data in the linear, low q region where non-ideal behavior is not observed nor expected. This seemingly intractable state of affairs encountered in this study is unfortunate, but until a more ideal system of charged anisotropic particles is discovered or invented, it is believed that this study will serve as an instructive lesson and a good foundation until that time.

The short time behavior of the correlation functions from which free diffusion may be extracted was investigated by expanding the short time region using a sample time a factor of 10 less than the time used for the measurement of a long time correlation function. An example of a correlation function measured in this fashion is displayed in figure 5.6 where this short time correlation function ($\Delta\tau = 10\,\mu s$) is spliced with its long time ($\Delta\tau = 100\,\mu s$) counterpart (sample 5 at 70 deg.). The diffusion constant recovered from the short time function alone is $2.48 \times 10^{8}\,\text{Å}^{2}/s$ and can be identified as the average value of the free diffusion constant which is exactly that calculated from the measured histogram analysis. As mentioned before, this short time region where free diffusion is observed is pushed to shorter and shorter times until only the long time value could be recovered at the

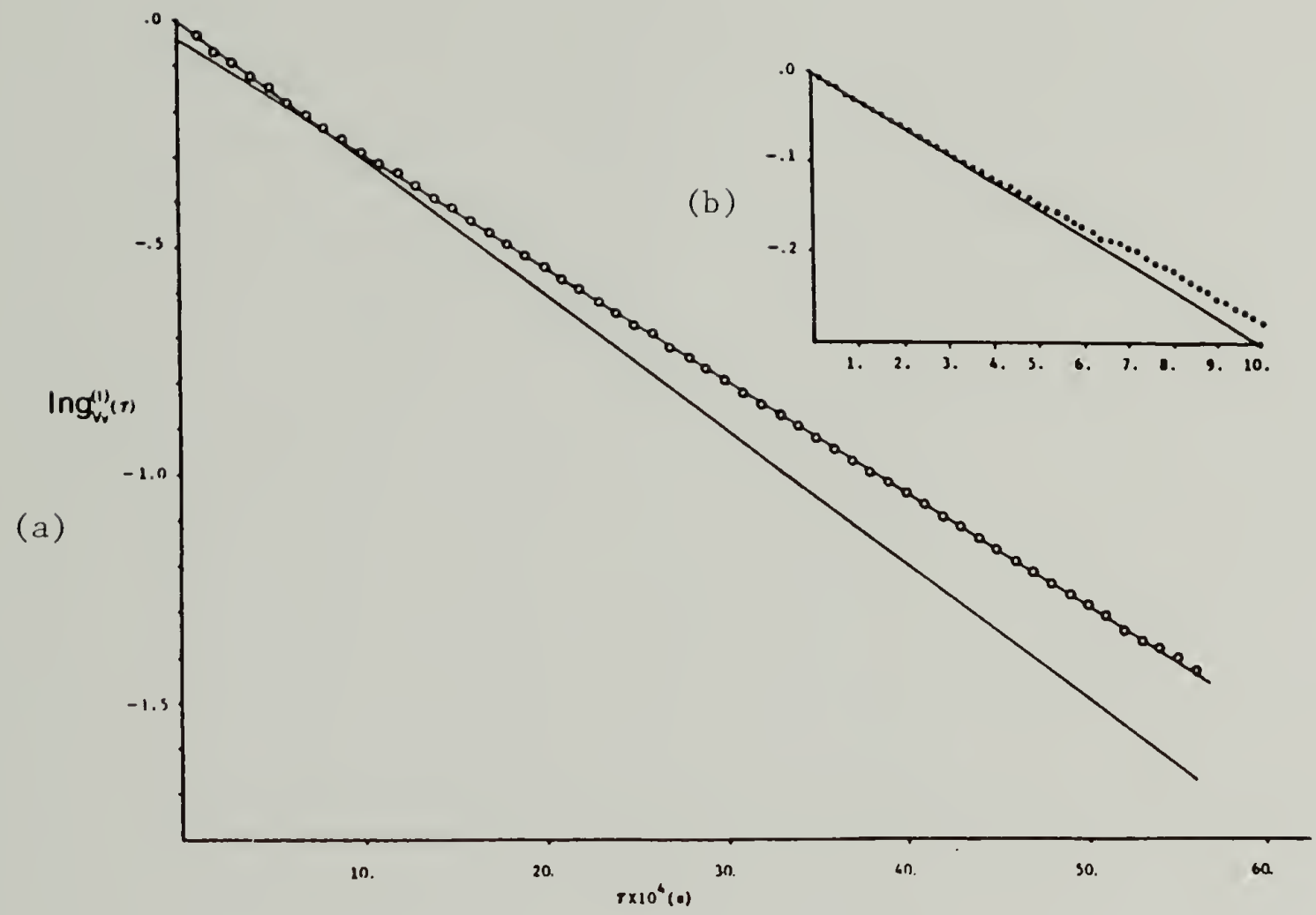

Figure 5.6 (a) The natural log of $g_{VV}^{1}(q,t)$ for sample 5 collected at 70 deg. at a sample time of 100 μs. The line through the data points in the long time region can yield the long time or "interacting" translational diffusion constant. The line drawn through the data points at the earliest times represents and can yield the free translational diffusion constant. (b) This insert is the same correlation function but measured at a sample time of 10 μs. The line drawn through this data better displays the initial slope.

highest concentrations.

Values of D_L/D_o, where D_o is that recovered from the short time measurement, are plotted versus concentration in Figure 5.7. The smooth curve through the data is the result of the theoretical calculation by Hess and Klein (eq. II.48). The DLVO parameters D_κ and ψ_o were floated independently through their relationship to the static structure factor (Hayter-Penfold) until a best fit was obtained by iteration. Because the structure factor algorithm by Hayter-Penfold employs the DLVO potential in the description of the macroions interacting over large distances, the DLVO parameters thus fit represent the large r tail of the potential and thus must be characterized as being effectively renormalized as defined by Alexander. The values of these renormalized parameters are $D_\kappa^* = .03$, $\psi_o^* = 29.\text{mV}$; indicating the coulomb potential as being weak and softly screened as evidenced by the height of the maxima representing nearest neighbor shells displayed in the measured absolute structure factor. The surface potential, 29.mV($Z \sim 144e^-$), is similar to others found in large particles displaying similar structure. The particle value (144) calculated from Gauss' law must be assumed to be an average over time and over particles as it has been shown that the total change in some protein molecules may fluctuate about an average value.[78] The two other theoretical calculations of Hess and Klein displaying the C and $C^{1/2}$ concentration dependencies are not plotted here. Their applicability to this system and the significance of their drastic over-

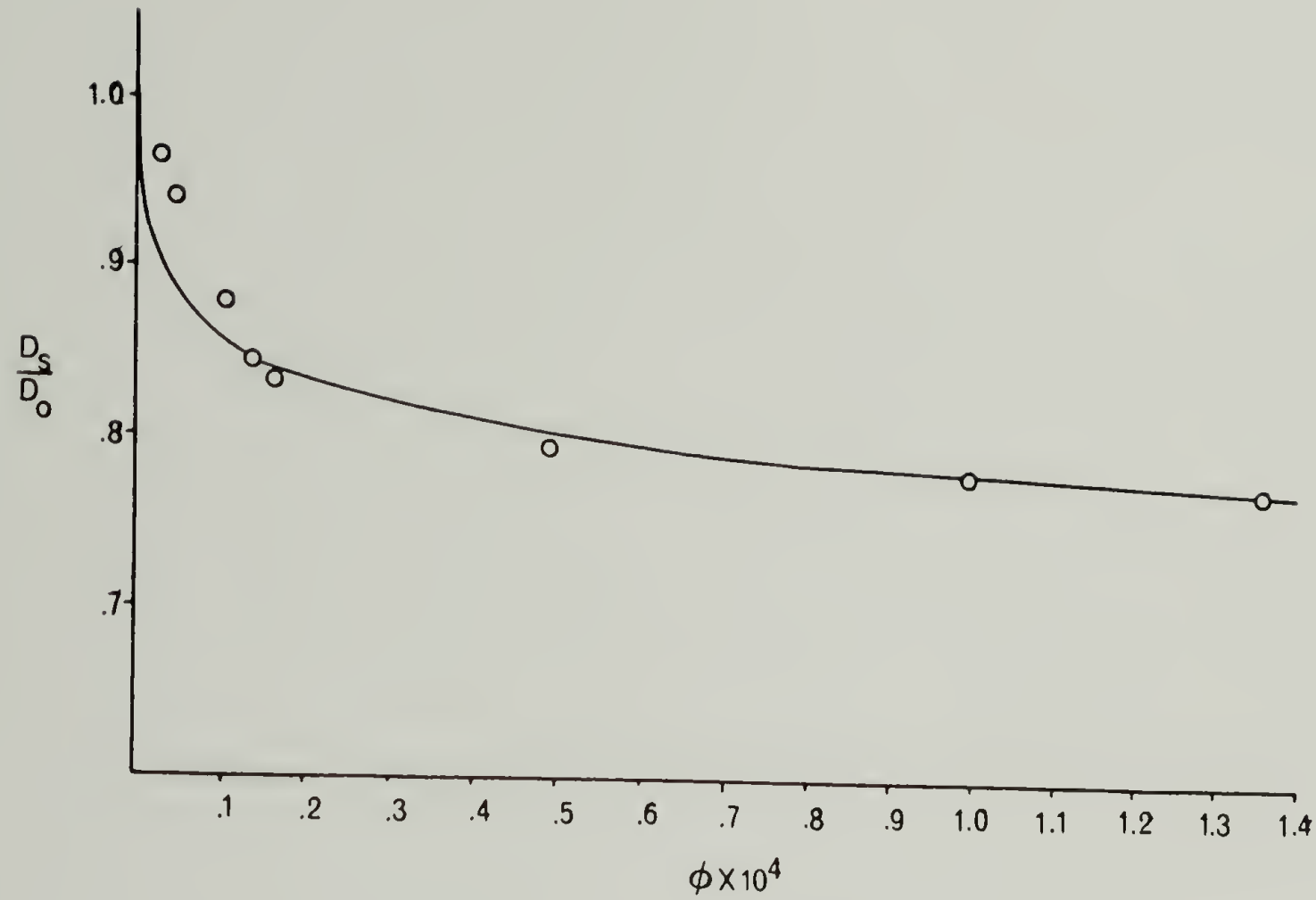

Figure 5.7 The concentration dependence of the long time translational diffusion constant. The smooth curve is the result of the calculation of Hess and Klein using a best fit set of renormalized DLVO parameters. The approximate error is displayed by the size of the circles labeling the data points.

estimation of the diffusion constant in comparison to eq. II.48 will be discussed in the concluding chapter of this work.

2. I_{Hv} Correlation functions and decay rates.

Using the same criterion involved in accumulating I_{Vv} spectra, I_{Hv} measurements were made throughout the q range studied. The rotational diffusion constant, 6Θ, is extracted from the linear regression $q^2 \to 0$ intercept of the $\bar{\Gamma}_{Hv}$ versus q^2 plots constructed from these 8 solutions. These are listed in Table 2. Linearity throughout the q range studied was observed in all $\bar{\Gamma}_{Hv}$ plots obtained from each solution, two of which are shown in Figure 5.4 (upper curves with a non-zero intercept) along with their Γ_{Vv} counterparts. Correlation coefficients recovered from the least square analysis for all 8 solutions were greater than .999. Apparently, sources of non-linearity as those affecting I_{Vv} spectra are evidently not present in I_{Hv}. The reason why will be revealed at the end of this section.

A similar correspondence in form occurs between I_{Hv} and I_{Vv} correlation functions, a form nearly identical, expect for a change of scale, to the I_{Vv} spectra displayed in Figure 5.3. Non-single exponential behavior is observed at very early times, times smaller in general than those in I_{Vv}, the correlation functions tending toward single exponentiality throughout the rest of the time domain. In general, the I_{Hv} spectra had lower second cumulants and lower chi squares for their cumulant fits than their I_{Vv} counterparts. It is

known that depolarized spectra suffer less from dust and aggregation than do polarized spectra.

Short time measurements of the I_{Hv} spectra were attempted in an effort to investigate the possible time dependence of the rotational diffusion constant. This was accomplished in a way analogous to their I_{Vv} counterparts. The initial slopes of the short time correlation functions for 6 samples were extrapolated to $q^2 \rightarrow 0$ to yield a short time value for the rotational diffusion constant. These are plotted in Figure 5.8 versus concentration along with their long time counterparts. The smooth curves drawn through the data points are not theoretical fits of any kind but only meant to guide the eye. As shown, the short time value at the lowest concentration, $1170.s^{-1}$, is very nearly that of the free value calculated from the measured histogram analysis ($6\Theta_o = 1151.S^{-1}$). The trend of 6Θ versus concentration tracks that of the long time values. The values at the lower concentrations are much larger and eventually merge asymtotically with the long time values at high concentrations where only single exponential decay is observed. The significance of this will be brought forth in the discussion section where speculation as to the mechanism of this concentration dependence will be presented.

At this point in this presentation, it is possible to discuss the important relationship between the effect of the form factor argument on the static and dynamic correlation functions. In Figure 5.2, it can be seen that the static form factor argument $\vec{q}\cdot(\vec{b}_l^{\,i}(0)-\vec{b}_m^{\,j}(0))$

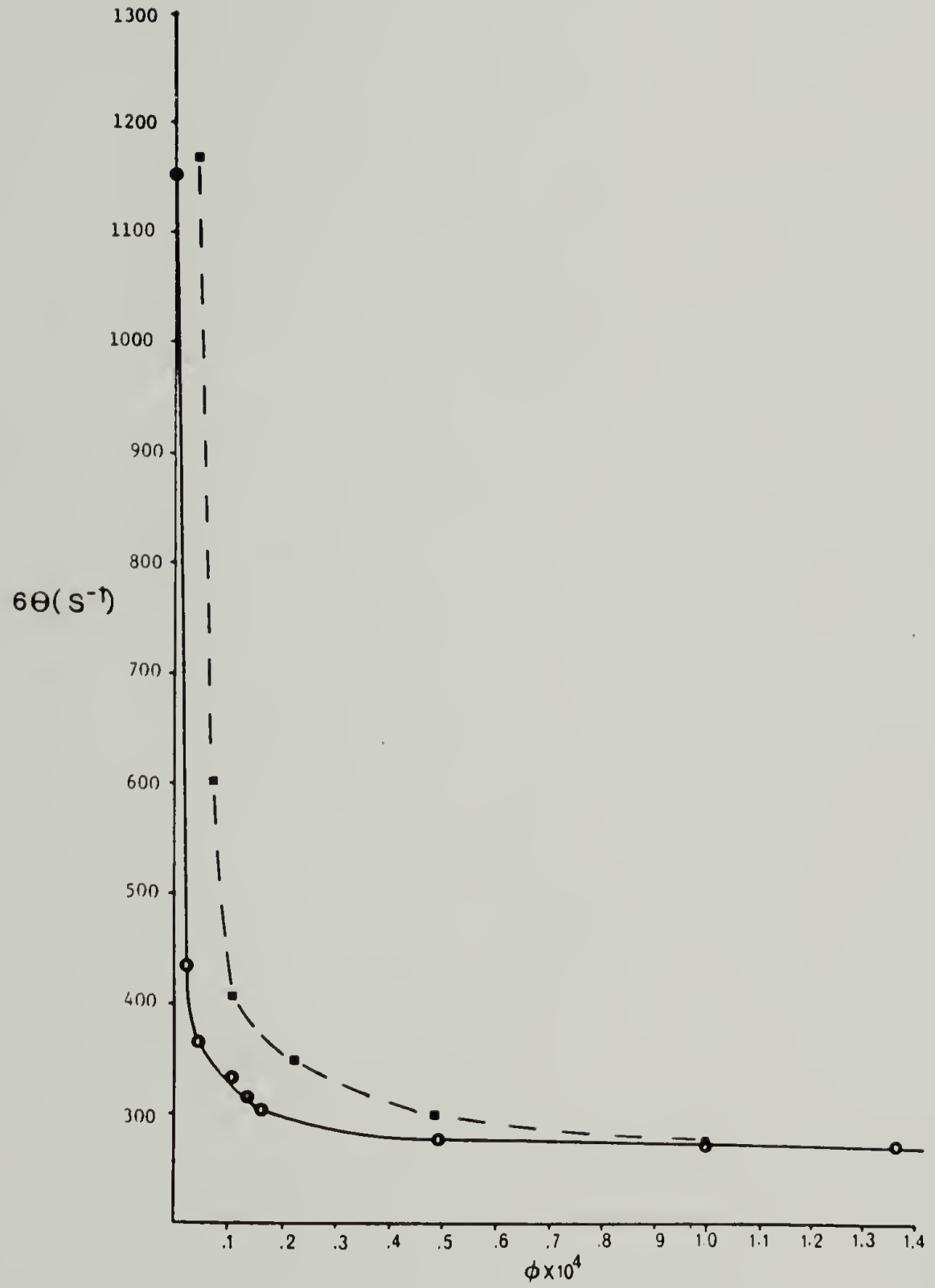

Figure 5.8 The long(o) and short(■) time concentration dependence of the rotational diffusion constant. The solid and dashed curves are not fits of any kind but only meant to guide the eye.

manifests itself over the entire q range studied, ranging from 1.1 to 2.1 over the q range considered in the static and dynamic intensity measurements. If this quantity displayed a detectable time dependence, it would manifest itself in a dynamic measurement as a second single exponential of increasing amplitude with q in both the polarized and depolarized dynamic $g^{(1)}(q,t)$ correlation function. As has been discussed, single exponetial behavior in both the polarized and depolarized dynamic spectra were observed at high q where the form factor would have its largest effect. This is also a clear test of the assumption that $\alpha_{zz}(t) \sim \bar{\alpha}$ for all q in the polarized spectra. Therefore, the onset of a positive deviation from linearity in $\bar{\Gamma}_{Vv}$ versus q^2 at the higher angles (while single exponentiality is retained) must be a result of polydispersity and/or the decay of the memory function at high q not optical anisotropy nor the manifestation of a dynamic form factor phenomenon. This also indicates that the mean polarizability is more sensitive to particle size than is the optical anisotropy, even though the particle volume is still recognized as being the weighting factor for both. This is also evidenced by the fact that the depolarized dynamic correlation functions have smaller normalized second cumulants than their polarized counterparts. This observation validates Pecora's[56] argument that for dynamic measurements, the form factor argument may be removed from consideration in the dynamic correlation function and treated as a static amplitude factor with a q dependence in $g^1_{Vv}(q,t)$, providing the particle is not too large. Evidently, these particles fall into

this regime. The form factor, of course plays an important role in the static polarized and depolarized correlation functions however. Recognizing these observations preserves the integrity of the previous analyses based on single exponential decay of the polarized and depolarized dynamic correlation functions assuming the time dependence of the form factor argument can be neglected and the anisotropy as it is involved in the polarized scattering can also be neglected.

C H A P T E R VI

DISCUSSION and CONCLUSION

In light of the presence of formal theoretical treatises for the concentration dependence of translational diffusion and the absence of such for rotational diffusion, translation and rotation will be discussed separately.

In Figure 5.7 is shown the concentration dependence of the translational self-diffusion constant and the results of the Hess and Klein theory (eq. II.48, smooth curve) based on the FPE using a non-WCA, MMCA and the best fit parameters for the renormalized DLVO potential. Following the theoretical curve, a rapid drop at very low concencentrations is observed followed by a wider range where the rate of decrease is small. Gaylor[79] has obtained results qualitatively similar by Monte-Carlo computer simulations. It is obvious that the agreement at concentrations greater than $\phi = 1.5 \times 10^{-5}$ is good while at lower concentrations, the theory overestimates the measured diffusion constant. A legitimate question is whether this break point in concentration has some significance. This match and mismatch between the theory and the measured data in the high and low concentration regimes respectively is a very important feature, one which reiterates the meaning and applicability of the WCA techniques used to calculate self-diffusion in interacting systems. Before explaining these features specifically, lets review briefly the

origins of the three theoretical approaches for self-diffusion in an effort to unravel a hierarchy of interrelations.

The foundation of the WCA is the linearization of the Boltzmann factors whose argument is the pairwise interparticle potential energy U(r), this linearization being valid only when $U(r)/kT \ll 1$. This approximation was then employed in: 1) the reduction of the N-particle potential and the equilibrium static distribution in the SE, this resulting in the equation for self-diffusion (eq. II.42) linear in C; 2) the linearization of the pair probability distribution function to obtain the DH form for the static structure factor which was then used to evaluate the memory function calculated within the MMCA and which was also used in both $G_s(q,t)$ (mean field form) and $h_D(q)$, this result yielding an expression for self-diffusion (eq. II.47) having a $C^{1/2}$ dependence; 3) In what is equivalent to a WCA, was the reduction of the FPE to obtain the SE, therefore, any application of the WCA while using the SE is actually a performance done twice. In the final most accurate description of translational self-diffusion, eq. II.48 based on the FPE within a non-WCA MMCA, the structure factor algorithm employed has deficiencies which, although are not related to the WCA directly, are related to the treatment of the N-body interaction potential and the form used for the pair potential itself.

First consider the validity of the WCA itself. Using the best fit renormalized DLVO parameters, a value for U(r) for a pair of

particles at a concentration of $\phi = 1.5 \times 10^{-5}$ is approximately .9kT indicating that a weak and influential coupling is still present at this concentration, the coupling increasing to kT and higher at the higher particle densities. Thus, the onset of a weak coupling regime is reached by sufficient dilution of the interacting particles to concentrations below about $\phi = 1.5 \times 10^{-5}$. This concentration identifies a transition to a regime of deficient theoretical applicability with regard to the WCA. Consider then the applicability of the results based on the WCA in this ultradilute regime. In a WCA, $Q^* = R\varepsilon\psi_o$ where if 29. mV is used as the potential, an effective valence of about 11e- is calculated in contrast to 144e- using the full DLVO result. Using this charge (11e-) and the best fit screening length, equations II.42 or 47 are found to give excellent agreement with the measured data in the $\phi<1.5 \times 10^{-5}$ regime while serious deviations are found when they are applied to higher concentrations where the WCA is no longer valid. The onset of this weak coupling regime can also be identified by comparing the interparticle spacings with the correlation length κ^{*-1}. It is found that this inverse Debye length corresponds quite well with the interparticle spacings calculated for $\phi = 1.5 \times 10^{-5}$ (59831.A). Hastings, however, found in a study of colloidal crystals, that κ^{-1}, on the basis of best fit criterion was approximately L/2 at a number of concentrations. He stated that this was apparently required if particles are to feel each other continuously. It should be recognized that the value of κ^{-1} determined here by the methods described is one that only appears to

govern the dynamical behavior based on the models assumed and by no means is it sufficiently determined for any critical comparison with previous findings. Thus the physics upon which the theories for self-diffusion are based are borne out remarkably by experiment. The reason why the WCA results do not apply or work at high concentrations is because the WCA is invalid there. The reason why the non-WCA result does not work at low concentrations is a result of minor deficiencies embodied in the approximations used to calculate $S_c(q)$ from the OZ equation and not necessarily a defect in the theory of diffusion itself. The approximations involved in solving analytically the OZ equation which were discussed in Chapter II.B.2 are known to result in structure factor algorithms which reproduce only the main features of experimentally derived particle center structure factors. The deviations are reflected into ways that are due to two different although related effects. The use of the MSA closure relation is an approximation known to be somewhat deficient in the treatment of the short range (small distance) part of the radial distribution function. This deficiency is related to the rejection of certain types of cluster integrals in the MSA representing higher order N-body interactions than those which are encompassed by the superposition approximation. The defect is reflected in the large q, $q > q_{max}$ region mostly as a difference between the actual and predicted positions of the secondary maxima and minima in $S_c(q)$. Although other closure relations such as the hypernetted chain approximation are known to be more accurate, they do not lead to analytic results. Another more

significant deviation is found at low $q<q_{max}$ region. The use of a screened Coulomb potential is itself only a convenient and approximate form for the actual pair potential and in addition, only represents the tail of the potential at large distances away from a macroion. Authors[75] have suggested that the overestimation of the $q<q_{max}$ region of actual measured $S_c(q)$ curves and the almost zero value predicted for $S_c(0)$ is a result of the inappropriateness of the screened Coulomb potential. The deviations thus mentioned become larger for lower particle densities. The use of an $S_c(q)$ algorithm such as that by Hayter and Penfold who employ a screened Coulomb potential and the MSA, in the integration over q found in eq. II.48 would result in an overestimation of the self-diffusion constant. As the deviations in $S_c(q)$ manifest themselves at low concentrations, the "added area" obtained through the integration over q would result in the overestimation of the self-diffusion constant only in the low concentration regime. This is indeed displayed in Figure 5.7.

In concluding this discussion of translational diffusion, consider the difference between the self-diffusion results based on the FPE and SE. As shown, the FPE non-WCA approach alone yields a corrrect prediction of the self-diffusion constant over a large range of concentrations while the SE, even when treated numerically in an effort to bypass the WCA, fails to reproduce the observed trend, the deviation errs toward values predicted using the WCA. Hess[80] has addressed the problem of using the SE in detail. As mentioned in

Chapter II, the SE is derived from the FPE by an expansion of the spacial gradient $\partial/\partial r$ and with respect to the inverse friction coefficient ζ^{-1}. For a weakly interacting system, these expansion parameters are convergent as the momenta are strongly overdamped by the solvent and decay on a much shorter time scale than do the position variables. In an interacting system, the added influence of interparticle forces cause the momenta to decay on a time scale near that of the particle positions themselves while the momenta become damped by the interparticle potential as well as the particle solvent Brownian interaction. Most systems under scrutiny thus far were weakly interacting thus justifying the neglect of the momenta in what has become an almost universal acceptance of the equivalence of the SE and FPE's. In the strongly interacting systems discovered and addressed in recent times, the two equations are found to be coincident only at $q \to 0$ for any level of interaction, while at arbitrary q, deviations are quite large. In fact, Hess has shown that the correction terms are on the order of $(\frac{m}{\zeta^2})(\frac{\partial \vec{F}_i(\{r\})}{\partial r_i})$ where $\vec{F}_i(\{r\})$ is the interaction force on the i th particle due to all others. Hess has concluded that for coincidence of the two equations to be assured, this term which is related to the memory function must be much less than 1. Using actual experimental parameters from the study of Gruner and Lehman,[32] this term is actually found to be almost equal to 1. Thus the FPE is superior to the SE when dealing with strongly interacting systems. The coincidence of the SE and FPE's in their accurate prediction of the diffusion data in the low density, weakly inter-

acting regime is additional evidence of the deficiency of the SE. In conclusion, either the SE or FPE solved in a WCA can be expected to be accurate only in regimes where the actual physics can be represented within a WCA, the MMCA correcting the results only slightly, not altering its general form. The approach of Hess and Klein based on the FPE within a non-WCA, MMCA is valid for strongly interacting systems and has been found to be entirely consistent with the experimental observations presented here.

Another important feature which must be addressed here as it has not been addressed anywhere else is the fact that in the case of self-diffusion, a larger hindrance of free diffusion is predicted by the weak coupling theory while the strong coupling theory predicts the correct result, it predicting a much weaker concentration dependence at the higher concentrations. In addition, the results of the strong interaction theory correctly predicts a leveling off of the self-diffusion constant with particle density, this occuring at a particle density such that the interparticle potential energy is approximately kT while the weak coupling theories do not. This indicates that once a particle becomes trapped within a Coulomb potential repulsive cage which is approximately kT in depth, as the particle density increases above that point, the actual potential well might not get any deeper as a result of mutual cancellations taking place when summing the N-body potential. In the report of Hess and Klein[1,47] where they specifically address their calculation of self-diffusion by the FPE

within the non-WCA MMCA, they display a curve analogous to the one presented here in Figure 5.7 representing the theoretical curve predicted using the parameters taken from the study of Gruner and Lehman. In calculating the pair potential energy at the break point estimated from their curve, a value of 2kT is found which is rather consistent with the behavior reported in this study.

Concentration dependencies of rotational diffusion, in the past, have been thought to be a result of hydrodynamic interactions originating through torques exerted on a particle by propagating supporting fluid vortices created by the rotatory motion of other particles. In this limit, cluster expansion techniques employing various forms for the rotational Oseen tensor have yielded an Einstein type relation[42] $\Theta = \Theta_o(1 - \frac{4}{15}\phi)$ indicating a very weak concentration dependence as was the case with translational diffusion. In a more advanced treatment employing the projection operatory technique, Wolynes and Deutch[81] calculate the single particle relaxation time of coupled translational rotational Brownian diffusers in terms of the dynamic $(\dot{g}_2)$ and static (g_2) pairwise orientational correlation functions. These results are essentially those of Keyes[60] described earlier, yielding a single exponetial decay for the single particle orientational correlation function. The decay rate is that of free diffusion modified by a correction factor dependent upon $\dot{g}_2$ and g_2 which themselves are cast in terms of an invariant expansion of the two particle distribution function which in turn can only be

calculated with knowledge of the potential of mean force. Their discussion considers only spherically symmetric hydrodynamic forces which give rise to no concentration dependence and unfortunately, they do not consider any anisotropic force fields which they state would cause a concentration dependence. Concentration dependencies based on electroviscous effects[72] are also impossible as these are local in character if present at all and are therefore independent of macroion concentration. The presence of some kind of interparticle torque arising from anisotropic interparticle interactions must be invoked to explain the trend displayed in Figure 5.8.

A phenomenological examination and explanation of the nature of the isotropic and anisotropic interparticle forces existing between macroions is possible upon inspection of Figures 5.1, 5.7 and 5.8. This discussion is facilitated by the presumed origins of the Coulomb potential field addressed in Chapter II.B.1. and the theoretical results of Chapter III describing the static and dynamic correlation functions. Consider first how the presence of both isotropic and anisotropic interparticle forces are reflected in both the static and dynamic correlation functions. In accord with the predicted behavior of such interacting systems, a certain self-consistency must exist between the dynamic correlation functions, yielding translational and rotational diffusive behavior and what is expected in the static properties.

From the concluding discussion of translational diffusion, the

isotropic radially symmetric part of the total Coulomb potential is reflected by an observed hindrance of free translational self-diffusion while at the same time, the particles locate themselves in local minimums of potential energy created by the N-body potential energy field, this correlation in position being borne out by peak structure in the measured absolute static structure factor. The dynamic behavior is excellently described by the procedure of Hess and Klein using the Hayter-Penfold particle center structure factor algorithm which also fits nicely the peak maximum in the measured absolute static structure factor.

Simultaneously, a concentration dependence of rotational self-diffusion is observed arising from postulated anisotropic interparticle interactions of the Coulomb monopole-induced dipole type. These anisotropic interparticle interactions also reveal themselves in the absolute static structure factor where interparticle 0-0 and/or 0-P correlations are evident. Thus, in a large array of particles, each particle tends to locate itself in local minimums with respect to its orientation as well as position. In terms of the harmonically bound Brownian particle model, the potential well enveloping each virtual lattice site is shallow, approximately kT in depth or greater for the particle densities considered. The break point in the translational diffusion versus concentration curve signifies that the interparticle potential energy has reached kT. Notice that in Figure 5.8, that a rapid upward trend of 6Θ with concentration for both the

short and long time values takes place in a way remarkably similar to what is observed in translational diffusion (fig. 5.7). It should be recognized that the effect is quite large, the hindrance of free rotational diffusion displayed in Figure 5.8 being a factor of 4 in total while the decrease observed between the highest and lowest concentrations being a factor of 2 and 3 for the long and short time values respectively. This seems to indicate that the curvature of the potential well governing rotational motion (of the O-O and O-P type) is much steeper than for translational (P-P) motion around each lattice site. Notice also that the break point in concentration before the rapid upward trend occurs in rotational diffusion takes place at approximately the same interparticle separation as it does for translational diffusion. The ultimate question is: what is the magnitude of the anisotropic interparticle potential energy and how does the resultant force retard free rotational motion. In accord with the postulated form of the anisotropic interparticle potential energy arising from the monopole-induced dipole interaction (eq. II.13), a magnitude can be estimated once a value for the ionic polarizability is estimated.

From the theory of Osawa,[21] in the zero electric field limit, the static ionic polarizability is determined by the mean square fluctuating dipole which is proportional to the approximate volume, ν, available for the potentially polarizable ions in the counterion atmosphere to move in. This is given by:

$$\langle \mu^2 \rangle = (\frac{3}{4\pi}) kT\nu\varepsilon_o \qquad (1)$$

The polarizability is given by:

$$\alpha = (\frac{3}{4\pi})\nu\varepsilon_o \qquad (2)$$

where the polarizability is expressed in units of ε_o. This equation must be modified for non-spherical particles such that becomes a tensor quantity. The anisotropic contribution to the total potential energy, $U_a(r)$, is given by the common monopole-inducted dipole interaction:[22]

$$U_a(r) = -\frac{1}{2}\frac{Q^2\alpha}{4\pi\varepsilon\varepsilon_o r^4} \qquad (3)$$

The volume of the equivalent sphere of the particles studied here from which the ion atmosphere is excluded is 915. Å. The counterion atmosphere should extend great distances from the particle surface as would be surmised by the magnitude of κ^{*-1}. To attempt an estimate of this volume is quite difficult, it could be determined experimentally however by dielectric dispersion measurements.[82] The volume required represents that available for polarizable or displaceable counterions, which would not include ones strongly bound to the particles surface. There is however, a competition between the ability of the monopole moment of one macroion to effect the potential energy of a counterion

contained in the atmosphere of another and also one between this and the Brownian forces themselves. Certainly, the monopole-monopole interaction is sufficient to influence the static and dynamic behavior of the macroions. The Brownian forces which are kT forces, are however short lived and undirectional in nature. This fact is the reason why long lived and directional interparticle energies on the order of kT are able to affect the long time behavior of the macroparticles. The weak interaction theory of self-diffusion, for instance, predicts that even forces much lower than kT are still able to effect considerably the long time behavior of macroparticles. Similarly, one could expect in analogy that a similar state of affairs would characterize the macroion-counterion interaction. Thus, it is quite a complication to somehow estimate the imaginary volume characterizing the effective region which a macroion can perturb the counterion atmosphere of another in the long time limit. In an attempt, first consider the non-spherical particles to be spherical with an equivalent radius of 915. Å. Next, let the imaginary volume be that represented by an imaginary sphere with a radius 3000. Å which would be a conservative estimate as the ion atmosphere could be expected to be much larger. Using the calculated value for ν in eq. V.2 and using the resultant polarizability in eq. V.3 it is possible to calculate the anisotropic component of the total potential energy. Assuming an interparticle spacing indicative of the sample of highest concentration (27800 Å) is yielded $U_a(27800) \backsim kT/350$, which indicates that the anisotropic part is weak as compared to the isotropic part

but by no means should this be considered negligible. This value could be quite larger by increasing the estimation of the effective ionic volume. Intense discussion exists in the literature concerning the nature of counterion deformation under an electric field for both charged proteins[82,83] and latexes, the review of this subject is beyond the scope of this work. Studies have specifically addressed[82,83] the polarizability versus inverse Debye length, however, these were carried out on non-interacting systems (κ^{-1} very much less than the interparticle separation). The magnitude of the polarizability at low fields suggests the large effect the deformed atmosphere may have on the dielectric properties especially if the polarizability is anisotropic.

The actual mechanism proposed for the retardation of rotational diffusion with concentration concerns the effect of a dipole induced in the counterion atmosphere of one particle by another macroion such that this dipole fixed spacially in the long time limit in the direction of the inducing field must retard the free rotational motion of its' parent macroion embedded within as this charged particle must follow its atmosphere. Thus there exists some kind of coupling between a macroparticle and its atmosphere and this coupling should exhibit a time dependence consistent with the observed results of the short time rotational diffusion constant versus concentration study. This proposed mechanism can be justified through experimental and theoretical documentation. This mechanism is similar to those

proposed[82,83] for the electric field orientation of charged DNA's due to anisotropic counterion flow. In the case of the system studied here, the field is provided by the monopole moment of a nearest neighbor.

The relaxation time or times characterizing the redistribution of a perturbed counterion atmosphere surrounding a spherical or non-spherical macroion can be measured through dielectric dispersion while the polarizability or mean square dipole can be measured through dielectric increment measurements. The ionic polarizability has also been shown[82] to effect the interpretation of transient electric birefringence data from which the rotational, diffusion constant can be obtained. Concentration dependencies of rotational diffusion of interacting (but not through long range Coulomb forces) concentrated protein solutions have been observed and attributed to particles physically touching each other as predicted they should by the formula $CL^3 \sim 1$ where L is the length of a DNA or protein particle. Experimental investigations of the dielectric increment or dispersion behavior of charged protein particles has been reviewed by both Tanford and Oosawa and will not be discussed here. Measurements have been carried out on charged polystyrene latexes and were found to exhibit pronounced polarizabilities, these systems however were non-interacting. Regarding the theoretical aspects of the relaxation times of the counterion atmosphere, Kirkwood and Schumaker as well as Oosawa have calculated the largest relaxation time to be on the order

of L^2/D' where L is the largest dimension of the particle while D' is the translational dissusion constant of a counterion. D' is expected to be smaller as compared to its free value as it is caught in the potential of the macroion. For most systems including this one, the relaxation time is quite small, on the order of a few microseconds. Further insight into the counterion relaxation may be found in comparing the short with the long time rotational diffusion constants versus concentration. Just as was the case with translational diffusion, over the time period a long time correlation function is measured (approx. $50X10^{-4}$ s), a particle rotates an appreciable fraction of its full rotational period ($1/6\Theta$). Over this period, the counterion atmosphere can reconstitute itself many times, the total effect on the macroparticle manifesting itself only in the long time limit. In performing a short time measurement of the rotational diffusion constant, dynamics of the macroparticle on the time scale over which the counterion atmsophere is reshaping itself is probed. It is felt that an analogous situation as was encountered with the short time measurement of translational diffusion is also encountered in short time rotational diffusion. At short times, the macroparticle can rotate at a faster rate than it can over longer times where many relaxation periods of the atmosphere can manifest itself. The short time limit obtained apparently does not yield free rotational motion except at the lowest concentration measured. It could be that measuring a rotational relaxation time on a time scale much shorter than the ones used here to extract a short time value for 6Θ through

short time measurements of the depolarized dynamic correlation function would be necessary to effectively separate the long and short time behavior and therefore possible extract $6\Theta_o$. Anyway, increasing the concentration of macroions increases the anisotropic interparticle potential energy and thus the coupling between an atmosphere and its particle. This should and does result in a similar trend for the short time and long time limits of 6Θ with concentration. It is encouraging to note that at the lowest macroion concentration where anisotropic interparticle interactions are smallest, a free value for the rotational diffusion constant is recovered while at this concentration, the isotropic component still affects a hindrance of translational diffusion as it should since it is much stronger.

The results of the static measurement of the depolarized intensity indicate the presence of 0-0 and/or 0-P interparticle correlations. Because a sphere has no detectable or preferential orientation, an 0-0 type of correlation simply means that a given pair of particles are orientated relative to each other over some long time characterizing one full rotational period. In this case, increasing the magnitude of the interaction by decreasing the interparticle spacing would cause an increased retardation of free rotational diffusion, thus implicit in a 0-0 correlation is a dependence upon the position of a nearest neighbor and thus the concentration. A 0-0 correlation implicitly contains 0-P correlations as a result of this as would be the case with any interparticle force dependent upon

interparticle distances. A correlation purely of the O-P type would be characterized by one particle exhibiting a preferential orientation, not just any orientation with respect to another. This is possible if one recognizes the non-spherical geometry of these particles whose average geometrical ellipticity is about 2. For a non-spherical particle, the ionic polarizability becomes a tensor quantity. From the theory of Oosawa, the ratio between the parallel and perpendicular components of the polarizability with respect to the long symmetry axis is a factor of 5 for an ellipticity of 2. This would increase the estimated effective anisotropic contribution from that calculated for an equivalent sphere by a factor of 5 to give a value of the potential of about kT/70 based on the previously stated parameters. It seems reasonable that rotational diffusion around some preferential particle fixed direction is occuring while this direction itself is changing as a neighboring particle inducing the dipole itself translates around. It is this type of motion that characterizes the "rotational diffusion constant." Regarding an attempt to model the hindered rotational diffusion process along the lines of the simple harmonically bound Brownian particle model used for translational diffusion, one can perform a variable transformation from $x(t)$ representing a particle position to a angular variable $\Omega(t)$ in the associated Langevin equation (eq. II.24). The harmonic frequency ω in the case of rotation would model the rotational motion of a particle within a cage defined by its asymmetric counterion atmosphere. The mathematical form of the coupling term embodied in

the harmonic frequency which is dependent upon the concentration is an unknown at the present time. Performing a transformation such as this would yield a form identical to eq. II.24 and thus would have a similar solution, unfortunately the analogy can be carried no further. As far as a more advanced treatment of hindered rotational diffusion resulting from the mechanism proposed above, there are none at the present time. Schurr[58] however, has proposed a theory for the hindered rotational diffusion constant of a Debye (Brownian) model fluid of interacting permanent dipoles in the short time limit. This theory is of no use as it does not apply here even though it represents work along the same lines as that which would be required here.

In conclusion, it would be interesting to make measurement such as this presented here on charged particle of other shapes[84] or possibly higher anisotropies. One might possibly make polyvinylidenefluoride latexes which could be heat treated to their piezoelectric points converting them into little bar electrets which when coated with surfactant might act as a solution of interacting permantent dipoles prevented from coagulation by a high monopole moment. Also, this study has revealed that much work needs to be done in the field of the physical chemistry of non-ideal electrolytes such as aqueous surfactant solutions. Schwan,[18a] et. al. discovered that extremely large static dielectric constants (10^4) are present in aqueous latex suspensions ($\kappa a << 1$) and that it is greatly dependent

upon concentration ($d\varepsilon/dc$ positive). It has been questioned as to whether or not static dielectric constants of this size are consistent with the screened Coulomb form. Clearly this should be resolved. The work of Frolich and Genzel[85] have clearly shown that if interparticle pumping occurs at the resonance frequency of the low lying giant dipole vibration characteristic of the fluctuating counterion atmosphere, this may be responsible for large interactions which can be both attractive and repulsive if the critical interaction distance $(\alpha/\varepsilon_s)^{\frac{1}{3}}=R^*$ is in the range of the interparticle spacing. If R^* is as large as κ^{-1}, this scenerio should be investigated. Recently, much inquiry has been focused on the phenomenon of surface plasmons observed in colloidal suspensions of small metallic particles. Interesting dispersive behavior can occur in the visible region where plasmon modes can be excited at resonance. Analogously, Schwarz[18b] recognized that colloidal particles and their counterion atmospheres can be considered as dielectric spheres exhibiting a surface conductance. At the light frequency used for scattering measurements (10^{14} Hz), any surface plasmon should be highly overdamped. Colloid particles of a size comparable to the wavelength of visible light should experience different electric field strengths at different parts of its surface which might produce overdamped surface currents which would relax on the time scales of macromolecular diffusion. An entirely new explanation invoking plasmon theory is being sought[86] with regard to the solidlike structures exhibited by the interacting virus suspensions in contrast to the apparent success of the Coulomb

solid model. The ordering and role of water molecules is also being investigated. There is also no reason why the rotational diffusion constant of the optically isotropic and geometrically spherical polystyrene latexes which can exhibit very strong Coulombic interparticle interactions, much stronger than this system, cannot be measured by transient electric birefringence to yield information on the role played by the ionic polarizability in affecting rotational diffusion in those systems. The absolute static structure factor could not be obtained as backup evidence in those systems however.

REFERENCES

PART II

1 W. Hess and R. Klein, Ad. in Phys. 32, No. 2, 173 (1983).

2 P.N. Pusey and R.J.A. Tough, "Dynamic Light Scattering and Velocimetry: Applications of Photon Correlation Spectroscopy," edited by R. Pecora (Plenum, 1984).

3 Sir G. Stokes, Trans. Cambridge Phil. Soc., 8, 287 (1847); ibid. 9, 8 (1851).

4 A. Einstein, Ann. Physik, [4], 19, 287 (1906); ibid., 34 591 (1911).

5 F. Perrin, J. Phys. Radium, [7], 7, 1 (1936).

6 W.J. Moore, "Physical Chemistry," (Prentice Hall).

7 A.R. Altenberger and J.M. Deutch, J. Chem. Phys., 59, 894 (1973).

8 P. Pieranski, Contemp. Phys., 24, 27 (1983).

9 P. Debye and E. Huckel, Physik. Z., 24, 185 (1923).

10a R. Hastings, J. Chem. Phys., 68, 675 (1978).

b R. Hastings, Phys. Letters 67A, 316 (1978).

c R. Hastings and J. G. Daly, J. Chem. Phys. 85, 294 (1981).

11a J. G. Kirkwood and J. C. Poirier, J. Phys. Chem., 58, 591 (1954).

b J. G. Kirkwood, "Theory of Solutions," (Gordon & Breach, New York, 1968).

12 M. G. Hodgins, O. C. Hodgins, D. W. Kupke and J. W. Beams, Proc. Nat. Acad. Sci. US 72, 3501 (1975).

13 S. Alexander, P.M. Chaikin, P. Grant, G.J. Morales, P. Pincus and D. Hone, J. Chem. Phys., 80, 5776 (1984).

14 W.H. Shih and D. Stroud, J. Chem. Phys., 79, 6254 (1983).

15 E.J.W. Verwey and J.T.G. Overbeek, "Theory of the Stability of Lyophobic Colloids," (Amsterdam 1945).

16 B.V. Derjaguin and L. Landau, Acta. Physiocochim., 14, 633 (1941).

17 S. Takashima, J. Chem. Phys., 70, 1372 (1966); Biopolymers, 5, 899 (1967).

18a H.P. Schwan, G. Schwarz, J. Maczuk and H. Pauly, J. Phys. Chem., 66, 2626 (1962).

b G. Schwarz, J. Phys. Chem., 66, 2636 (1962).

19a J.G. Kirkwood and J.B. Schumaker, Proc. Nat. Acad. Sci., 38, 855 (1952).

b J.G. Kirkwood and J.B. Schumaker, Proc. Nat. Acad. Sci., 38, 863 (1952).

20 C.T. O´Konski, J. Phys. Chem., 64, 605 (1960).

21 F. Oosawa, "Polyelectrolytes," Marcel Dekker, Inc., New York (1971).

22 Y. Marcus, "Introduction to Liquid State Chemistry," (Wiley Interscience, 1977).

23 J.G. Kirkwood, J. Chem. Phys., 3, 300 (1935).

24 M. Born and H.S. Green, Proc. Roy. Soc. A188, 10 (1946).

25 J. Yvon, "La Theorie Statistique des Fluides et l´Equation d´Etat," Actualities Sci. Ind. 203 (1935).

26 N.N. Bogoliubov, J. Phys. USSR 10, 257, 265 (1946).

27 J.K. Percus and G.J. Yevick, Phys. Rev. 110, 1 (1958).

28 J.M.J. van Leeuwen and J. de Boer, Physica (Utrecht) 25, 792 (1959); M.S. Green, J. Chem. Phys., 33, 1403 (1960).

29a J.B. Hayter and J. Penfold, Mol. Phys. 42, 109 (1981).

b J.P. Hansen and J.B. Hayter, Mol. Phys. 46, 651 (1982).

30 R.G. Palmer and J.D. Weeks, J. Chem. Phys., 58, 4171 (1973).

31 M. Baus and J.P. Hansen, Phys. Rep., 59, 1 (1980).

32 F. Gruner and W. Lehman, J. Phys. A: Math. Gen., 12, L303 (1980); Light Scattering in Liquids and Macromolecular Solutions," edited by V. DeGiorgio, M. Corti and M. Giglio (New York: Plenum); J. Phys. A: Math. Gen., 15, 2847 (1982).

33 J.C. Brown, P.N. Pusey, J.W. Goodwin and R.H. Ottewill, J. Phys. A: Math. Gen. 8, 664 (1975).

34a P.N. Pusey, J. Phys. A: Math. Gen., 11, 119 (1978).

b P.N. Pusey, Phil. Trans. R. Soc. Lond., A283, 429 (1979).

35 M.C. Wang and G.E. Uhlenbeck, Rev. of Mod. Phys., 17, 323 (1945).

36 J.A. Marqusee and J.M. Deutch, J. Chem. Phys., 73, 5396 (1980).

37 W.B. Veldkamp and J.R. Votana, J. Chem. Phys., 72, 2794 (1976); R.S. Hall and C.S. Johnson, Jr., J. Chem. Phys., 80, 4251 (1980).

38 G. Phillies, J. Chem. Phys., 60, 976 (1974).

39 W. Dieterich and I. Peschel, Physica 95A, 208 (1979).

40 H. Mori, Prog. Theo. Phys., 33, 423 (1965).

41 B.J. Berne and D. Forster, Ann. Rev. Phys. Chem., 22, 563 (1971).

42 M. Muthukumar and K.F. Freed, J. Chem. Phys., 78, 497 (1983); ibid. 78, 511 (1983).

43 W. Hess and R. Klein, J. Phys. A: Math. Gen., 13, L5 (1980).

44 L. Onsager, Ann. N.Y. Acad. Sci., 46, 241 (1945).

45 S. Harris, Mol. Phys., 26, 953 (2973); J. Phys. A., 10, 1905 (1977).

46 W. Hess and R. Klein, Physica 105A, 552 (1981).

47 W. Hess and R. Klein, J. Phys. A: Math. Gen., 15, L669 (1982).

48 J.W. Strutt (Lord Rayleigh) Phil. Mag. [4] 41, 107, (1871).

49 P. Debye, J. Applied Phys., 17, 392 (1946).

50 M. Smoluchowski, Ann. Physik, [4] 25, 205 (1908); Phil. Mag., [6] 23, 165, (1912).

51 A. Einstein, Ann. Physik, [4] 33, 1275 (1910).

52 C. Tanford, "Physical Chemistry of Macromolecules," (John Wiley & Sons, Inc.).

53 B.J. Berne and R. Pecora, "Dynamic Light Scattering," (Wiley Interscience, 1976).

54 H. Maeda and N. Saito, Poly. J., 4, 309 (1973); J. Phys. Soc. Japan, 27, 984 (1969).

55 A Wada, N.C. Ford and F.E. Karasz, J. Chem. Phys., 55, 1798 (1971).

56 R. Pecora, J. Chem. Phys. 49, 1036 (1968).

57 J.J. van Aartsen, Euro. Poly. J., 6, 1095 (1970).

58 J.M. Schurr, Mol. Phys., 40, 1025 (1980); CRC Crit. Rev. Biochem., 4, 371 (1977).

59 D.R. Bauer, G.R. Alms, J.I. Brauman and R. Pecora, J. Chem. Phys., 61, 2255 (1974).

60 T. Keyes, Mol. Phys., 23, 737 (1972).

61 G.R. Alms, D.R. Bauer, J.I. Brauman and R. Pecora, J. Chem. Phys, 59, 5310 (1973).

62 W.A. Steele, J. Chem. Phys., 38, 2404 (1962); ibid., 38, 2411 (1962).

63a P.A. Egelstaff, D.I. Page and J.G. Powles, Mol. Phys., 20, 881 (1971).

b J.H. Clark, J.C. Dore, G. Walford and R.N. Sinclair, Mol. Phys., 31, 883 (1976).

64 D.E. Koppel, J. Chem. Phys., 57, 4814 (1972).

65 J.C. Brown, P.N. Pusey and R. Dietz, J. Chem. Phys., 62, 1136 (1975).

66 G. Odian, "Principles of Polymer Chemistry," (Wiley Interscience).

67 F.J. Rahl, M.A. Evanco, R.J. Fredricks and A.C. Reimschuessel, J. Poly. Sci. 10, 1337 (1972).

68 R.H. Ottewill and D. Rance, Croatica Chem. Acta, 50, 65 (1977).

69 K. Shinoda, M. Hatoud and T. Hayashi, J. Phys. Chem., 76, 909 (1972).

70 G.C. Kresheck, "Water: A Composite Treatise, Vol. 4, Aqueous Solutions of Ampiphiles and Macromolecules" Chap. 2, edited by Felix Franks (Plenum Press, 1975).

71 G. Loveluck, J. Phys. Chem., 64, 385 (1960).

72a E. Nowak, J. Chem. Phys., 79, 976 (1983).

b S. Gorti, L. Plank and B. R. Ware, J. Chem. Phys., 81, 909 (1984).

73a C.M. Sorensen, R.C. Mockler and W.J. O'Sullivan, Phys. Rev. A., 14, 1520 (1976).

b B. Herpigny and J.P. Boon, "Light Scattering in Liquids and Macromolecular Solutions," edited by V. Degiorgio, M. Corti and Giglio, Marzio (Plenum, N.Y., 1980).

74 P.S. Russo, K.H. Langley and F.E. Karasz, J. Chem. Phys., 80, 5312 (1984).

75 M. Medina-Noyola, J. Chem. Phys., 77, 1428 (1982); M.J. Grimson, ibid., 79, 1070 (1983).

76 A. Vrij, J. Chem. Phys., 71, 3267 (1979).

77 G.H. Meeten and P. Navard, J. Poly. Sci. Phys. Ed., 22, 2159 (1984); G. Oster, Chem. Revs. 43, 319 (1948).

78 J.G. Kirkwood, J. Chem. Phys., 2, 767 (1934).

79 K.J. Gaylor, I.K. Snook, W. van Megen and R.O. Watts, Chem. Phys., 43, 233 (1979).

80 W. Hess and R. Klein, J. Phys. A: Math. Gen., 14, L145 (1981).

81 G. Wolynes and J.M. Deutch, J. Chem. Phys., 67, 733 (1977).

82 D.C. Rau and V.A. Bloomfield, Biopolymers, 18, 2783 (1979).

83 M. Hogan, N. Dattagupta and D.M. Crothers, Proc. Nat. Acad. Sci. USA., 75, 195 (197).

84 N.A. Clark, J. Physique Lett., 46, L-277 (1985).

85 H. Frolich Physics Letters, 39A, 153 (1972), ibid. L. Genzel, 65A, 371 (1978).

86 D. W. Kupke, private communication.